CUTTINGS ANALYSIS IN DRILLING

PERFORMANCE EVALUATION AND FORMATION IDENTIFICATION

by © Igor Kyzym

A thesis submitted

to the School of Graduate Studies in partial fulfillment of the

requirements for the degree of

Master of Engineering

Faculty of Engineering and Applied Science

Memorial University of Newfoundland

May 2018

St. John's Newfoundland and Labrador

Abstract

This investigation describes multiple methods for drilling cuttings collection in laboratory and field conditions. The methodology for cuttings sample preparation and its following analysis is also suggested. The analysis mainly focuses on cuttings size, ways of its graphical and numerical representation and its relationship with drilling parameters. Research shows that such parameter as a coarseness index can be easily calculated and can be used as a reliable indicator of the cuttings size. The relationship between rate of penetration, weight on bit, flow rate, bottom hole pressure, torque on bit, mechanical specific energy and cuttings size have been established in this research. Also, the overall effect of these parameters on drilling efficiency have been evaluated. Both, field and laboratory, data shows good correlation between the above-mentioned parameters and coarseness index. Research also shows that cuttings can be used for formation identification and construction of geological cross-sections. Analysis of the field and laboratory data indicates that type and strength of the formation affect drilling parameters. It also affects size distribution of generated cuttings and its relationship with drilling parameters. This shows that cuttings can be used as a valuable source of information in evaluation of drilling performance, drilled formation and can greatly help with better understanding of the drilling mechanism.

Acknowledgement

I would like to express my genuine gratitude to my supervisor Dr. Stephen Butt for his professional supervision, continuous guidance, academic and financial support throughout this research. Dr. Stephen Butt provided me with an opportunity to participate in multiple projects, field trials and an internship, during which I gained extensive knowledge and invaluable experience.

I would like to thank all Drilling Technology Laboratory members at Memorial University of Newfoundland; especially Rosana Reyes, Pushpinder Rana, Solomon Ansah, Abdelsalam Abugharara, Hongyuan Qiu for their assistance, suggestions, and their friendship.

Finally, I would like to express my deepest gratitude to my parents and my sister, who have been a constant source of support and encouragement during my studies and all my life.

Table of contents

List of Tables

List of Figures

Nomenclature

ROP	Rate of penetration
WOB	Weight on bit
TOB	Torque on bit
MSE	Mechanical specific energy
BHP	Bottom hole pressure
PSD	Particle size distribution
LWD	Logging while drilling
HSI	Hydraulic horse power
BHA	Bottom hole assembly
LPT	Linear position transducer
CI	Coarseness index
SSA	Specific surface area
N	Rotary speed
A_b	Area of the cross-section of the bit
q	Flowrate
ρ	Density of drilling fluid
C_d	Nozzle discharge coefficient
A_t	Total flow area of the nozzles
ROP_n	Rate of penetration for rotary speed n

List of Appendices

CHAPTER 1

INTRODUCTION

This chapter gives an introduction to drill cuttings analysis as an important source of information which can provide not just data about subsurface formations, but also be used as an indicator of drilling efficiency and related issues, such as hole cleaning, wellbore stability, etc. It can contribute to better understanding on the drilling process and its following optimization. It states the potential use of cuttings analysis in real-time drilling performance evaluation.

1.1 Research Context and Motivation

Well drilling is a process of drilling an opening in the ground for the following extraction of certain type of natural resources, for injection fluids to a subsurface reservoir or subsurface formations evaluation. As the most complicated, is usually considered drilling of an oil and gas wells, which requires penetration to much higher depths, comparing to water or any other type of wells. Considering the fact that oil production more than tripled

over last 50 years, the majority of shallow deposits have been almost depleted [1]. This made oil companies move towards more intricate sources of hydrocarbons (mostly deep-water wells). Drilling of deeper wells always requires more time, which also means higher overall cost of the project. Nowadays, during times of high market competition and relatively low oil price, cost optimization is extremely important. One of the possible ways to decrease the time required to drill a well and reduce the cost is an increase in rate of penetration (ROP). Oil companies can noticeably cut oil production cost just with a couple of percent increase in ROP. Many parameters affect ROP and it is very important to understand how each of those parameters affects it. Another way to decrease the drilling cost, is to reduce non-productive time (NPT), which accounts up to 32 percent of drilling operation cost for deep water wells [2].

Better understanding of drilling process, bit-rock interaction in particular, can help to accomplish both solutions mentioned above. Massive amount of data need to be collected and processed to understand which processes occur between the bit and drilled formation and how they affect drilling efficiency. It is also very important to look for new sources of information and new approaches for its analysis. Drill cuttings is a great source of information. It represents the result of bit-rock interaction and provide valuable information about rock cutting mechanism. This research focuses on analysis of cuttings size and its relationship with major drilling parameters, such as a rate of penetration, weight on bit, bottom hole pressure, flowrate, etc. It also discusses the effect of certain formation properties on cuttings size and deformation mechanism.

The outcomes of this research can potentially contribute to drilling optimization, well planning process, drilling fluid specification, develop new downhole equipment and bit technologies, etc.

1.2 Research objectives

The main purpose of this research is to establish the relationship between major drilling parameters and size of generated cuttings through the extensive set of laboratory and field experiments. As an interim step in this research, the procedure for drill cuttings collection and preparation for analysis to be proposed. Also the investigation on numerical representation of particle size distribution must be performed and the most optimal solution will be recommended. Based on the laboratory experiments, the relationships between parameters such as rate of penetration (ROP), weight on bit (WOB), bottom hole pressure (BHP), flowrate, torque on bit (TOB), mechanical specific energy (MSE) and cuttings size to be established. Similar relationships must be established based on the field data. Additionally, the effect of rock properties on drilling parameters and cuttings generation mechanism to be discussed in this thehis.

1.3 Thesis outline

Chapter 2 presents a review of the different methods and equipment required for cuttings collection and analysis. It describes methods, apparatus, and limitations for each of the method. This chapter also describes multiple ways for particle size distribution (PSD) representation and briefly explains the techniques used for numerical representation of the

cuttings shape. It includes a section about evaluation of formation properties based on cuttings analysis. The final part of the chapter discusses the effect of drilling parameters on cuttings size, and established relationships between them.

The information presented in this chapter helps to identify a suitable method for cuttings analysis for this research, as well as an optimal way to represent cuttings size. It also summarizes the outcome of the similar investigations performed by other researchers. This builds the foundation for the comparison and discussion of the results presented in this thesis.

Chapter 3 presents the results of the experiments conducted in the laboratory. They are a more extensive version of the experiments conducted by other scholars. These experiments are strictly based on use of PDC bit in a rotary drilling, while prior research was performed only on rotary percussion drilling or rotary drilling with use of diamond coring bits.

This chapter includes brief description of the lab scale drilling simulator, double-cutter PDC drilling bit, preparation of synthetic rock, test procedure. It also includes procedure for cuttings samples preparation and analysis. This chapter presents in detail the relationships that were established between the parameter that represents cuttings size and various drilling parameters.

Chapter 4 presents the results of the field trials. This chapter has a similar structure to the structure of Chapter 3. Due to the limitation of the drilling rig only one drilling parameter, the WOB, was varied throughout the experiments. Nevertheless, different formation were drilled during the field trials and the effect of their properties on the deformation

mechanism and cuttings size is discussed along with the relationships between ROP, WOB and cuttings size parameter are presented.

This chapter also includes the description of the field trials site, site geology, drilling equipment.

Chapter 5 presents the newly designed Logging While Drilling (LWD) system and its major components. It briefly discusses the capabilities of the system and meaning of recorded parameters. It provides information on the drilling equipment and conducted field trials. It presents the relationship between certain rock drilling rig parameters and formation strength. The results of ore-waste boundaries investigation and the importance of cuttings analysis in formation evaluation are also discussed in this chapter.

Chapter 6 summarizes major outcomes of the research. It includes concluding observations and the most relevant results. It states the importance of research, its potential and recommendation for future work.

CHAPTER 2

REVIEW OF CUTTINGS COLLECTION SYSTEMS AND METHODS OF ITS ANALYSIS

Drilling cuttings have always been used as a reliable source of information about subsurface formations. Analysis performed on cuttings can provide real-time information during the drilling process that may affect subsequent drilling, provide stratigraphic information, and give early indications of possible hydrocarbon presence. In addition, drill cuttings are the representation of the subsurface formation that can provide information not available from any downhole measurement. Cuttings can provide geochemical and paleontological data. They allow direct measurement of grain density, grain size, and pore morphology [7]. Cuttings also affect drilling fluid properties, annular-pressure losses, hole cleaning, wellbore stability/integrity, rate of penetration and have many other drilling considerations [3], [4], [8]. Cuttings properties such as particle-size distribution, volume, shape, etc., can indicate the start of a drilling problem and can help on the decisions to

improve performance. Also drill cuttings can be used for prediction of rate of penetration and overall evaluation of drilling process efficiency. Cuttings are an important source of information, because they represent the process of bit, rock, and fluid interaction [5], [6]. Reliable measures must be in place for taking accurate samples and reporting related properties to enable the drilling engineer to make meaningful correlations. Although automation and real-time measurements have simplified cuttings analysis, the logic behind the process still needs to be decided by the drilling experts. Ensuring reliable data and using it properly remain a challenge to improve drilling performance [3]. This proves the importance of drill cuttings monitoring on a continuous basis.

2.1. Manual and automated cuttings sampling

Ideally, cutting samples should be the same as the ones produced in the wellbore, where a bit and drilling fluid are interacting with the rock, directly affecting the drilling process. The closest place possible for cuttings collection is a return flowline that directs mud to the shakers.

There are several manual and automatic ways of obtaining and analyzing cuttings in the mud flow, including [3]:

- In-Line Measurement: Instrument is inserted into a pipe and takes measurements as the mud circulates;
- At-Line Measurement: Sample is collected and tested manually on-site;
- On-Line Measurement: Sample is collected and tested via bypass line;

- Off-Line Measurement: Sample is collected and tested manually in a laboratory setting.

Regardless of the automation stage, the sample needs to be collected from the mud return flowline. Such locations are inaccessible, and the modification of the flowline or installation of the bypass line is required to collect the sample. Figure 2.1 shows one of the earliest setups (left) for this purpose along with a modern arrangement (right). As an example, a set-up required for at-line measurement is shown in Figure 2.2. It depicts the return flowline with a control valve and a line for a sample collection.

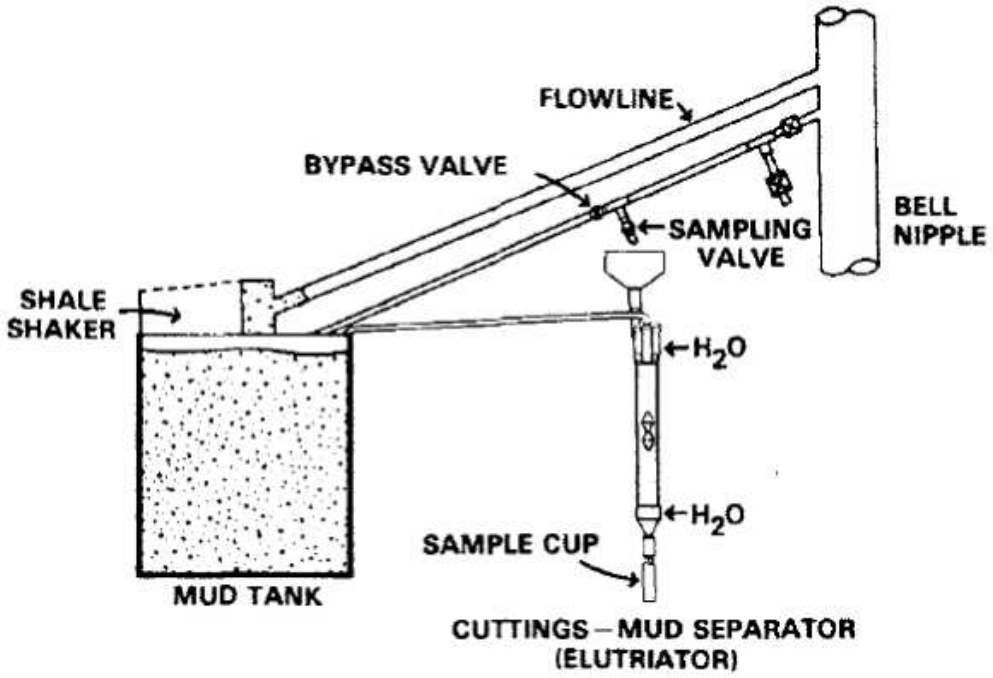

Figure 2.1 – Simple sampling setup (left) and recent sampling set-up with PSD analyzer (right) [3]

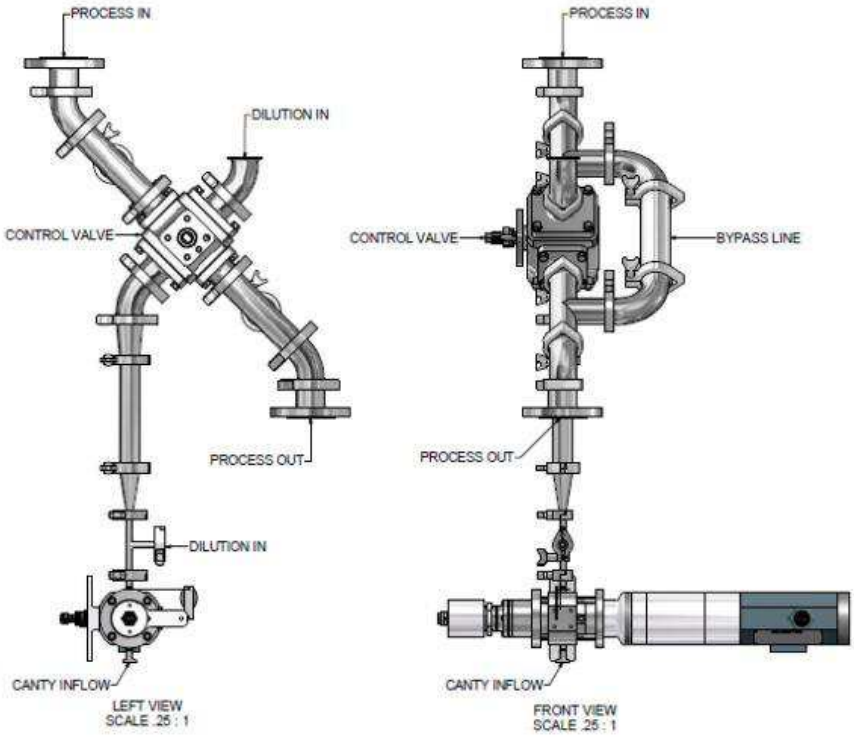

Figure 2.2 – At-line mud particle analyzer [3]

Another similar system for at-line sample collection was presented in [9]. The system (Figure 2.3, on the left) consists of three modules: a mud pump, a mini-shaker, an elutriator and sample collection unit. In this system mud flow saturated with cuttings is diverted at the bell nipple through a small diameter hose to the mini-shale shaker. Mud samples are collected with certain time interval from the small diameter hose to the collection column (Figure 2.3, on the right). The last one incorporates an elutriator, which is used to remove any remaining drilling muds [9].

If equipment required for the cuttings collection is not installed and it is impossible to collect samples from the flowline, the next place to gather cuttings is the “possum belly”.

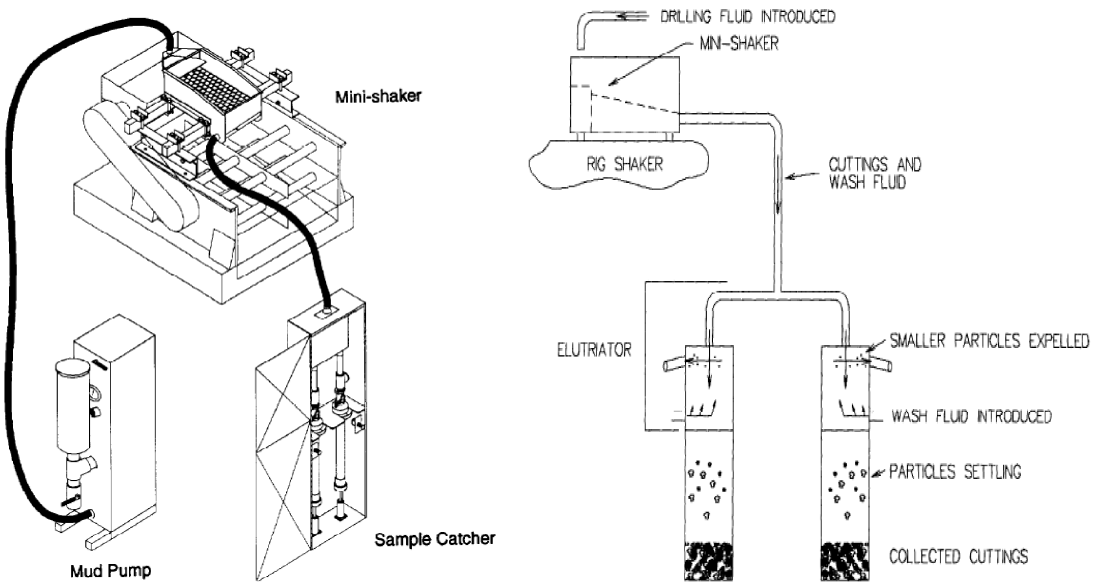

Figure 2.3 – Automated Cuttings Sampler system (left) and collection column with elutriator (right) [9].

Possum belly represents top part of the shale shaker that accumulates the mud before it passes through the shaker sieves (Figure 2.4).

Figure 2.4 – Shaker table and possum belly [3]

Figure 2.5 shows cuttings collected in the possum belly (a) and cuttings collected in the end of the shaker table (b). It can be observed that a majority of fine cuttings are lost because of the course sieve size of the shaker screen and cuttings tend to stick together in the sample collected at the shaker table. This will potentially lead to loss and misinterpretation of collected data [9], [4].

(a) **(b)**

Figure 2.5 – Cuttings samples collected at (a) the possum belly and (b) the end of the shaker [3]

Even though samples collected in the possum belly provides more reliable data, it is important to remember that the cuttings concentration can differ depending on the location in the possum belly the sample is collected from. Cuttings settle down and accumulate very fast at the bottom of the possum belly. Also, some cuttings can to wonder in the possum belly for long time and distort gathered data. The investigation has to be done and the best location for sample collection must be picked. The concentration of the cuttings is much higher towards the bottom and center of the belly (Figure 2.5, 2.6). Reliable data, suitable for analysis, can be obtained only if all the samples are collected from the same location.

If the samples are collected from different locations, analysis will be misleading and can cause interruptions in the drilling process.

(a)

(b)

Figure 2.6 – Cuttings samples collected from (a) the middle and from (b) the side of the possum belly [3].

It also important to keep in mind that there is a time delay between when the cuttings are produced at the bottom of the hole and when they are collected for analysis. This time delay will depend on the well diameter and depth, mud type and flowrate, size of the drill string, properties of drilled formation, etc. The specific calculation must be developed and

followed to establish the proper link between the cuttings sample and the depth is has been collected from.

A number of cuttings flow meters were developed to quantify the cuttings return. One of the most common methods is to estimate the weight of cuttings flow on a shale shaker via a collection device and strain gauges. Such system can provide an accurate real-time cuttings return volume measurement based on known rock density. Some of these systems even apply correction factor to account for errors caused by the coat of mud over cuttings. In other words, they can calculate the volume of equivalent dry cuttings mass or volume. Comparison of measured cuttings volume and theoretical return volume, cuttings recovery ratio can be calculated to reflect hole cleaning efficiency [11], [12]. Also, multiple systems based on image analysis of the cuttings have been developed. They are able to monitor the loading of cuttings on shale shaker in real-time and warn the operator if something unusual happens [13]. However, these systems are not able to quantify volume, size, or shape of the cuttings.

More advanced systems for at-line analysis have been recently developed. They do not require collection of the sample and can provide real-time data. One of such system, based on image analysis, was presented in 2017 by Han *et al.* Figure 2.7 (a) and (b) illustrate the design concept. Figure 2.7 (c) present the testbed setup and (d) shows the field setup with an explosion proof enclosure. A profile laser scanner, 2D and 3D cameras are used along with specific software to produce and analyze data [10], [19]. Image analysis technology in discussed in greater detail in subsequent sections of this chapter.

2.2 Methods of drill cuttings analysis

Cuttings can be analyzed from different perspectives: size, shape, physical and petrochemical properties, etc. This research is mainly based on analysis of cuttings size and its relationship with drilling parameters. To characterize cuttings size of the whole sample, particle size distribution (PSD) is required. PSD is list of values indicating what sizes of particles and in what proportion (usually by mass) they are present in a test sample.

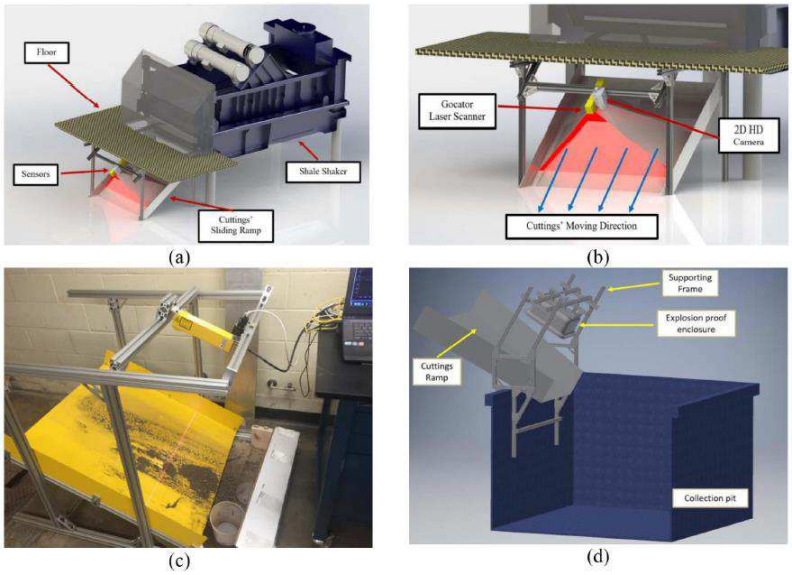

Figure 2.7 – Austin cuttings monitoring testbed design [10]

PSD can be presented as mathematical function, table, graph or can be used to derive a single numerical parameter to characterize cuttings size [14].

There are many different methods to determine particle distribution, some of them are discussed in this section. The choice of a particular method depends primarily on a dispersion level of a sample, i.e. on the degree of fineness of the sample. Also, some

methods can be preferred for samples which particles are suspended in liquid media. Sometimes tables or charts, like one shown in Figure 2.8, can be used to quickly identify suitable methods.

2.2.1 Sieving analysis

The most common and technologically simple method of particle size determination is sieving analysis.

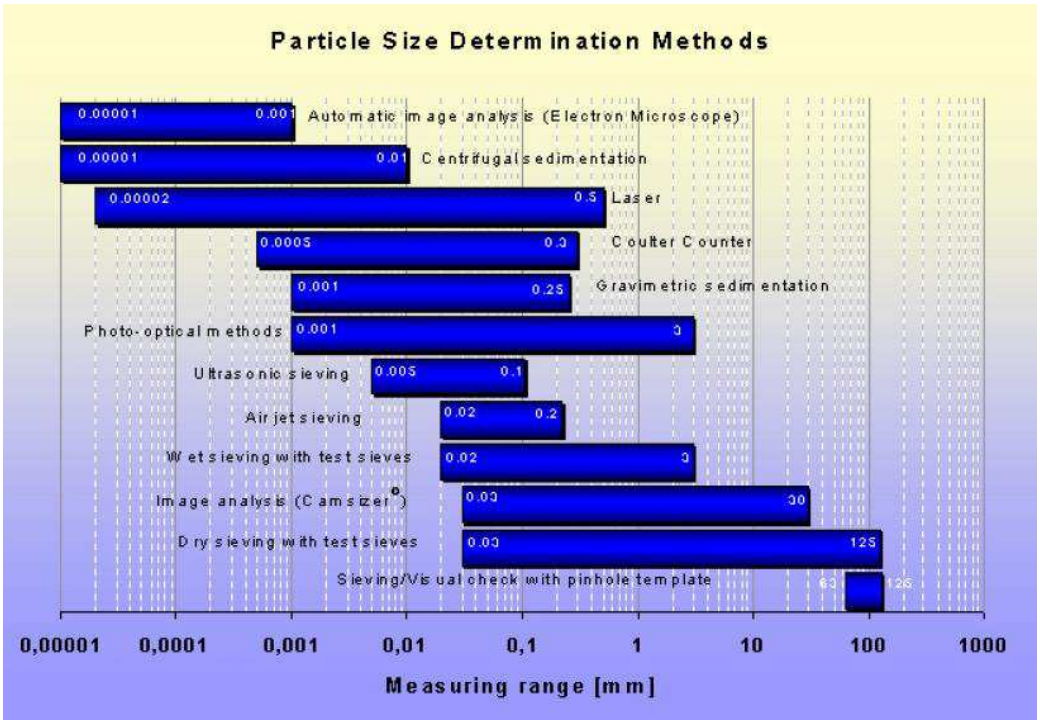

Figure 2.8 – PSD determination methods [15]

Particle distribution analysis for sieving analysis is normally done by weight, and more rarely by volume. A set of sieves with appropriate mesh sizes must be picked for analysis. Mesh size and number of sieves is based on type of desired data, minimum and maximum

size of particles present in the sample, required precision, available time for analysis, etc. During the sieving, particles are subjected to horizontal or vertical movement (or both), forcing particles to pass through the sieves. The likelihood of particles passing through the sieve depends on the mesh size, particle size, time and intensity of the sieving action. After the sieving is complete, weight of each fraction is measured and recorded. Later these values are used to derive particle size distribution.

Depending on the material and the requirements for sieving result, various sieving methods are used for determining particle size and distribution. A basic differentiation is made between the following parameters:

i. Automatization:

- manual sieving;
- mechanical sieving.

Usually manual sieving is only done for a quick on-site analysis when no sieving machine is available. The results of this type of sieving can very subjective. They are affected by force and intensity of sieving, type of action, time, which can differ from test to test and person to person. Mechanical sieving is performed with using of sieve machine (Figure 2.9) and can be subcategorized by the type of sieving action: throw-action and horizontal sieving. Horizontal sieving is preferable for samples with long, flat, needle-shaped particles. Horizontal sieving ensures movement of particles in one (horizontal) plane and reduces chances of sieve mesh getting clogged with irregular shaped particles. For this reason, horizontal sieving is recommended for analysis of large samples [15].

ii. Number of sieves:

- single sieve;
- sieve set sieving.

Single sieve used only when the percentage of undersized or oversized particles has to be determines. Sieve set sieving must be carried out when the complete particle distribution of the sample is required. The more sieves are included in the set, the more detailed analysis can be performed.

Figure 2.9 – Sieving machine [15]

iii. Dry and wet sieving.

Most sieving processes are carried out on dry materials. However, there are many applications in which wet sieving cannot be avoided, e.g. when the material to be tested is already present as suspension or when a very fine sample tends to form lumps while being dried. Wet sieving is very similar to dry sieving. The major difference is that the sieving

liquid is introduced to the top sieve and the shaking action continues till the liquid leaving sieving set runs clear with no solid particles [15]. The main advantage of the sieving is its simplicity and that there is no upper limitation on the particles size.

2.2.2 Laser diffraction

Laser diffraction is one of the most widespread method used for the particle size measurement. The device for laser diffraction consists of a central measuring unit and a dispersion unit. There are two semiconductor lasers located in the central measuring unit, which usually ensures measuring range from 0.08μm up to 2000μm. Normally particles bigger than 2000μm cannot be tested by this method. The laser diffraction method makes use of a laser light which is scattered by a suspended particle, when passing through. Depending on the size and optical properties of the particles, the light scatters at a particular spatial angle. These angle patterns, after passing through condensing lens, are detected, and measured by photodetector arrays (Figure 2.10). Data received from photodetectors is analyzed by a computer and used to calculate size distribution of particles [16].

2.2.3 Image analysis

Modern image processing facilities can perform analysis off-line, on samples analyzed in the lab, or even perform analysis on-line, on cuttings samples moving on the shaker table or special facility installed after it. For off-line (static) analysis, individual high-resolution pictures are taken and later processed using the software, which generates PSD data in form of a table or a graph.

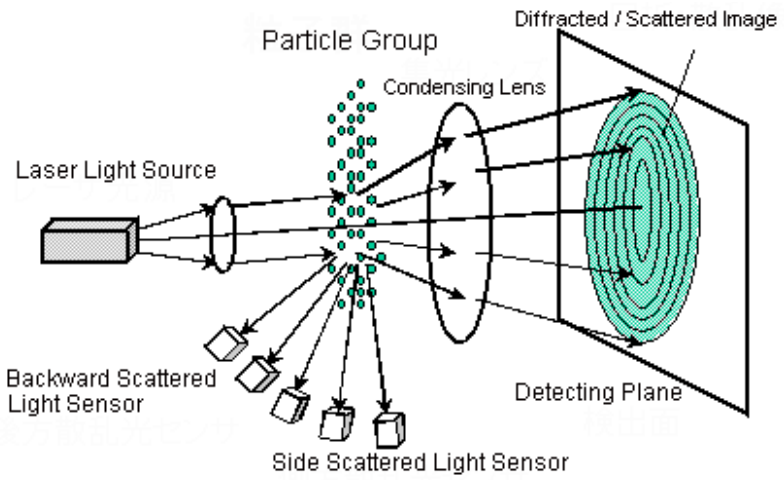

Figure 2.10 – Laser diffraction principle [19]

Depending on type of the analyzing facility, length and width (2D cameras) or length, width and thickness (3D cameras) can be measured [13], [17], [18].

Some software, used for analysis, can also provide information about particles shape. On-line, or dynamic, analysis performed on cuttings moving on shaker table, usually cannot provide PSD data and its results can only be used for indication of issues related to cuttings removal efficiency, wellbore instability, etc. Nevertheless, certain technologies can perform analysis on cuttings flow and obtain precise PSD, for instance, the CAMSIZER Image Analysis Technology. It projects a beam of light on the particles freely falling from the chute and two cameras record the projected shadows. The process is illustrated in Figure 2.11.

Figure 2.11 – CAMSIZER Image Analysis technology [19]

Patented camera technology consists of the main camera that measures big particles and zoom camera measures small particles (Figure 2.12). These different range cameras ensure high resolution and wide measuring range. They work similar to regular digital cameras and captures not the actual particle, but its reproduction in square pixels. The size of the pixel is different for two cameras: 75 and 15 μm for basic and zoom camera respectively (Figure 2.13 a). Detection of the particle is possible only when two or more pixels have been activated. This means that even particles as small as 30 μm can be detected. High resolution of CAMSIZER pictures makes it possible to calculate various lengths, widths, equivalent diameters, etc. Shape metrics including sphericity, aspect ratio, symmetry can also be calculated [19].

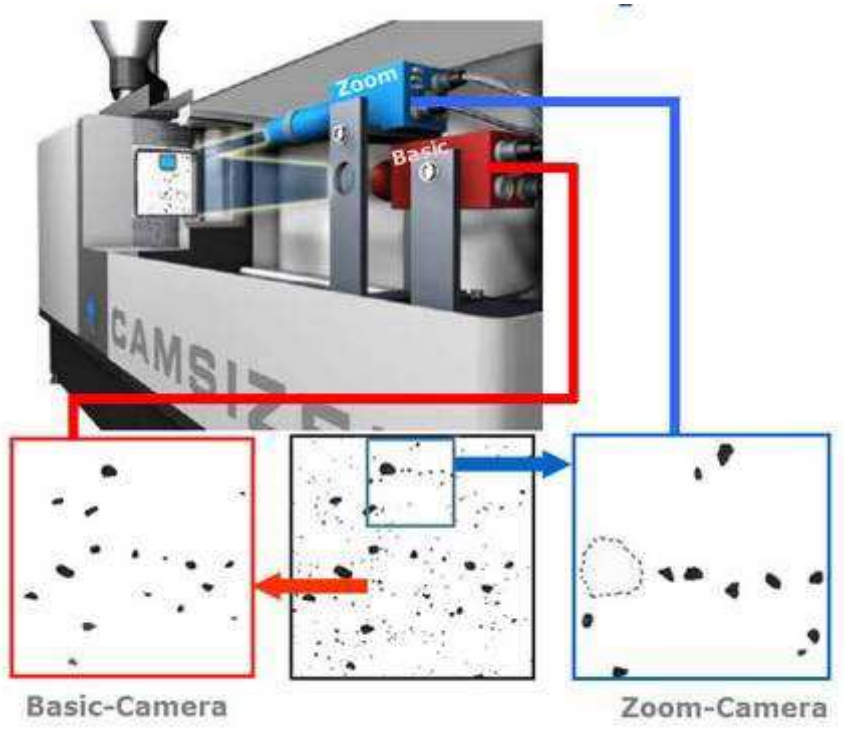

Figure 2.12 – Basic and zoom cameras [19]

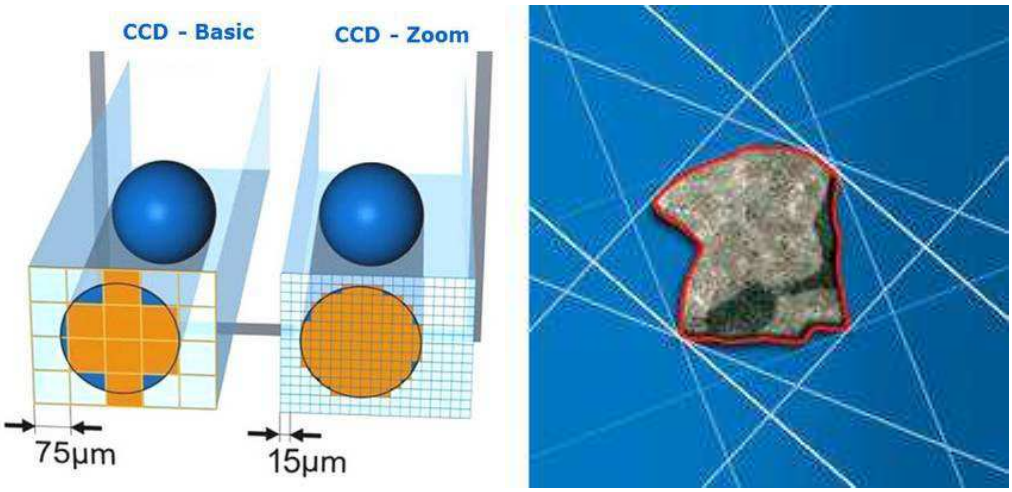

a) **b)**

Figure 2.13 – Particle detection: a) Pixel size for basic and zoom cameras; b) Particle scanned in multiple directions [19]

2.2.4 Focused beam reflectance measurement (FBRM)

This method can perform measurements on particles suspended in liquid media, thus it can be used as an in-line method and can obtain real-time PSD data. During the measurements, the probe based instrument is inserted directly into a pipe under an angle. It ensures that the particles can flow easily across the probe window where the measurements take place. A laser is projected through the probe tube and a set of optics and focused on sapphire window. The beam is scanning across the particles as they flow past the window (Figure 2.14 a) [3], [20]. As the beam scans across the flow, individual particles will backscatter the laser light to the detector. These pulses of backscattered light are counted, their duration is measured and later used to calculate a chord length of each particle (Figure 2.14 b).

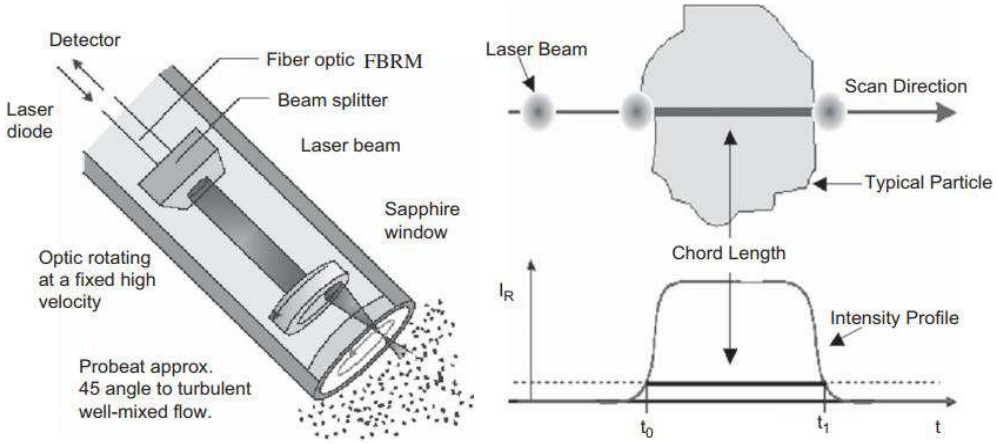

Figure 2.14 – a) The focused beam reflectance method (FBRM) probe technique; b) Measurement of a particle chord length using the FBRM technique [20]

The chord length is directly related to particle size. Thousands of particles are measured and counted every second, what provides high frequency and high precision data. Similarly to laser diffraction, testing is limited to particles smaller than 2000μm.

2.2.5 Ultrasonic extinction

Ultrasonic extinction technology can be used as in-line and on-line method. This technology is using sound waves, thus can be used in opaque media with concentration of solids up to 70 % vol. [3]. Cuttings suspended in liquid media flow between ultrasonic transducer and detector. An electrical high radio frequency (RF) generator is connected to the transducer. The generated ultrasonic waves with the certain lengthwave (λ) are transmitted through the suspension and interact with the particles (Figure 2.15). This interaction results in an attenuation of the intensity of the ultrasonic waves. After passing the measuring zone the ultrasonic waves are received by an ultrasonic detector and are reconverted into an electrical signal. The extinction of the ultrasonic waves is calculated from the ratio of the signal amplitudes of the generator and the detector side [21].

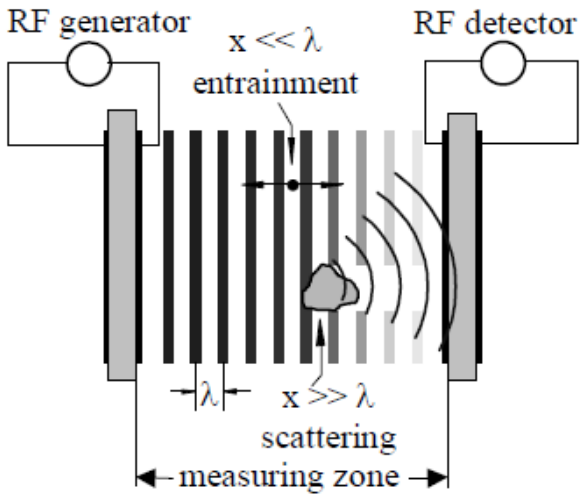

Figure 2.15 – Schematic of the measuring principle [21]

The extinction level is dependent on the thickness of the suspension layer, the projection area-concentration, and the related extinction cross section caused by particles. This data is processed, and PSD is generated by a software.

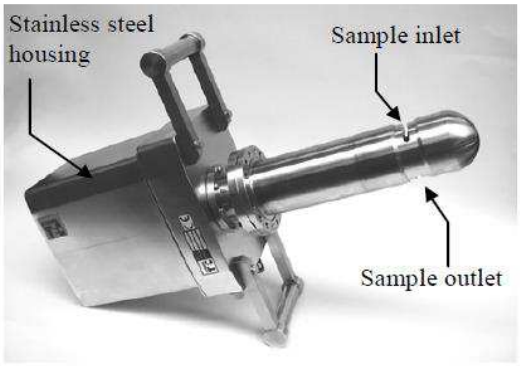

Figure 2.16 – Technical realisation of Ultrasonic Extinction for in-line particle size analysis (Sympatec OPUS) [21]

2.3 Graphical and numerical representation of sample's cuttings size and shape

As it was already mentioned, particle size distribution is a representation of the whole particle sample. It indicates what sizes of particles are present in what proportions (relative particle amount as a percentage where the total amount of particles is 100 %) in the sample. Most usually PSD is represented as a graph, where the cumulative percentage of the particles fractions is plotted against cuttings size in log coordinates (Figure 2.17). Cumulative percentage can represent the amount of particles of certain size or below (cumulative passing or finer percentage); or the amount of particles of certain size or above

(cumulative remaining or coarser percentage). The percentage can be measured by weight or by volume. PSD can be also represented as a mathematic function or a data table.

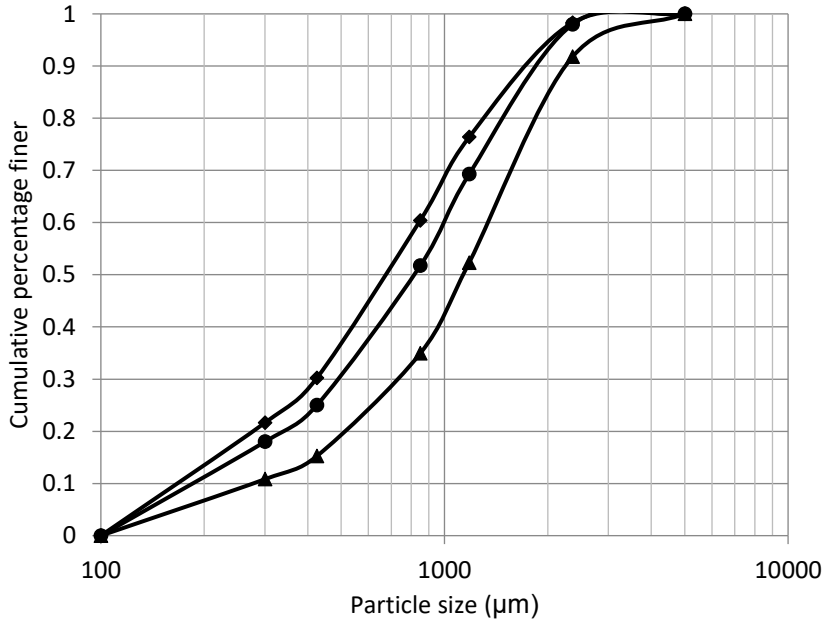

Figure 2.17 – Particle size distribution

Also, PSD can be plotted in logarithmic coordinates. In this case, both x-axis, which represents particle size and y-axis, represents cumulative percentage are plotted logarithmic coordinates (Figure 2.18) This type of the plot is also called Rosin-Rammer-Sperling diagram [22], [6].

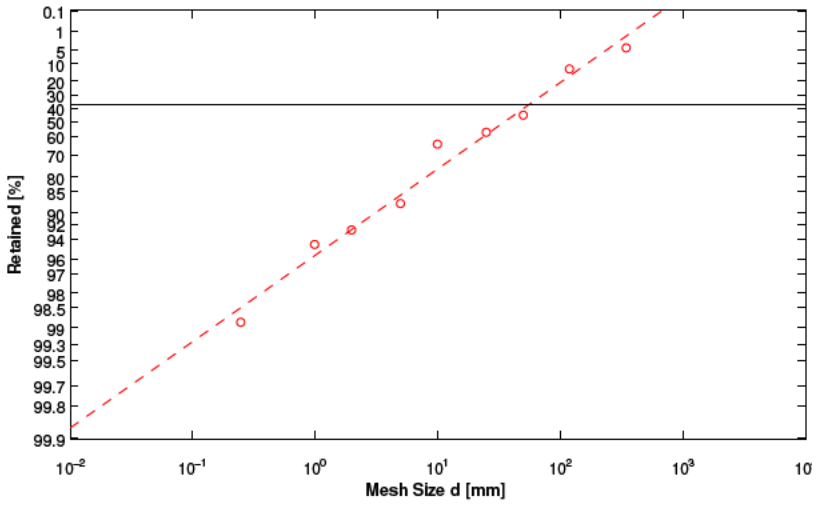

Figure 2.18 – Particles size distribution in log-log coordinates [22]

The main advantage of this diagram that PSD can be plotted as a straight line. However, it largely compacts the region above 50% and especially above 75% [23].

Even though PSD provides detailed information about particles in the sample, it is not always the best option to represent the cuttings size. During the analysis, when the cuttings size must be related to some other parameter and many samples have to be compared, it is better to have PSD represented as a single number. For this purpose, such parameters as coarseness index (CI) and mean particle size can be used. Mean particle size is known as the median diameter D50 and represents the particle diameter at 50% in cumulative distribution. In other words, 50% of the sample are larger that median diameter and 50% are smaller. The parameter of D36.79 (36.79% of the sample is bigger than this size) also sometimes called mean particles size and is used to characterize particles sample. This number was originally derived for coal, but also can be used for any material prepared by grinding, crushing or milling [22], [24], [25].

Another numerical parameter, that can represent a sample of particles called a coarseness index (CI). It is a non-dimensional value, that is calculated by adding cumulative weight percentage of particles retained in each sieve [6], [26]. Table 2.1 and Equation 2.1 explain the way CI is calculated,

$$CI = \sum_{n=1}^{i} (W_i + W_{i+1}), \tag{2.1}$$

where W_i – weight percentages of different fractions.

Table 2.1 – Coarseness index calculation

Size (mm)	Weight (%)	Cumulative weight (%)
+2.36	7.52	7.52
-2.36+1.18	27.44	34.96
-1.18+0.850	12.83	47.79
-0.850+0.425	20.98	68.77
-0.425+300	7.34	76.11
-300	23.89	100.0
∑	100	
Coarseness index (CI)		335.15

Based on previous research [40], mean particle size and coarseness index show similar relationship with major drilling parameters and are interchangeable. However, this may be different for other type research.

Numerical representation of particles shape is more challenging and usually requires high definition images and specialized software. Image analysis can be performed in different ways, as different shape characteristics may be required for different type of analysis. One of the oldest and the simplest ways to represent a particle shape is a length to width ratio.

However, this parameter does not always provide accurate results, especially for very irregular-shaped particles, because it narrows down particle representation to a square or a rectangular shape. It does not account for particle circularity of angularity.

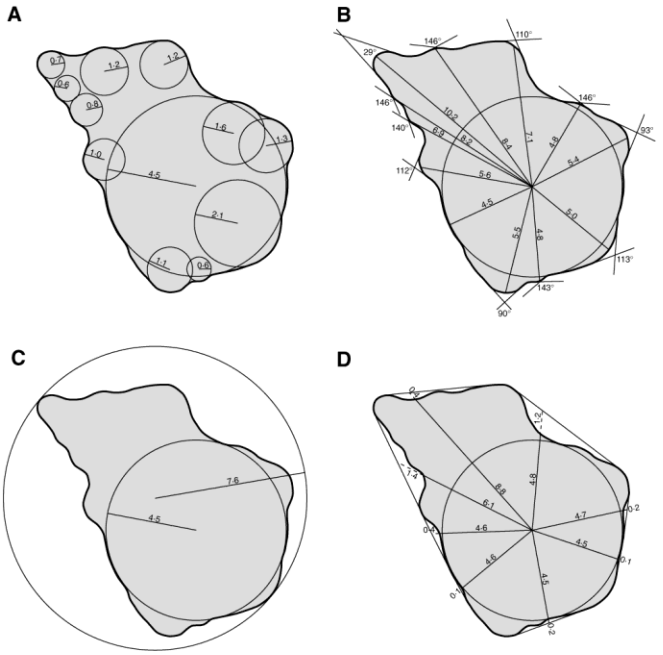

Figure 2.19 – Diagrams illustrating the measurements made for determination of: a) particle roundness; b) angularity; c) circularity and d) irregularity [27]

Modern software can evaluate such parameters as roundness, angularity, circularity, irregularity, etc. (Figure 2.19) [27]. Another parameter called “spike factor”, which is a characteristic of angularity can be obtain. Good correlation between this parameter and rock abrasiveness can be observed for certain types of rock and materials (quartz, silica sand, etc.) [28].

2.4 Cuttings analysis in evaluation of formation properties

Drill cuttings can provide quick and useful information on properties of drilled rock, especially when cores are not available. Several properties can be determined from cuttings:

- Acoustic properties;
- Mechanical properties;
- Petrophysical properties and others.

Multiple techniques have been developed for determination of P and S-wave velocities from measurements on cuttings. One of the techniques suggest performing measurements on a single cutting. Edges of the cutting need to be flattened on the grinding machine. Later sonic transducer and receptor along with other equipment are used to measure the velocities [29].

Unconfined Compressive Strength (UCS), which is normally defined by performing standard ASTM test on cores, can also be measured by testing cuttings. The indentation test is performed on individual cuttings. The research showed that indentation index has a strong correlation with UCS. However, cuttings require thorough preparation for this test. Cuttings are embedded in the acrylic resin disks, which act as a confining environment and prevent the tensile splitting of the cuttings. The disk surface is polished, and the indentation test is performed on cuttings surface. During the test, load-displacement curve is plotted and the slope of the curve represents an indentation number or index [29], [30], [31]. A lot of research was also done on evaluation of petrophysical porosity and permeability

measurements on cuttings [29], [32], [33]. Other properties such as saturation, pore-size distribution, thermal dilution, electrical resistivity can be defined from specific cuttings tests [29].

2.5 Effect of drilling parameters on cuttings size

Very limited research has been done on drill cuttings in terms of its relationships with drilling parameters. Nevertheless, it has been reported that rate of penetration has a very strong correlation with drill cuttings size. A set of experiments was performed in the field [6], using percussion drilling rig. During the experiments, all the parameters of the rig were kept constant. Depths and time of drilling were recorded and cuttings samples were collected for corresponding intervals. Sieving analysis performed on cuttings samples and such parameters as coarseness index and mean particle size were derived. Strong relationship between ROP and above-mentioned parameters was established (Figure 2.20, Figure 2.21). Size of drilling cuttings increase with increase of ROP. It was also indicated that specific surface areas (SSA) tend to increase with decrease of ROP. This can be explained by the fact that decrease in ROP cause decrease in cuttings size and smaller particles size is always associated with higher surface area [6].

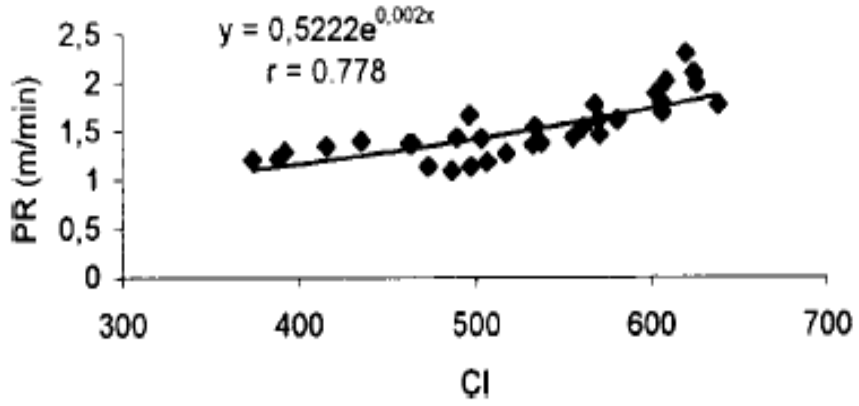

Figure 2.20 – The relationship between rate of penetration and coarseness index [6]

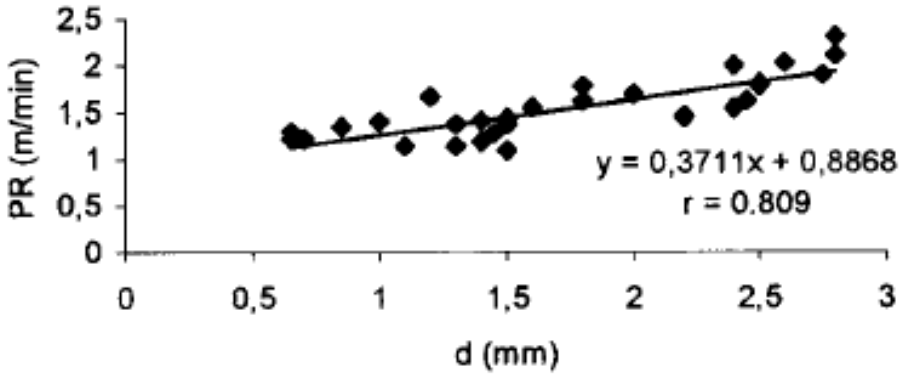

Figure 2.21 – The relationship between rate of penetration and mean particle size [6]

Another set of laboratory experiments was performed with use of coring bits (pin, hybrid, impregnated bits) [34]. Sieving analysis was performed on cuttings and mean particle size (D50) for each sample was calculated. It was reported that cuttings size increases with increase of weight of bit and with increase of ROP (Figure 2.22). This tendency can be

observed for all types of tested bits. Rotary speed and specific energy also seems to have strong correlation with mean particle size. Particles size decreases with increase of rotary speed. This can be explained by crushing and regrinding of the cuttings, before they were removed with drilling fluid. This regrinding process also causes increase in specific energy (Figure 2.23) [34].

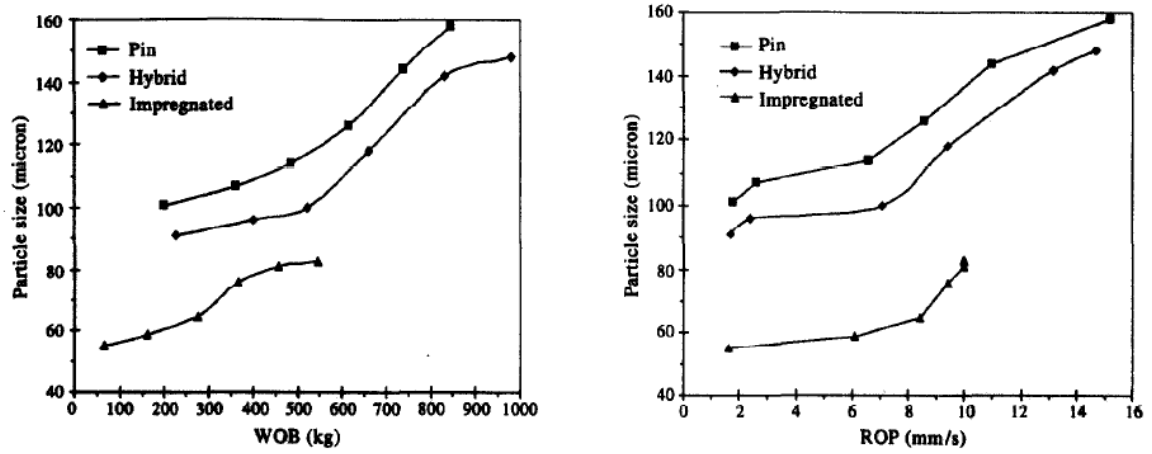

a) **b)**

Figure 2.22 – The graphs of the particle size of the detritus versus weight on bit (a) and rate of penetration (b) [34]

Another phenomenon, that was observed during these experiments, that the fraction of fine particles tends to decrease drastically with increase of WOB (increase in ROP). This indicates more efficient cutting mechanism under higher WOB [34].

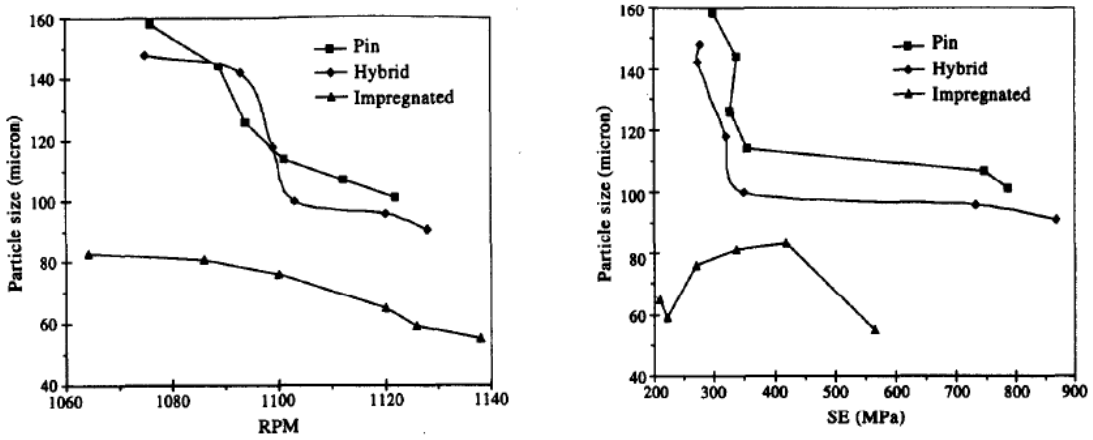

a) b)

Figure 2.23 – The graphs of the particle size of the detritus versus rotary speed (a) and specific energy (b) [34]

Another research [5] also indicates that the decrease in size particles contributes to increase of mechanical specific energy. Exponential relationship between minimum particle size and MSE was established (Figure 2.24).

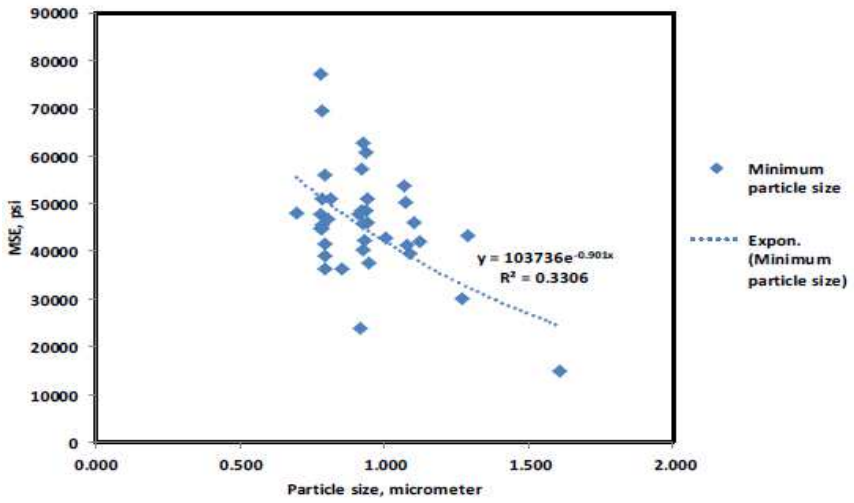

Figure 2.24 – The relationship between minimum particle size and mechanical specific energy [5]

It was also observed that maximum particle size has no apparent correlation with MSE. This fact does not necessarily contradict the hypothesis about regrinding. The regrinding process may affect only smaller particles and the maximum particle size does not have to change [5].

CHAPTER 3

LABORATORY EXPERIMENTS AND DRILL CUTTINGS ANALYSIS

Based on the literature review and previous investigations, bottom hole pressure (BHP), flowrate and weight on bit (WOB) are among the most important factors that affect drilling performance. An extensive set of laboratory drilling experiments was conducted to evaluate the effect of these factors on drilling performance and size of generated cuttings. This chapter describes a laboratory set-up, test procedure and results. The relationship between cuttings size and drilling parameters are discussed in great detail.

3.1 Experimental laboratory set-up

An existing laboratory drilling rig, which includes a rotary head, loading system, high pressure drilling fluid circulation system and data acquisition system was used to perform

the drilling tests. A collection system for the drill cuttings was added to the system. Figure 3.1 shows the schematic of the experimental set-up.

The rotary system is powered by an electric motor, which is mounted on a carriage that travels vertically along the frame pillar on rack and pinion gear. A loading system applies downward force on the bit and consists of the motor, drilling string and suspended weight. The suspended weight allows to increase a weight on bit up to approximately 2500 N.

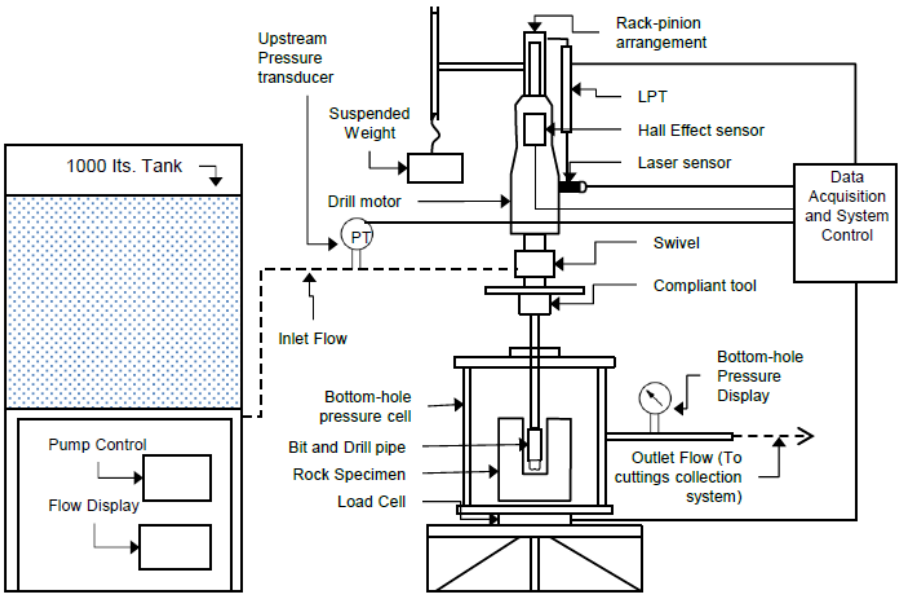

Figure 3.1 – Laboratory drilling set-up [35]

The drilling fluid circulation system mainly consists of high pressure triplex pump, which circulates water through a swivel, drilling string, drilling bit nozzles and bottom hole pressure cell. The pump features adjustable flowrate up to 150 l/min. The bottom hole pressure cell that holds rock specimen, is located at the bottom of setup. It is designed to operate under pressure up to 2500 kPa [36], which can be adjusted by needle valve installed

on the fluid outlet line. The drill string that transfers torque from the motor to the bit, is inserted through the top plate of the pressure cell. A brass bushing and lip seal is installed in the top plate to centralize the drilling string and minimize leaks during the experiments. The bottom hole pressure cell set-up shown in Figure 3.2. Another part of the drilling set-up is a compliant tool with a polished steel disk mounted on it, which allows to measure rotary speed. The disk also allows to measure a relative displacement between tool's parts if it is set to a compliant mode.

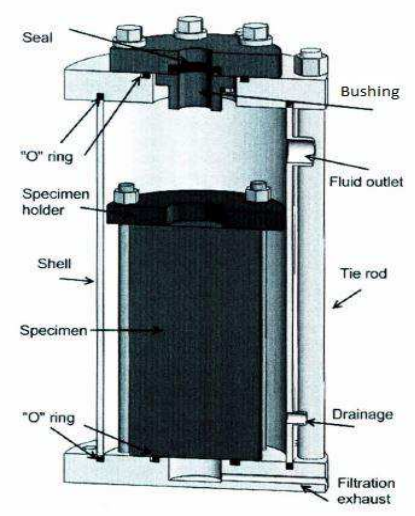

Figure 3.2 – Bottom hole pressure cell [36]

Finally, a cuttings collection system allows a collection of the cuttings samples with particles size over 67 μm. It is a very simple set-up which consists of 20-gallon container with an orifice in the bottom and a sieve underneath it. Water with crushed rock flows from the bottom hole cell to the collection container and then slowly flows through the sieve. Cuttings retained in the sieve are later analyzed in the lab. The cuttings collection system is schematically shown on Figure 3.3.

3.1.1 Sensors and Data Acquisition system

A set of sensors is installed on the drilling set-up to record various drilling parameters. One of them, is a linear position transducer (LPT) that measures the displacement of the drilling bit. It is installed on the carriage of the motor and free end of its cable is attached to the frame. A relative displacement of the earlier mentioned compliant tool (between the top and bottom part of the tool) is measured by a laser sensor mounted on the motor head.

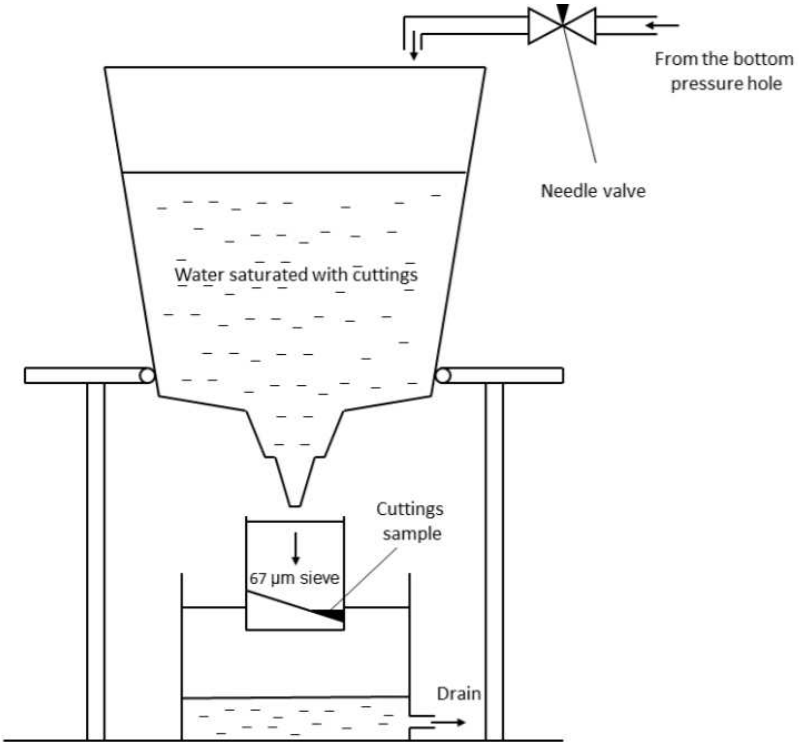

Figure 3.3– Schematics of cuttings collection system

The laser beam travels vertically down from sensor and reflects from the polished steel plate mounted on top of the compliant tool. The time of the beam travel is recorded and is later used to calculate relative displacement of the tool. Data from this sensor is also used

to calculate a rotary speed of the bit. For this purpose, six grooves were cut on the top plate (Figure 3.4). Every time the laser beam hits a groove, a spike on the displacement versus time graph appears. Six spikes represent one full rotation of the bit. A Hall Effect sensor is installed next to the electric motor to measure current, which is later used to calculate torque based on method presented in [35].

All the sensors mentioned above are connected to a single data acquisition (DAQ) system and all the parameters are recorded with 1000 Hz sampling frequency. A dial pressure gauge, installed on the side of the cell, is used to monitor bottom hole pressure. More details on DAQ system can be found in [36].

Figure 3.4 – Top plate with grooves mounted on the compliant tool

3.1.2 Drill bit characteristics

Due to high popularity of PDC bits in the drilling industry, a two cutter PDC bit with diameter of 35 mm is used for the drilling experiments. This bit is a perfect fit for a laboratory drilling simulator and is suitable for drilling 4 inch rock specimens. The cutters are brazed to a steel body under 25° side-rake and 25° back-rake angle. The cutters have a 0.15 mm long chamfer with 70° back-rake angle. The PDC bit is mounted on a steel base which used as a coupling to attach the bit to the drilling string. Two nozzles were drilled through the base to introduce drilling fluid to the rock surface [35]. The bit and the steel base with nozzle configuration are shown on Figures 3.5 and 3.6 respectively.

Figure 3.5 – Two cutter PDC bit

3.2 Rock specimen preparation

Drilling tests were performed on the synthetic rock specimens. They were prepared by pouring concrete of specific recipe into 4-inch diameter plastic molds. The concrete slurry consists of aggregate, cement, water and superplasticizer.

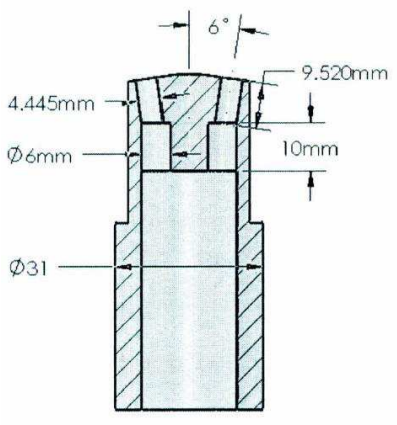

Figure 3.6 – Steel base with nozzles configuration

The aggregate sample was sieved and a particle size distribution diagram (Figure 3.7) plotted using obtained data (Table 3.1).

Table 3.1 – Particle size distribution of aggregate material

Size (μm)	Weight (%)	Cumulative weight (%)
+4870	0.91	0.91
-4870+2360	22.91	23.83
-2360+850	32.80	56.63
-850+595	9.91	66.54
-595+425	8.67	75.21
-425+300	9.72	84.94
-300+150	11.10	96.04
-150+75	2.91	98.95
-75	1.05	100.00
∑	100.00	
Coarseness index (CI)		603.04

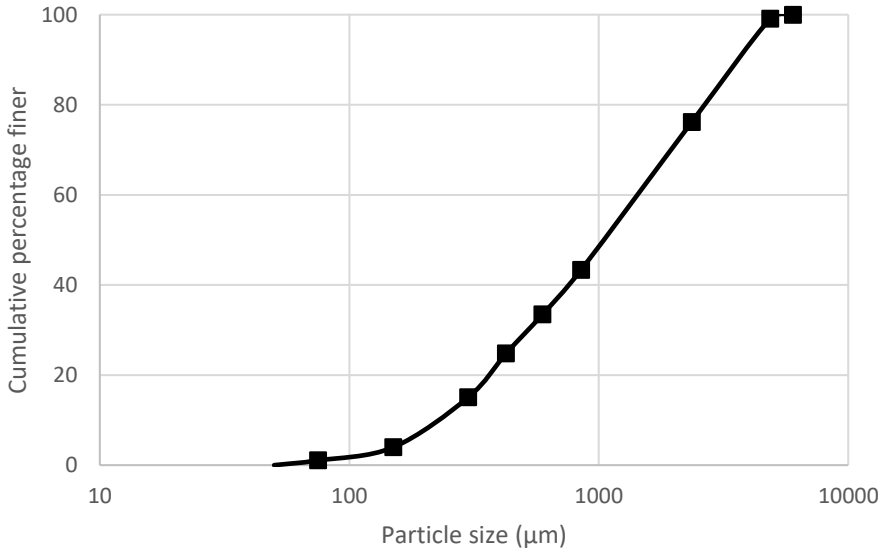

Figure 3.7 – Particle size distribution for aggregate sample

Procedure described in [37] was followed during concrete mixing and specimen preparation. The design quantities of the materials mentioned above are shown in Table 3.2.

Table 3.2 – Design quantities for synthetic rock material [37]

Materials	Design quantities	Used quantities (one batch)
A:C:W	3:1:0.45	3:1:0.45
Aggregate	30 kg	150 kg
Cement	10 kg	50 kg
Water	4.5 kg (4500 ml)	22.5 kg
Superplasticizer (Daracem 19)	60 ml	300 ml

Thorough following of the procedure and design quantities ensures that all prepared samples will have the same properties. Properties of the synthetic rock are shown in Table 3.3.

Table 3.3 – Properties of the synthetic rock [37]

Properties	Values
Unconfined compressive strength	49 to 55 MPa
Density	2313 kg/m^3
Mohr friction angle	42˚

This specific recipe was used due to multiple reasons:

- simulates medium strength natural rock, which is a very common type of formation;
- ensures depth of cut higher than the cutter's chamfer size, what is very important to maintain proper cuttings mechanism. Use of specimens with higher UCS, can lead to drilling with the depth of cut lower than the chamfer length under low WOB;
- provides proper aggregate bonding, what ensures that aggregate material in being cut or grinded by the bit, and not just pulled out from cement matrix.

3.3 Design of experimental matrix

Based on the literature review and previous investigations, bottom hole pressure (BHP), flowrate and weight on bit (WOB) are considered as the most important factors that affect drilling performance. All these parameters were varied in range that is allowed by experimental equipment for further evaluation of drilling performance and investigation of effect of these parameters on cuttings size.

Previous investigation [36] concluded that the optimal flowrate for a current experimental set-up varies for different BHPs, but is always in range between 90 and 115 l/min. For this

reason, four different flowrate values (90.7, 103.1, 109.3, 115.5 l/min) were picked for following testing. Also, three different values of BHP were tested during the experiments: 100, 200 and 300 psi (690 kPa, 1380 kPa and 2070 kPa), which simulate drilling at depth of 70, 140 and 210 meters respectively (drilling with water).

Finally, seven values of the last variable, WOB, were tested during the experiments: 153.2, 170.0, 186.8, 203.6, 220.4, 237.2, 254.0 kg (1502, 1677, 1832, 1997, 2162, 2327, 2492 N). A maximum value of the WOB is limited by capacity of the drilling simulator.

3.4 Test procedure

All the steps followed in the test procedure ensures the maximum quality of the drilling response and obtained data. After the specimen is placed inside of the pressure cell, a top plate of the cell is put in place and the pressure cell is checked for leaks. Then the desired flowrate value is adjusted using the knob on the pump and BHP value is adjusted by needle valve. A trial drilling test is performed, and needle valve is adjusted again if needed. Such trial tests are required when BHP need to be changed. Every rock specimen is predrilled for 15 mm to make sure that the PDC cutters are fully in contact with the rock. This ensures stable drilling parameters during the test. Before the start of the test, the drilling bit is kept off-bottom, and the pump and drill head are turned on. After final check of the flowrate and BHP, the bit is released. During each test bit drills 40 mm deep hole. After the drill head is turned off, the pump is kept running to flush all the cuttings to the collection system. Later all the cuttings are collected into a plastic bag. After each test, the collection system is cleaned to prevent mixing of cuttings from different tests.

3.5 Drill cuttings preparation and analysis

As it was mentioned before, after each test cuttings sample was collected in a tagged plastic bag. Later all cutting samples were moved to small steel containers and dried in the oven. It was observed that high oven temperature makes particle stick together and form relatively big lumps which can later affect sieving process. For this reason, all the samples were kept in the oven (Figure 3.8) under the temperature no higher than 50˚C and at least for 12 hours. Low temperature seems to prevent cuttings from sticking together. Dry samples were weighted before the analysis.

Sieving analysis was performed to obtain particle size distribution for each sample. This method of analysis was chosen, because of its simplicity and low cost. Standard sieving machine and sieves were used for analysis (Figure 3.9). Table 3.4 shows the mesh sizes of the sieves picked for analysis. Each sample was sieved on the machine for 1 minute. Longer duration of the sieving did not show any changes in weight of obtained fractions.

Figure 3.8 – Laboratory oven used to dry cuttings

Figure 3.9 – Sieving machine

Previous investigations [6], [40] proved that Coarseness Index (CI) can be used as an accurate representation of the particles size for the whole sample. Also, CI is much more convenient during the analysis than any type of graphical PSD representation. CI in a non-dimensional number, calculated by adding cumulative weight percentage of particles retained in each sieve. CI will vary depending on the mesh sizes of selected sieves, but will be suitable for comparison if the same set of sieves is used throughout the process. The meaning of coarseness index and its calculation are shown in detail in Chapter 2.

Table 3.4 – Sieves used for sieving analysis

Sieve No.	8	20	30	40	50	100	200
Mesh size (μm)	2360	850	595	420	300	150	75

3.6 Test results

The overall efficiency of the drilling process is complex and can be affected by numerous factors which include operating parameters, bit type and design, properties of the rock, drilling fluid properties, capacity of the drill, etc. In this section the effect of operating parameters on drilling performance and drill cuttings size is investigated.

3.6.1 Rate of penetration and weight on bit

As it was mentioned before, WOB, BHP and flowrate have great impact on drilling process and drilling efficiency. The effect of WOB on performance is shown on Figure 3.10. The trend shows that increasing WOB produces increase in ROP. The same trend was observed for all tested flowrates and bottom hole pressures. No founder point was observed, and it is possible to assume that ROP will continue to increase with higher WOB values. Testing of higher WOB is required to detect a founder point for this specific rock and drilling set-up. Unfortunately, it was impossible due to the limitations of the drilling simulator.

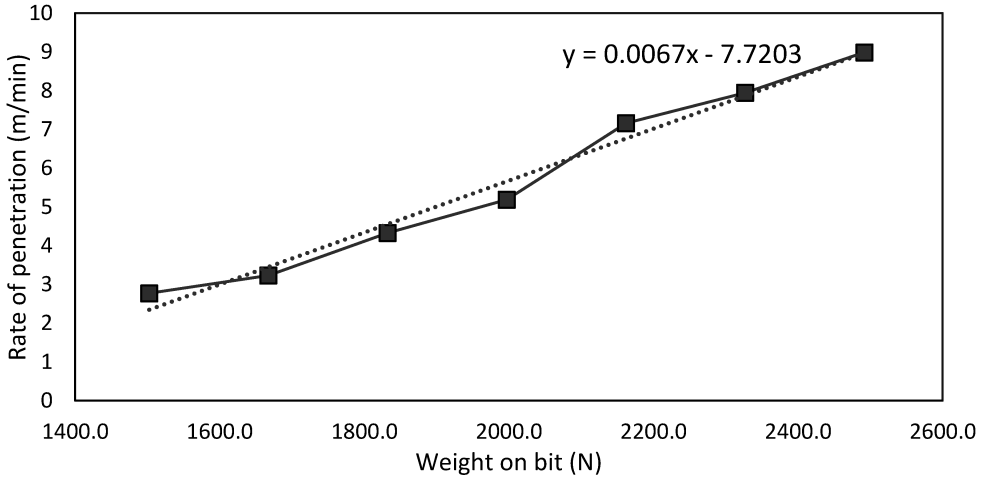

Figure 3.10 – Relationship between ROP and WOB

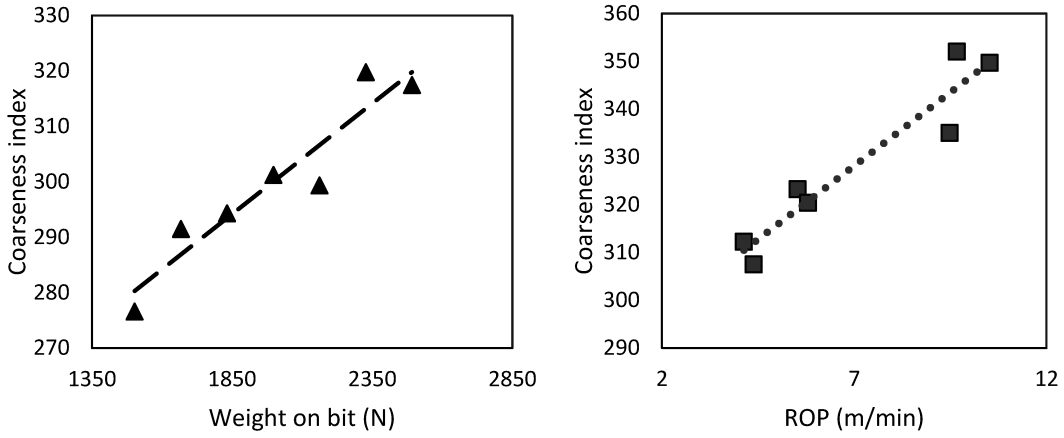

(a) **(b)**

Figure 3.11 – The relationship between CI and (a) WOB and (b) ROP

Coarseness index (CI) shows good relationships with ROP and WOB. CI tends to increase with increase of WOB and ROP (Figure 3.11). With increase of WOB drilling cuttings size increases, which indicates higher efficiency of the drilling process. This can be possibly explained by the fact, that under high WOB, cutters constantly and more aggressively "bite into" fresh rock generating coarser cuttings.

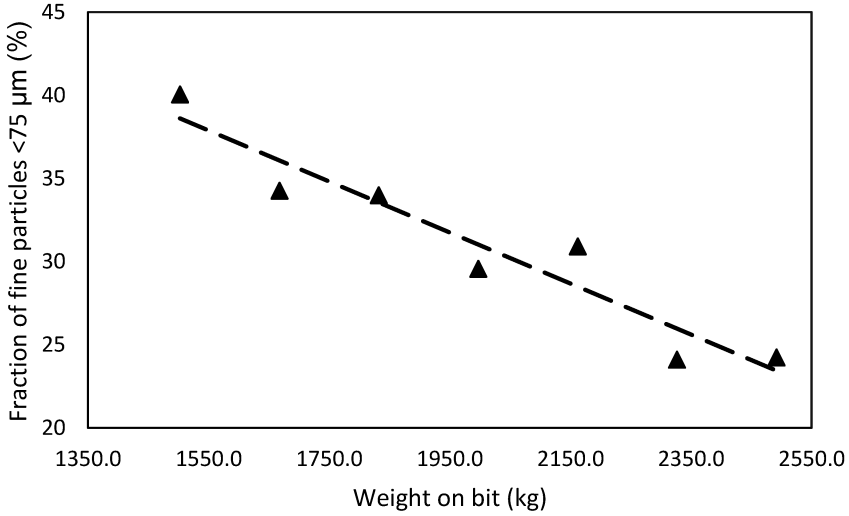

Figure 3.12 – The graph of finer particles fraction (<75 µm) vs. WOB

Figure 3.12 shows that the amount on fine particles decreases with increase of WOB. This indicates that the regrinding process is minimized and supports the statement that the rock cutting mechanism is more efficient under high WOB.

For more detailed analysis, mechanical specific energy (MSE), was calculated to evaluate drilling efficiency. The following formulas were used:

$$MSE = \frac{WOB}{A_B} + \frac{120\,\pi \cdot TOB \cdot N}{A_B \cdot ROP}, \tag{3.1}$$

where TOB – torque on bit, calculated used methodic described in [33];

N – rotary speed of the bit;

A_b – area of the cross-section of the bit.

Figure 3.13 shows that MSE decreases with increase in WOB and ROP. This further confirms the above-mentioned statement about drilling efficiency.

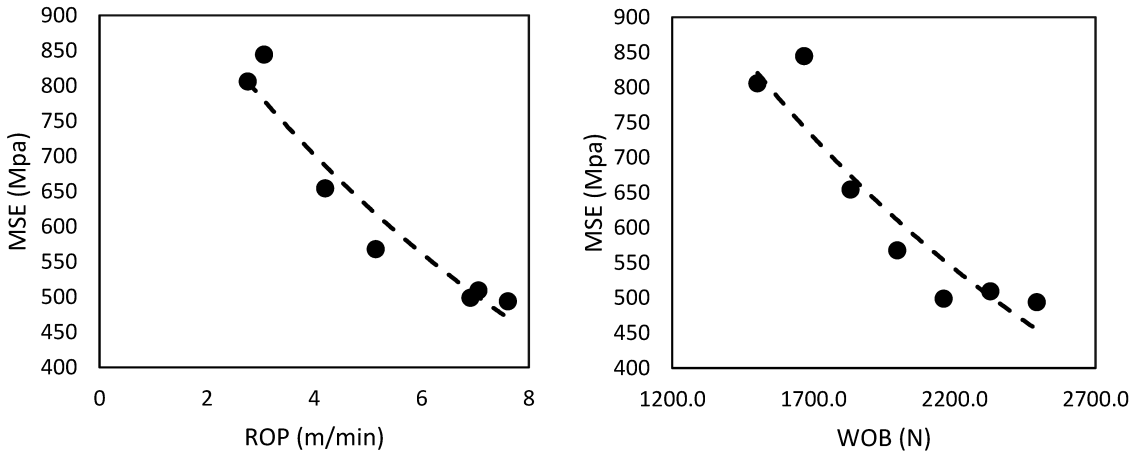

(a) **(b)**

Figure 3.13 – (a) MSE versus ROP; (b) MSE versus WOB

3.6.2 Flowrate. Bit hydraulics

As it was mentioned before, previous research [36] indicated that optimal flowrate is somewhere in range between 90 and 115 l/min. Four different flowrates in this range were tested. For each of these values, bit hydraulic horsepower per square inch (HSI) was calculated using the following formulas:

$$HSI = \frac{\Delta p_b \cdot q}{1714 \cdot A_b}, HP/in^2 \tag{3.2}$$

$$\Delta p_b = \frac{8.311 \cdot 10^{-5} \cdot \rho \cdot q^2}{C_d^2 \cdot A_t^2}, psi \tag{3.3}$$

where q – flowrate, gpm;

ρ – density of the drilling fluid, ppg;

C_d – nozzle discharge coefficient, for this bit C_d=0.7 [36];

A_t – total flow area of the nozzles, in^2.

Tested flowrates and corresponding HSI values are shown in Table 3.5.

Table 3.5 – Flowrate and corresponding HSI

Flowrate (l/min)	Flowrate (gpm)	Hydraulic horsepower (hp/in^2)
90.7	24	3.56
103.1	27.2	5.23
109.3	28.9	6.24
115.5	30.5	7.36

Figure 3.14 shows graph of ROP versus HSI. ROP tend to decrease slightly with increase of flowrate. However, very small change in ROP was normally detected for different flowrates and in most cases ROP versus HSI trend appeared to be a nearly horizontal line. This lead to a conclusion that the change of flowrate in this range has very little to no effect on ROP. Small reduction is ROP while drilling under high flowrate might be explained by higher pump-off force that counteracts the WOB.

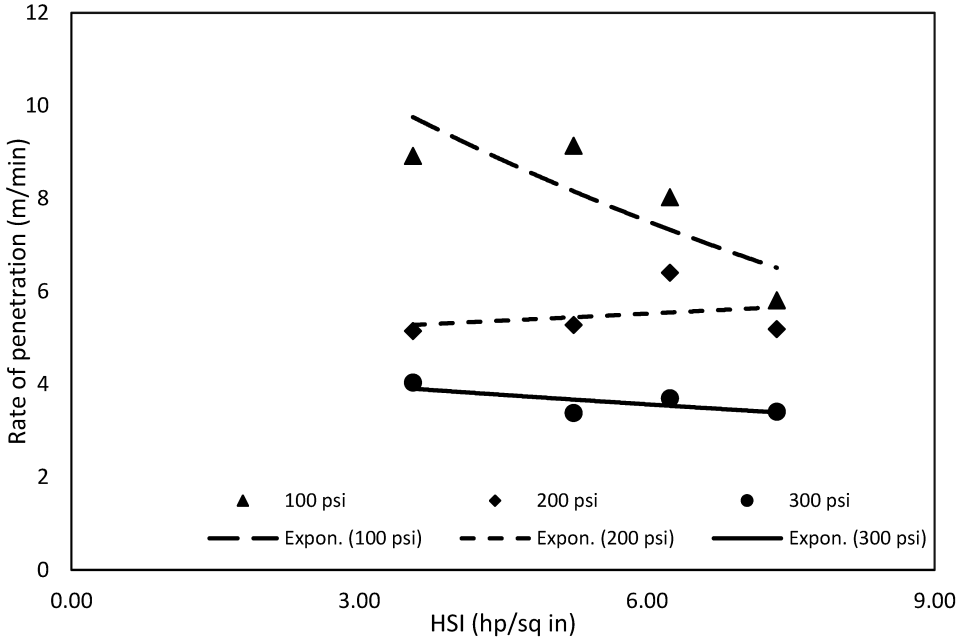

Figure 3.14 – Graph of ROP versus HSI

Figure 3.15 shows the relationship between MSE and HSI. It can be observed that MSE tend to increase with increase of HSI and this tendency can be noticed throughout all range of tested WOB and BHP. Also, Figure 3.16 shows that MSE versus ROP trendline shifts towards the top with increase of flowrate.

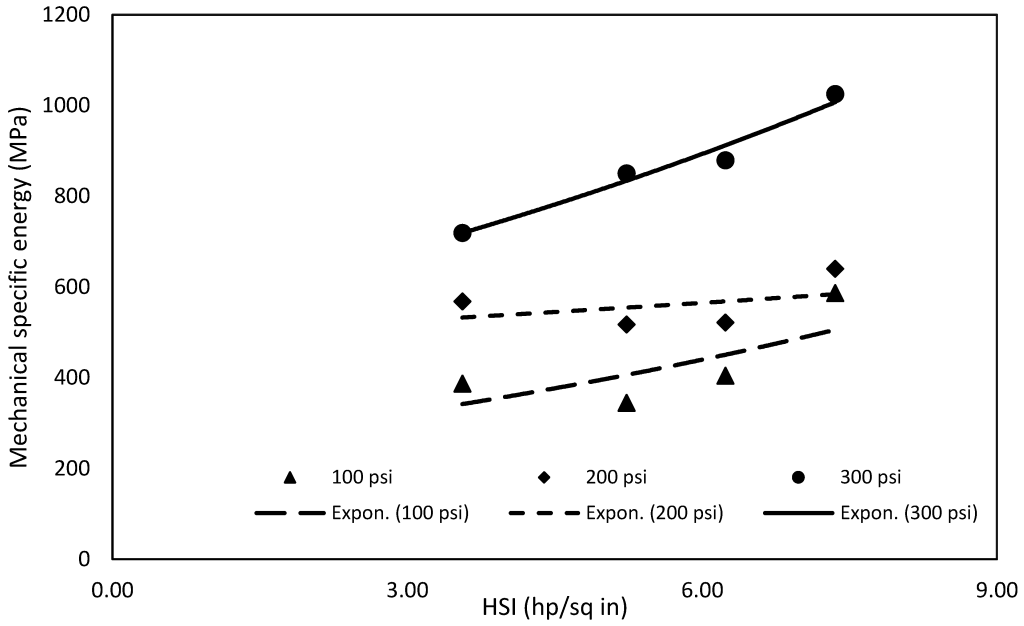

Figure 3.15 – The relationship between MSE and HSI

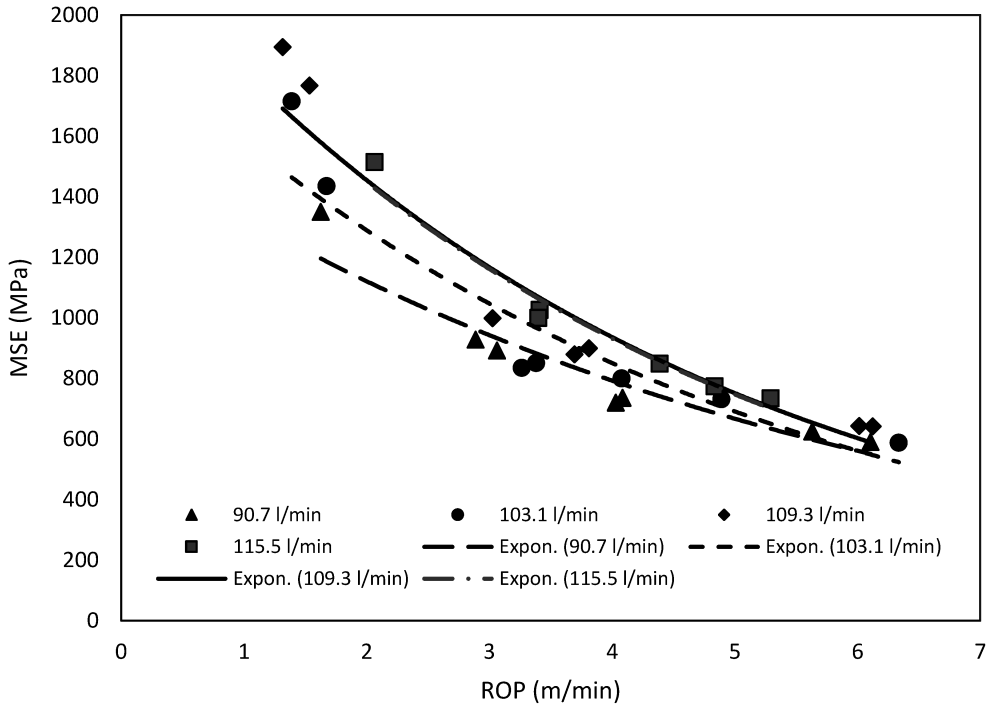

Figure 3.16 – The relationship between MSE and ROP

These observations lead us to a conclusion that flowrate of 90.7 l/min, which corresponds to 3.56 value of HSI, is the most efficient in terms of MSE. No significant change in ROP was noticed.

For the highest tested BHP of 300 psi, MSE vs. HSI curve is usually much steeper comparing to lower pressure values (Figure 3.15). It may be related to strong coupling effect of jet off force and BHP force, while drilling under high pressure conditions. In other words, under higher BHP, the effect of jet off force can become more significant for higher HSI values. These results are going along with conclusions made in [36], where it was asserted that the applied surface pressure from the jet force may play the role of hold-down pressure for the cuttings which are being generated. The application of a very high surface pressure may constrain the cleaning action. Even though high jet force can apply high drag removal force, the resultant pressure keeps generated cuttings in zone of penetration. This phenomenon is also known as a chip hold-down effect [36].

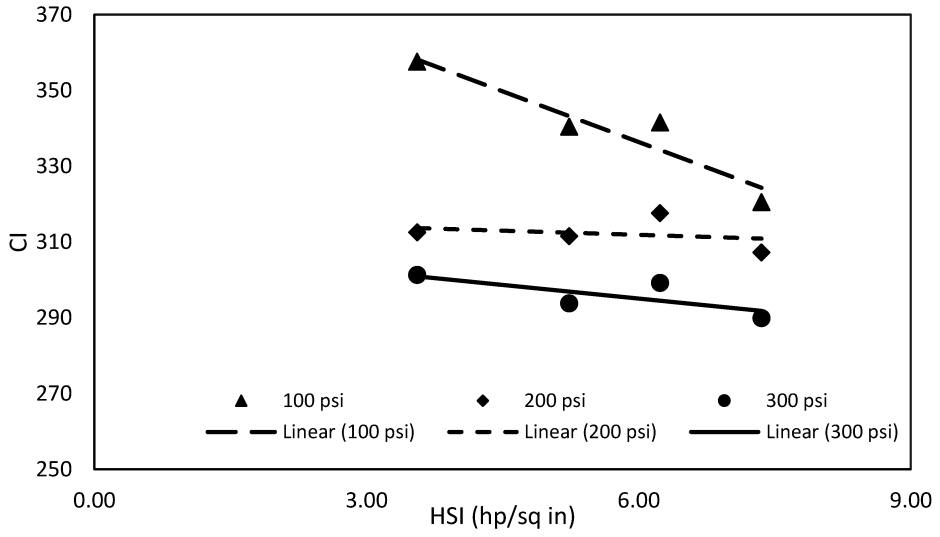

Figure 3.17 – The relationship between CI and HSI

Cuttings analysis also supports the above-mentioned hypothesis. It can be clearly observed that with increase of flowrate, e.g. higher HSI values, cuttings size decreases (Figure 3.17). It is also noticeable that for BHP of 300 psi, CI vs. HSI linear approximation slope is much higher, than for 200 or 100 psi. This observation proves that under high BHP, high flowrate can cause chip hold-down effect. This effect can lead to a lot of regrinding, which according to the literature mainly affects fine particles. Figure 3.18 shows the graph of fine particles fraction (<75 μm) versus HSI.

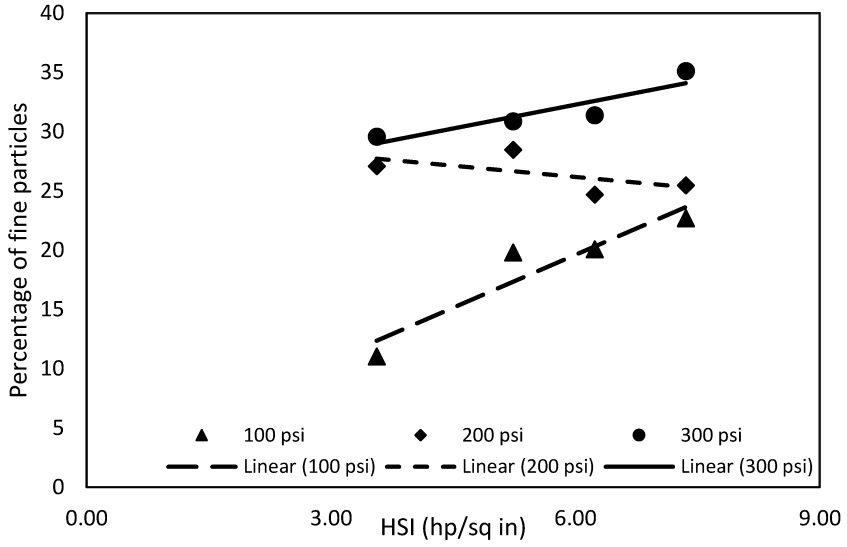

Figure 3.18 – The graph of percentage of fine particle (<75 μm) versus HSI

Even though the fraction of small particles almost always increases with increase of HSI, sometimes it shows the reverse trend (Figure 3.18, 200 psi). It does not necessarily contradict an argument regarding regrinding. Fine cuttings tend to form lumps or stick to coarser cuttings during drying. Part of fine cuttings can also be lost in the circulation system, thus affecting PSD of the sample.

3.6.3 Torque on bit

Torque on bit is defined as a reactive moment caused by friction forces between a bit and a rock. Due to small length and high torsional stiffness of the drill string, torque on bit is equal to the torque created by the motor. The motor torque is related to consumed current and have been calculated using the methodic described in [35].

The relationship between WOB, ROP and torque shown in Figure 3.19. High WOB drives drilling bit into the rock, causing higher friction forces and higher reactive moment. It was also noticed, that rotary speed decreases with increase in torque due to the nature of the electric motor. Nevertheless, rotary speed fluctuates less than 6% over range of WOB and does not affect overall outcome of the experiments.

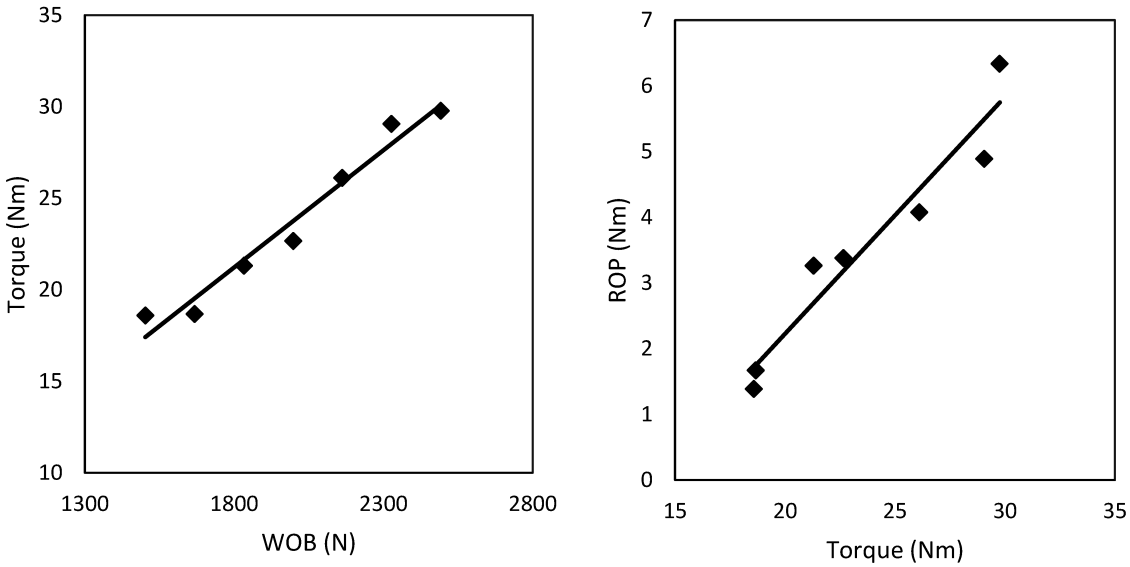

Figure 3.19 – The relationship between (a) WOB and torque, (b) ROP and torque

Increasing WOB produces an increase in torque, and consequently in ROP. Moreover, it is possible to assume that higher torque values can be associated with coarser cuttings. This is confirmed by graph below showing CI versus torque (Figure 3.20).

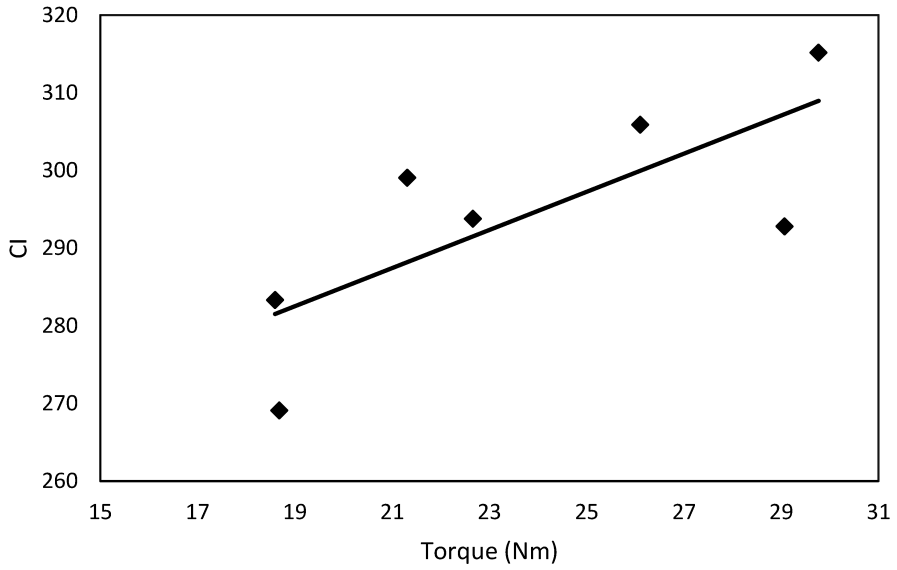

Figure 3.20 – The relationship between CI and torque on bit

3.6.4 Bottom hole pressure

It is well-known that high BHP pressure has negative impact on drilling efficiency. In order to explain the effect of BHP, rock failure mechanism caused by PDC cutter can be compared to standard compressive strength test. Schematic cutting action (a) and core specimen (b) with depicted principal stresses σ_1 and σ_3 are shown in Figure 3.21. When confining stress σ_3 is equal zero, principal stress σ_1 equals to unconfined compressive strength (UCS). This also represents conditions for atmospheric drilling (BHP=0). When $\sigma_3>0$, principal stress σ_1 equals to confined compressive strength (CCS). CCS value is

always bigger than UCS and it increases with increase in σ_3. This scenario represents pressurized drilling. Higher BHP causes higher stress σ_3.

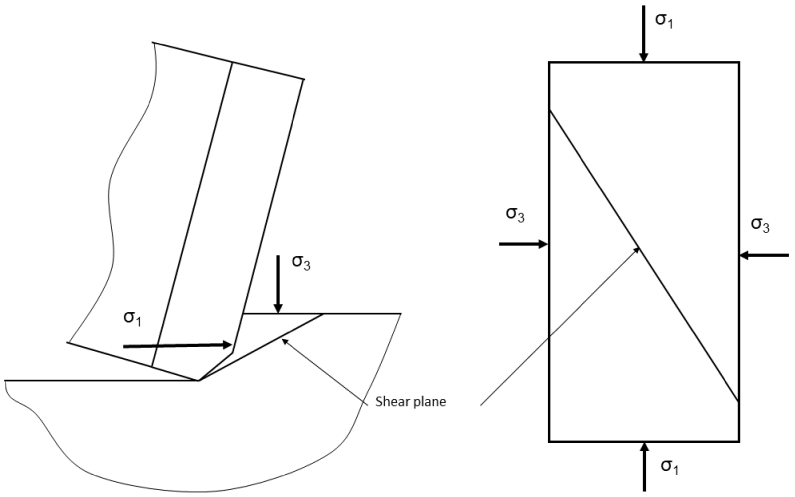

(a) **(b)**

Figure 3.21 – Principal stresses acting on the specimen during (a) cutting action and (b) compressive test

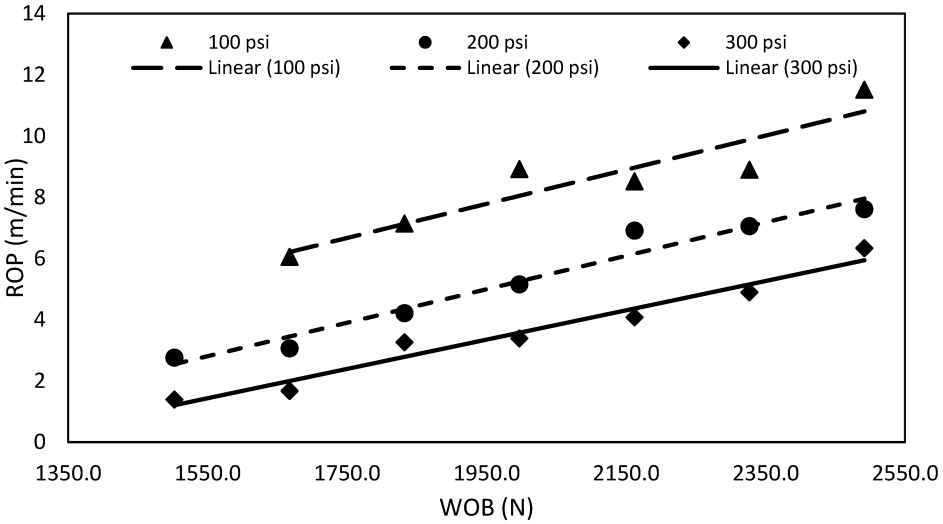

Figure 3.22 – ROP versus WOB for different BHP

High BHP “strengthening” effect causes increase in MSE, energy required to brake the rock. This will result in reduction of ROP and drilling efficiency. The effect of BHP on ROP can be seen in Figure 3.22. It is clear that ROP reduces with increase in BHP, as all ROP vs. WOB trendlines shift towards the bottom of the chart with increase in BHP. Also, the graphs of MSE versus BHP and ROP versus BHP, gives a great idea on the effect of BHP on drilling efficiency (Figure 3.23). Just an increase of 200 psi, which represents 140 meters in well depth, causes 70% increase in MSE and almost 50% drop in ROP.

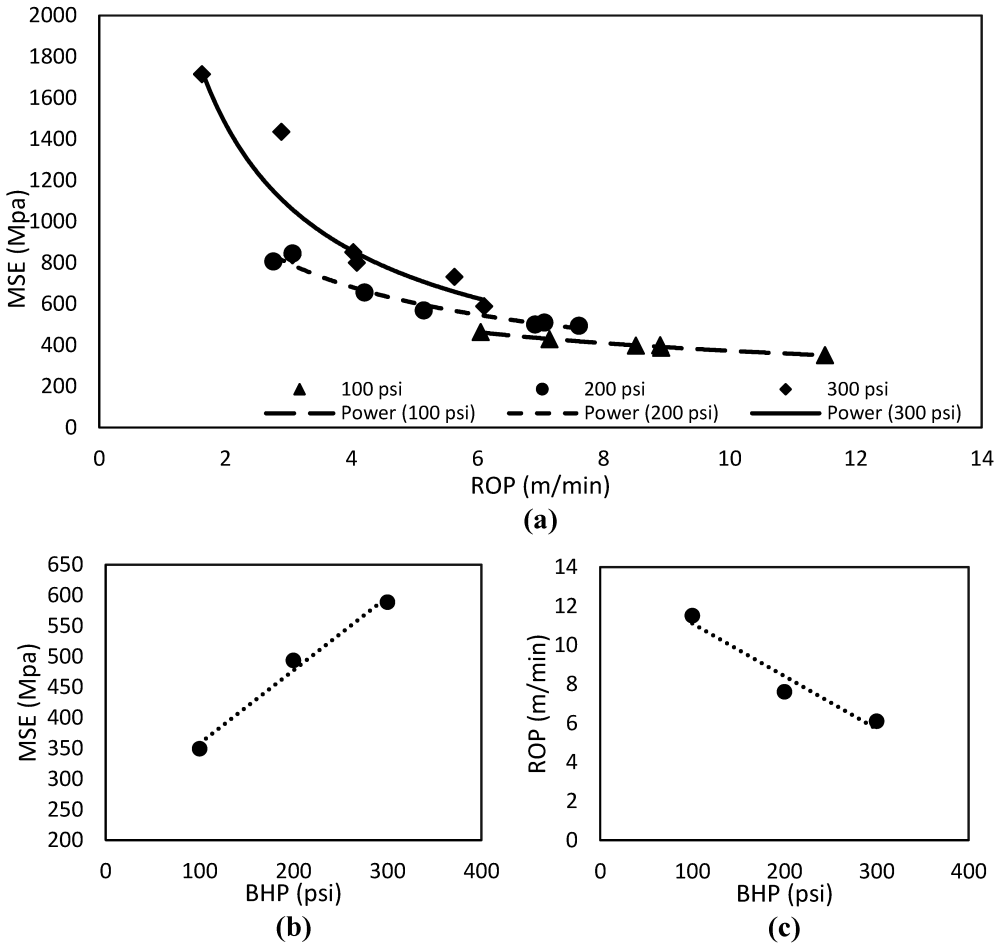

Figure 3.23 – The relationship between (a) MSE and ROP, (b) MSE and BHP, (c) ROP and BHP

Figure 3.24 shows the decrease in cuttings size with increase in BHP and confirms the decrease in efficiency during drilling under high pressure.

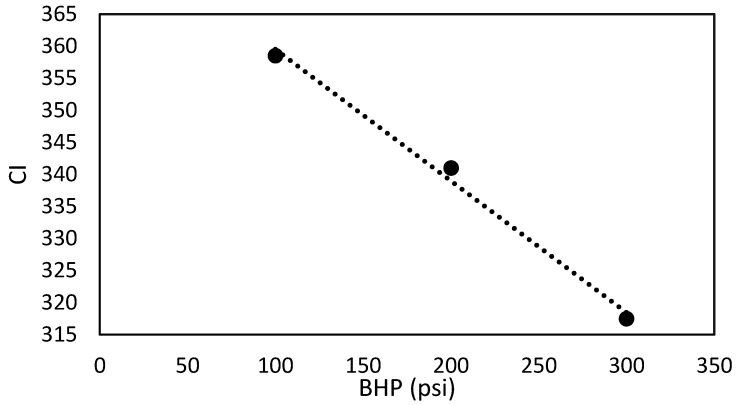

Figure 3.24 – CI versus BHP

It was reported that high BHP can obstruct bottom hole cleaning and sometimes even cause cuttings to lump and stick to the cutter [36], [38]. Figure 3.25 shows an increase in percentage of finer particles for higher BHP. It can be related to the crushing and regrinding of the particles that were confined in the hole due to high BHP. This observation supports the abovementioned statement, as regrinding mainly affect fine particles [38].

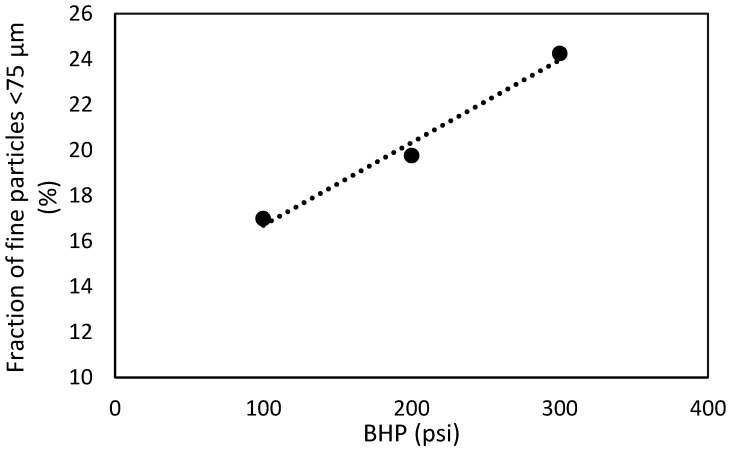

Figure 3.25 – The graph of finer particles fraction (<75 µm) vs. BHP

The results presented above show that the cuttings size has a good correlation with major drilling parameters. The established relationships are consistent throughout the range of tested parameters. These relationships allow to perform the reverse analysis and use cuttings to predict ROP and evaluate drilling efficiency. However, such analysis can be performed only on cuttings generated under the same conditions (bit, drilling mud, rock type and strength, etc.). To predict ROP for different type of rock, mud or bit, set of experiments similar to one described in this chapter, has to be performed. Also, it important to keep in mind that many factors can distort particle size distribution and affect the results. Cuttings samples can be incomplete, as some of them may be lost in the load cell or during the sieving. This also may lead to dilution of some samples. Particles can stick together during drying, thus also affecting PSD.

CHAPTER 4

FIELD TRIALS AND CUTTINGS ANALYSIS

Cuttings were collected during field trials to investigate the effect of drilling operational parameters and the formation characteristics on cuttings size. This allows to evaluate drilling performance based on cuttings size analysis and also potentially detect changes in cutting mechanism with changes in drilling parameters for certain type of formations. This chapter includes description of the equipment and site geology. It also includes the analysis procedure, its limitations and the results discussion.

4.1 Field trials drilling site and equipment

Several potential field sites for the trials were identified and evaluated on the Avalon Peninsula of Newfoundland, Canada. The site selected for the present study was a quarry site owned and operated by Greenslades Construction in Conception Bay South. The

location in quarry B (Figure 4.1) was picked, because of easy accesses and relatively large flat area, convenient for the trials.

Figure 4.1 – Field trial location [39]

During the trials in September 2014, drilling was performed by Brewster Well Drilling. An Ingersoll Rand T3W drill rig and pump truck were used (Figure 4.2). The parameters of the rig are mentioned in Table 4.1.

Figure 4.2 – Drilling rig and a pump truck

Table 4.1 – Ingersoll Rand T3W drilling rig parameters [39]

Rig parameter	Value
Thrust output	16400 lbs
Available torque	9660 lbs·ft
Stand length	20 ft

The rig was equipped with four drill bits that were used alternately during the drilling; however, this the investigation focused only on the results obtained during the drilling with PDC and RC bits. TSP bit data was not analyzed because of insufficient number of collected samples (less than 2 ft were drilled). Also, percussive bit is out of interest, as the research is focused only on rotary drilling. Several BHA configurations were tested under different values of weight on bit. Multiple sections were drilled with field scale compliant tool included in the BHA. Other parameters like flowrate of the drilling fluid system and rotary speed of the drill string fluctuated because of the nature of the drilling rig. The following parameters were recorded for each interval: drilling depth, net drilling time, feed pressure, rotary speed, pump flowrate. The data was obtained either through the rig's control panel or through direct measurement. Depth and time were later used to calculate ROP and feed pressure was used to calculate WOB. To compensate for the fluctuations of rotary speed, a normalized ROP value was calculated as follows:

$$ROP_{100} = ROP_n \frac{100}{n}, \tag{4.1}$$

where ROP_n– is rate of penetration corresponding to rotary speed n.

This means that the normalized ROP's values correspond to a rotary speed of 100 rpm.

4.2 Site geology

Preliminary mapping studies indicated that the rocks drilled would be grey and red shale potentially reaching granite basement. Multiple samples of grey shale, red shale and granite were collected from exposures on the surface of the field site for further rock strength evaluation by Point Load Index test. The results (Table 4.2) show that red and grey shales had approximately the same compressive strength value.

Table 4.2 – Unconfined compressive strength of the rocks [40]

Rock type	Value (MPa)
Grey shale	61
Red shale	56

However, grey shale (Figure 4.3 a) is much more fissile than red shale (Figure 4.3 b), because of its highly laminate structure. Granite compressive strength is, as expected, considerably higher.

During the trials, the formations and their boundaries were preliminary identified by color of the return water line (i.e. gray, red, and clear). Later, visual analysis on cuttings was performed to identify the formation type and construct geological cross section (Figure 4.4). It was assumed that formations are continuous in horizontal plane (between the wells). Question marks indicate the boundaries between formations that were not possible to define, because of lack of data.

(a) **(b)**

Figure 4.3 – Grey (a) and (b) red shale

Analysis showed that the drilled formations were prevalently grey and red shale. The upper 60 m consist of pure grey shale. Deeper formations are mainly consecutively changing, thin layers of grey and red shale, or red shale interbedded in a grey shale and vice versa. The last 15 m of Well 1 and 2 are mainly grey shale with a high content of quartz. The bottom sections of Wells 1 and 2 appeared to be highly heterogeneous due to the different amount of quartz in each sample. For this reason, no further cuttings analysis, or any drillability evaluation was performed for this section. Therefore, the investigation was focused mostly on the depth interval of 0-105 m for all three wells. Based on cuttings analysis, this interval consists from homogenous grey and red shale. The section from 72-90 m deep also has some quartz veins; however, the percentage of quartz is quite small, and it had a negligible effect on the drilling performance.

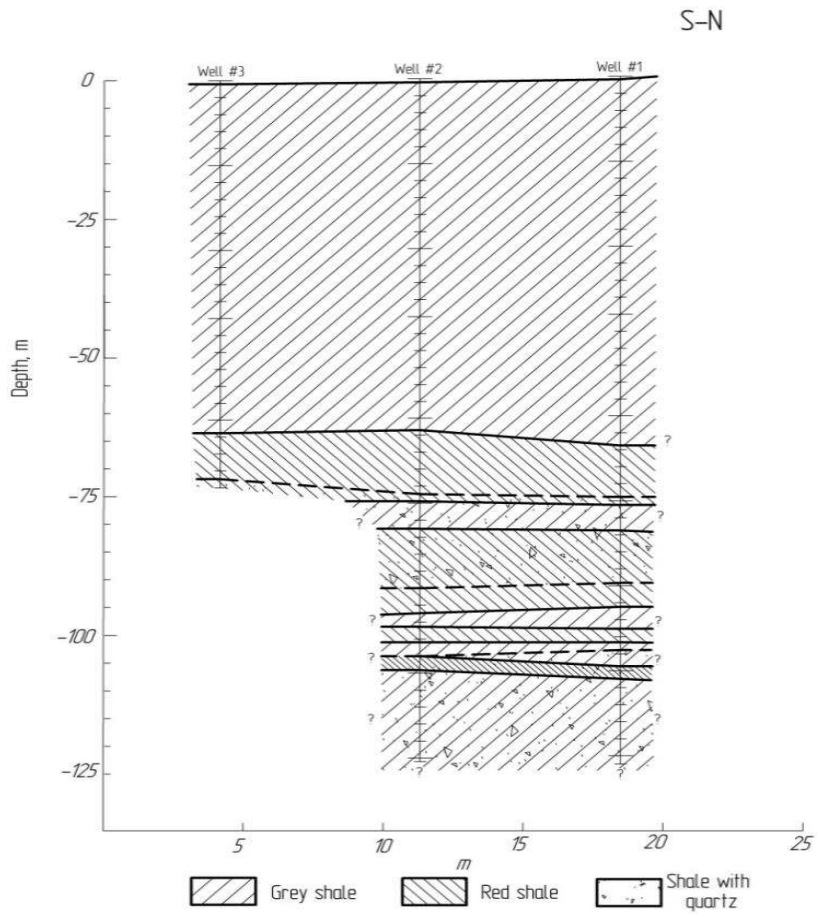

Figure 4.4 – Geological cross section of the site [40]

4.3 Cuttings collection and data analysis

Cuttings were collected during field trials for analysis and investigation of the effect of the drilling operational parameters. Samples were collected from the return mud (water) flow. After cuttings were collected in a bucket, they were given some time to settle down. Then, water was drained, and cuttings samples were placed in plastic bags. Each sample collected was tagged with the sample number, well number, date and bit type used for further relation with the measured parameters.

The procedure described in Chapter 2, was followed for sieving analysis. A subset of 100 grams from each sample was taken to perform sieving. According to ASTM standard, following mesh sizes were used for analysis:

- 2300 μm;
- 1180 μm;
- 850 μm;
- 425 μm;
- 300 μm;
- 100 μm.

For each cuttings sample, CI and mean particle size were calculated. Mean particle size was obtained from Rosin-Rambler diagram using Matlab code [22]. Later these parameters were correlated with WOB and ROP, based on analysis performed on multiple depth intervals. Also, it was found that bar PSD diagram (Figure 4.5) is a very convenient tool for comparison of cuttings samples. It allows a comparison of different fraction sizes for multiple samples. Each bar represents one sample and different color sections represent the percentage of cuttings retained in certain sieve size. For instance, green sections represent cutting bigger than 100 μm and smaller than 300 μm, red sections represent particles bigger than 300 μm and smaller than 425 μm, etc.

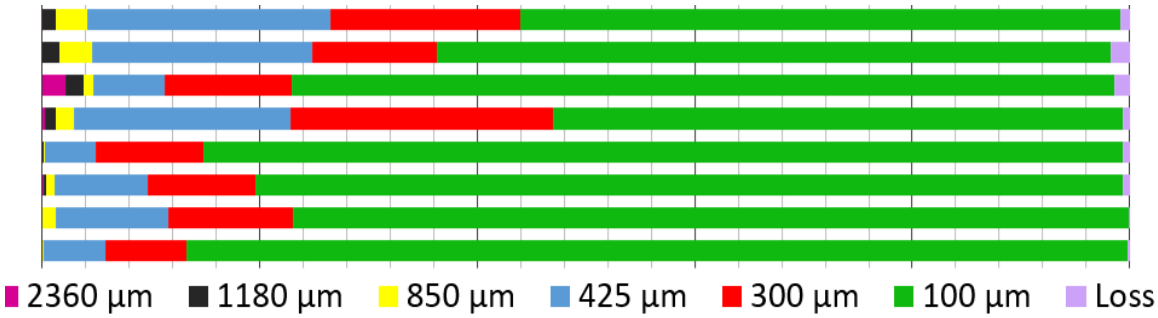

Figure 4.5 – Bar PSD diagram

4.3.1 Cuttings analysis in grey shale

The first analyzed section, represents 39.3-63.6 m interval of Well #1. Drilling was performed in the same lithology, with roller cone bit and no compliant tool was included in BHA. Cuttings samples 12-21 were collected during drilling this interval.

In Figure 4.6 a bar PSD diagram for this section is shown, along with CI, d, WOB and ROP values for each sample. However, samples 16-17 were not considered, because visual analysis of cuttings showed a high content of quartz in these samples.

These diagrams show that cuttings size has a tendency to increase first and then decrease after certain point. Conversely, WOB and ROP values are continuously increasing. From the CI and d plots it can also be observed that both parameters are equivalent for size representation.

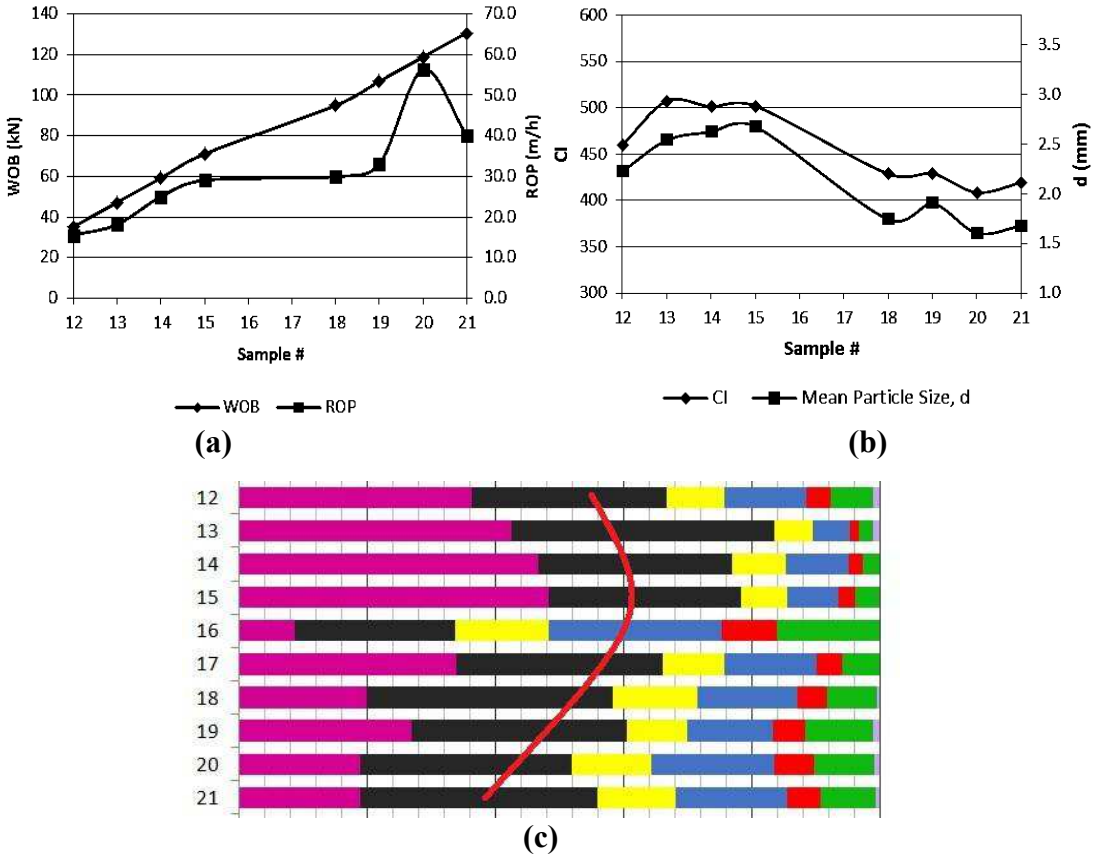

Figure 4.6 – PSD analysis for Section 1:

(a) – WOB and ROP trends; (b) – CI and d trends; (c) – Bar PSD

Another section (samples 18-21, Well #3, 82.3-91.4 m), which was drilled with a PDC bit and no compliant tool, shows the same results as Section 1. The corresponding results are shown in Figure 4.7.

Analyzing both sections, it is possible that after reaching a certain threshold value of WOB cuttings get smaller because of crushing and regrinding by the bit before they can be removed from the borehole with the drilling fluid. Threshold WOB seems to be an important parameter, because above it the cuttings size shows the reverse trend, which could indicate a change in cutting mechanism. In both cases (Section 1 and 2) this threshold

value approximately equals 70-75 kN. After this value, the positive relationship between ROP (WOB) and cuttings size changes into a negative one.

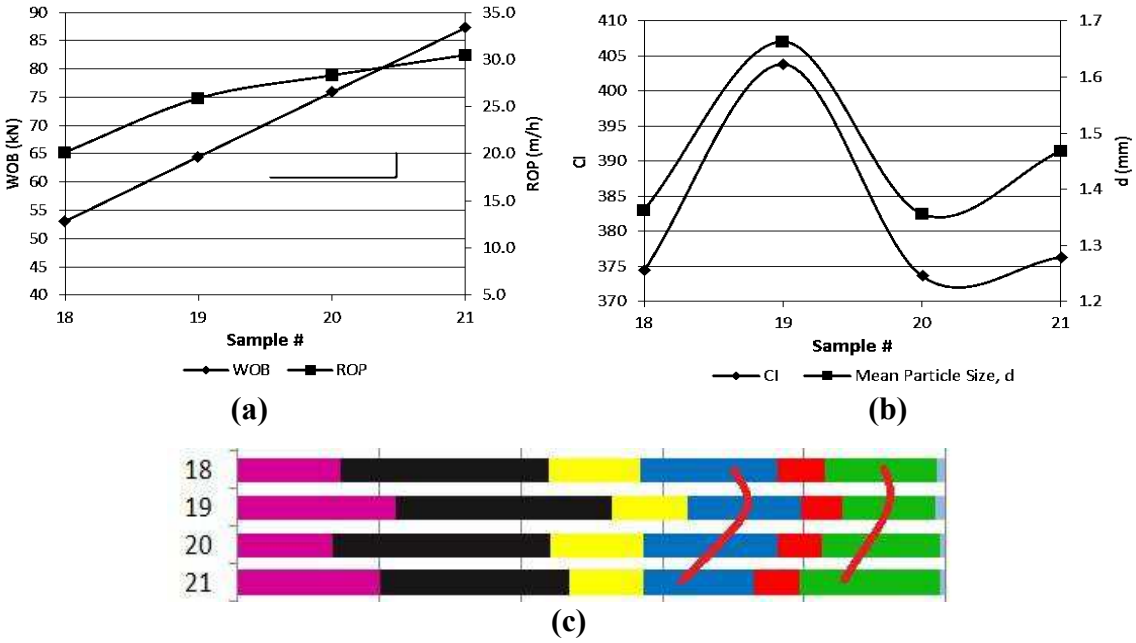

Figure 4.7 – PSD analysis for Section 2:

(a) – WOB and ROP trends; (b) – CI and d trends; (c) – Bar PSD

This phenomenon can be possibly explained by the laminate structure and brittleness of the grey shale. It is worth noticing that ROP is still increasing, while smaller cuttings are being generated. We might expect that, with more efficient cleaning of the borehole (a higher flowrate) ROP could be even higher, as additional energy would not be spent in regrinding cuttings. This leads to the conclusion that, for weak and fissile formations efficient cleaning may be extremely important factor.

The other two sections analyzed in grey shale lithology showed a negative relationship between ROP and cuttings size. In both cases drilling was performed with a WOB over 65 kN, which supports the hypothesis about cuttings regrinding after threshold value. On the

other hand, this can be explained by a possible change in the cuttings mechanism. Due to highly laminate structure of the grey shale, its shear strength along the bedding plane is very low. High WOB can contribute to the weakening of the formation by contributing to layers separation and also by introducing the tensile stress in the direction perpendicular to the bedding plane. This might cause extra fracturing in formation layers and the reduction in cuttings size. However, the ROP may continue to increase due to more efficient cutting mechanism (shear and tensile failure).

4.3.2 Cuttings analysis in red shale

During performing a drill-off test in red shale section of Well #3, cuttings samples 39-43 where collected (Section 3: 71.6-73.6 m). These samples contained quartz particles, but as the percentage was quite small and relatively constant throughout all these samples, it was assumed that it has no significant effect on the performance and PSD. Drilling was performed with the PDC bit and with the compliant tool in the BHA.

The bar PSD diagram for this section and the corresponding CI, d, WOB and ROP graphs are shown in Figure 4.8.

For drilling in red shale, the cuttings size and ROP (as well as WOB) have a positive relationship in all range of WOB; in other words, bigger cuttings are generated while drilling with higher ROP and WOB. Additional analysis performed on other sections in the red shale are consistent with this affirmation.

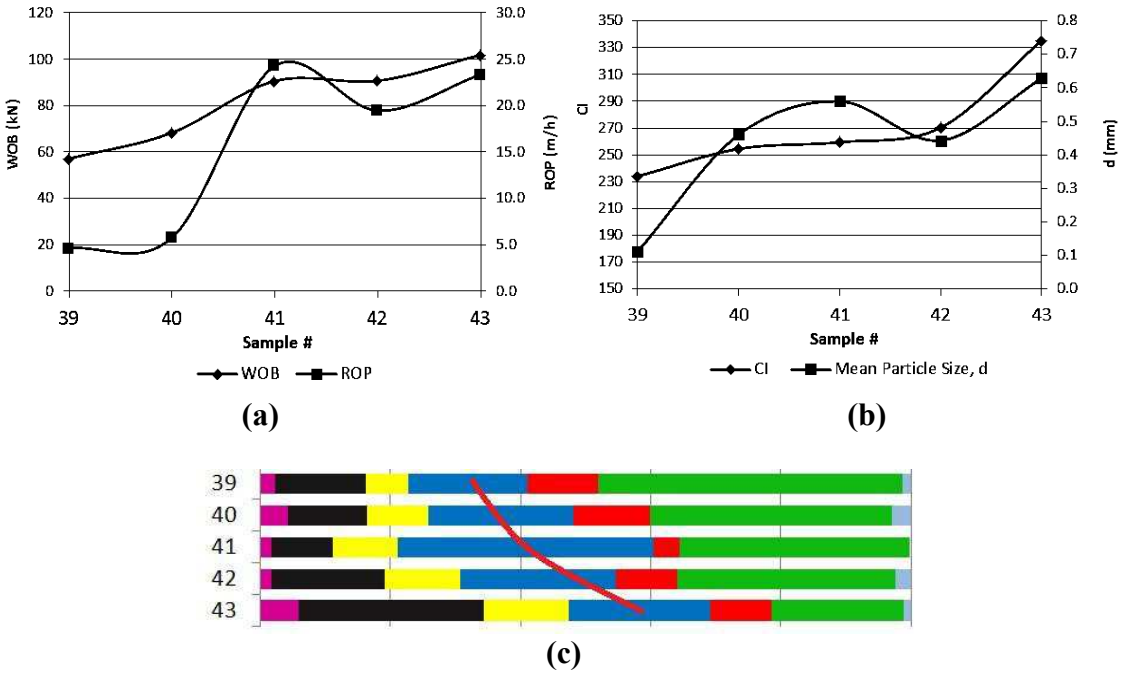

Figure 4.8 - PSD analysis for Section 3:

(a) – WOB and ROP trends; (b) – CI and d trends; (c) – Bar PSD

The same particle size analysis against performance parameters was made for the bottom section of Wells #1 and #2. Although it was mentioned that this formation was highly heterogeneous, the results obtained also support the statement that ROP and cuttings size have a positive relationship. However, is important to keep in mind that, in this case, change in cuttings size could be due to changing lithology (transition from quartz vein to shale and vice versa).

Also, due to natural fissility of the shale and friction between the drill string and wall of the well, cavings could occur and consequently affect original particle size distribution of the cuttings samples. In addition, heterogeneity in the formations and fluctuations in the flowrate and rotary speed might be another reason for the irregularity of the results.

CHAPTER 5

LOGING WHILE DRILLING AND CUTTINGS ANALYSIS IN ORE-WASTE BOUNDARIES IDENTIFICATION

5.1 Background

The discussion it previous chapters showed that drilling parameters have a strong correlation with the cuttings size. Also in Chapter 4, is was stated that cutting mechanism and consequently cuttings size distribution is affected by nature and properties of the drilled rock. Building on the laboratory and especially field results, an experiment was carried out to instrument a drilling and evaluate drilling rig parameters in order to determine geologic parameters that are critical to mining operations. The objective of this experiment was to establish the relationship between drilling parameters of the drilling rig and formation

properties. This relationship later to be used in identification of the boundaries between different formations (waster rock/ore). This chapter discusses specially designed equipment used for experiments and results of the small data set collected during field trials.

5.2 Introduction

Anaconda Mining Inc. currently operates the Pine Cove open pit gold mine and mill in the Baie Verte Mining District on the island of Newfoundland, and holds mineral rights for several other gold deposits in the region. The Pine Cove deposit's probable reserve estimation is shown in the table below. These reserves estimations for the Pine Cove Mine site as well as the daily production planning decisions are based on previous studies that assessed the geological setting and the status of the pit in order to obtain a model that can accurately predict the location, shape and grade of the ore deposits.

Table 5.1 – The resources and reserves of Pine Cove mine as of October 2015 [41]

Category	Tons	Gold (g/t)	Ounces
Indicated	1,560,000	1.67	83,685
Inferred	208,700	1.57	10,565
Probable Reserves	858,800	1.46	40,400

The geological studies include site mapping, diamond drilling, core sample analysis, borehole geocamera, laboratory testing of rock specimens and cuttings samples analysis. Currently, grade analysis on cuttings samples collected after blasthole drilling, is a final

step to ascertain ore presence. However, cuttings for the full length of the blastholes are sampled when the hole is finished, and it is impossible to determine the ore and waste rock contacts within a drilled blasthole. It has been shown that a thin high-grade zone can be mistakenly identified as a low-grade waste zone due to the dilution of the cuttings, resulting in reduced ore recovery. Anaconda estimates that approximately $1.4M of gold is not recovered from each bench due to this current methodology. Also, cuttings samples must be sent to the laboratory for analysis. It is a time-consuming process, and can potentially slow down the production.

It has been suggested that drilling performance analysis based on measuring various drilling parameters can potentially evaluate the geology. Several authors have indicated that there is a relation between the ground characteristics and the drilling parameters that allow obtaining properties such as hardness of the rock mass and the boundaries between different rock types [42], [43].

The purpose of this project was to collect enough performance data from the Pine Cove mine drilling equipment and compare it to other sources of data such as cuttings assay results and geological mapping in order to evaluate the potential of this technique to accurately identify the ore-waste boundaries.

A collaborative project between the Drilling Technology Laboratory (DTL) at Memorial University of Newfoundland (MUN) and MITACS graduate internships has been established in order to evaluate the feasibility and develop the procedures and devices for fast and precise identification of the ore-waste boundaries.

5.3 Logging while drilling (LWD) system and drilling rig equipment

The Logging While Drilling (LWD) system developed and installed on Atlas Copco T40 blasthole drilling rig (Figure 5.1).

Figure 5.1 – Atlas Copco T40 FlexiROC

FlexiROC T40 is a flexible and versatile tophammer drill rig, developed and designed for high performance in demanding construction applications. It's also a very efficient alternative for medium size quarrying jobs. Some of the T40 parameters are shown in Table 5.2.

Major LWD components include:

- hydraulic and pneumatic pressure transducers that measure the various drilling parameters;

- cable position sensor (string pot) that measures the travel of the hydraulic line carousel;
- Data Acquisition System (DAQ) to record the data from the sensors;
- electrical cables, pneumatic and hydraulic fittings to connect the sensors to the DAQ system.

Table 5.2 – Atlas Copco T40 parameters [44]

Parameter	Characteristic
Drilling method	Tophammer
Hole diameter	76 mm - 127 mm
Rock drill/DTH hammer size	COP 2560+
Maximum hole depth	28 m
Engine	168 kW

Five transducers were tapped into the system at the bulk head just outside the cabin of the rig. This is the bulk head in which the hoses run to the pressure gauges inside the cabin. Four transducers (5000 psi or 350 bar) (Figure 5.2) were tapped into hydraulic lines to measure the following parameters [45]:

- GF1: Feed pressure (0-50 bar);
- GH1: Percussion pressure (0-200 bar);
- GDP5: Damping pressure (0-70 bar);
- GRR2: Rotation pressure (0-200 bar);

and one transducer (200 psi or 14 bar) was tapped into pneumatic line:

- GA1: Flushing air (0-7 bar).

Figure 5.2 – Pressure transducers tapped into hydraulic lines [45]

Pressure snubbers were installed to protect the transducers from sudden pressure fluctuations.

A string potentiometer, used to measure hole depth, was mounted on the plate on top of the mast. The cable of the depth sensor was attached to a spring hooked onto a small pre-existing hole on the hose drum (Figure 5.3).

Figure 5.3 – Cable position sensor SR1A-125

All of the above-mentioned sensors are analog. The main characteristics of the sensors are shown in Table 5.3. All the sensors are connected to and powered from the DAQ system. DAQ system is installed in the waterproof enclosure on the left side of the drilling rig, next to the main electrical panel A1. The system itself is also powered from this panel. Two voltage regulators, fuse, on/off switch and a few terminals were installed for proper wiring.

Table 5.3 – Sensors characteristics

Parameter	Cable position sensor SR1A-125	Pressure transducer PX309-200A5V	Pressure transducer PX309-5KG5V
Measurement range	125 in	200 psi	5000 psi
Accuracy	0.5% FS	0.25%	0.25%
Environmental suitability	IP67	IP65	IP65
Operating temperature	-40˚ to 85˚ C	-40˚ to 85˚ C	-40˚ to 85˚ C
Measuring cable	0.034 in dia.	-	-
Measuring cable tension	23 oz. (6.4 N) ±30%	-	-
Output	0 to 5 Vdc	0 to 5 Vdc	0 to 5 Vdc

5.3.1 Data Acquisition (DAQ) system components

As already mentioned above, the DAQ system is installed in the enclosure (Figure 5.4, a) next to electric panel A1. However, it's only a part of the system and it includes the following component:

- Microcontroller Genuino Mega (Master board);
- Real Time Clock (RTC) breakout board;
- Micro SD breakout board;
- Analog to Digital Converter (ADC) board.

Another, integral part, of the DAQ system is a remote control (Figure 5.4, b) mounted in the cabin. Its components include:

- Microcontroller Arduino Nano (Slave board);
- LCD;
- I2C backpack for LCD;
- Keypad.

All the remote-control components are mounted inside of hand held enclosure. A brief description of each component and its specific function is shown below.

(i) Genuino Mega

The Genuino (Arduino) Mega is a microcontroller board based on the ATmega1280 (Figure 5.5).

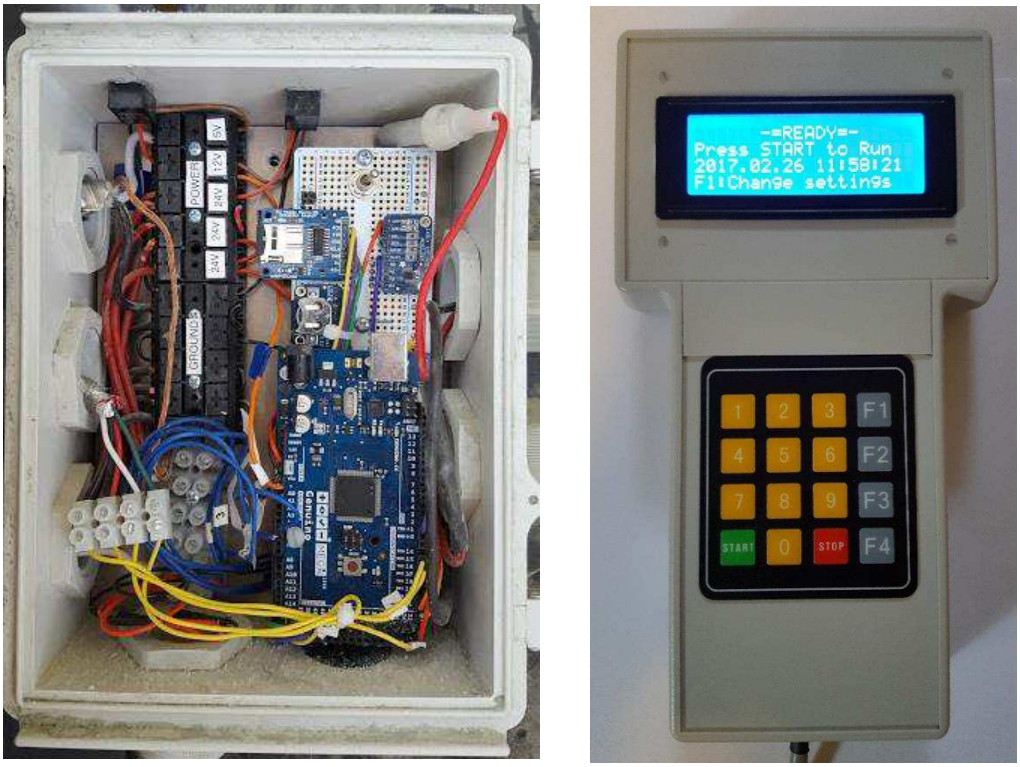

(a) **(b)**

Figure 5.4 – DAQ system (a) and remote control (b)

It has 54 digital input/output pins, 16 analog inputs, 4 hardware serial ports, a 16 MHz crystal oscillator, a USB connection, a power jack, an ICSP header, and a reset button. It contains everything needed to support the microcontroller. A big number of analog and digital pins allows future expansion of the system if required. Mega is powered from the electric panel A1 (24 V), and also provides power for the rest of the DAQ system components. This board functions as Master board. The sketch (code) uploaded to the board is shown in Appendix A.

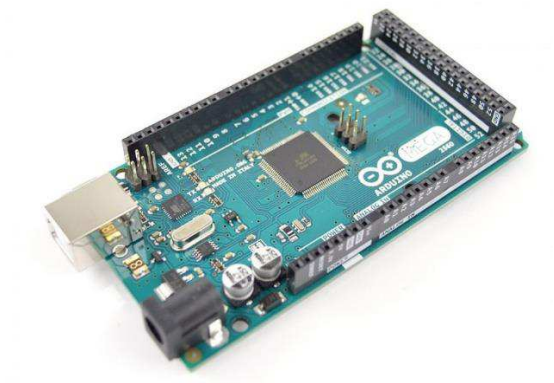

Figure 5.5 – Genuino Mega [46]

(ii) Arduino Nano

The Arduino Nano (Figure 5.6) is a small, complete, and breadboard-friendly board based on the ATmega328. Despite its small size it is a fully functioning microcontroller that features 8 analog and 13 digital pins. The Arduino Nano can be powered via 5V regulated power supply (pin 5V) or 6-20V unregulated external power supply (pin VIN). The second option was picked for the project, because an LCD connected to the board has higher voltage requirement. The sketch uploaded to Arduino Nano, which functions as a Slave board, is shown in Appendix B.

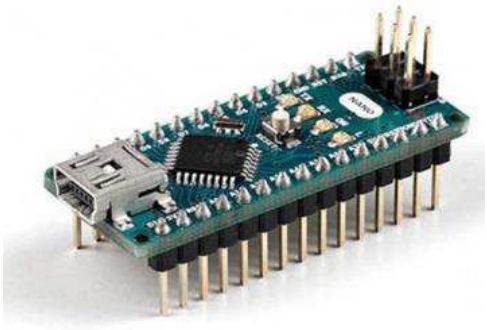

Figure 5.6 – Arduino Nano [46]

Table 5.4 – Pin connection for Arduino Nano

Boards	Pins			
Arduino Nano	VIN	GND	RX	TX
Genuino Mega	5 V	GND	TX3	RX3

(iii) LCD and I2C backpack

The main function of the LCD is to display the information required to operate the DAQ system. It includes controlling of data recording, monitoring the parameters, naming files, adjusting parameters, etc. A display with the definition of 4×20 characters was picked for this purpose. It usually requires a 16 pin connection with the microcontroller. To reduce the number of pins, a backpack board was used together with the LCD. It was soldered to the back of the LCD board. This allows a reduction of a number of pins required for connection from 16 to 4 (I^2C protocol). Also, the backpack features contrast adjustment. LCD and backpack are shown in Figure 5.7.

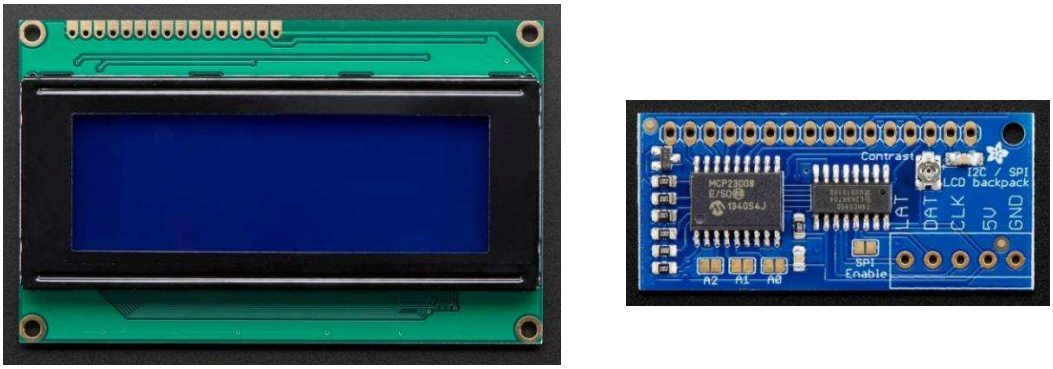

(a) **(b)**

Figure 5.7 – LCD (a) and backpack (b) [47]

The connection guide for LCD backpack is shown in Table 5.5.

Table 5.5 – Pin connection for LCD backpack

Boards	Pins			
Arduino Nano	5 V	GND	A5	A4
LCD backpack	5 V	GND	CLK	DAT

(iv) Matrix keypad

This keypad has 16 buttons, arranged in a 4×4 grid. It's made of a thin, flexible membrane material with an adhesive backing that can be easily attached to the enclosure. The keys are connected into a matrix, so only 8 microcontroller pins (4 for columns and 4 for rows) needed to scan through the pad. The keypad (Figure 5.8) is connected to digital pins 2 to 9 on Arduino Nano. Buttons Start, Stop, F1-F4 used for navigation and adjustments of DAQ system settings, while 0-9 used to name files.

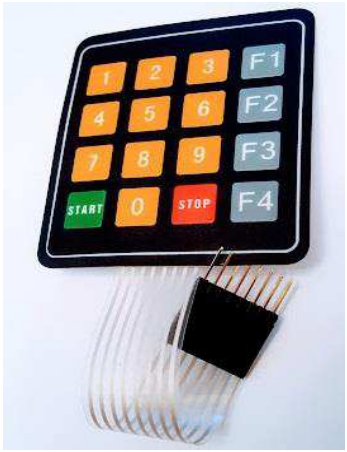

Figure 5.8 – Matrix keypad

(v) MicroSD breakout board

This board main function is to record the data on microSD card. A push-pull socket with card slightly over the edge of the board, so it's easy to insert and remove. It features an activity LED light up the card is written or being read. It also has onboard 5 to 3 V regulator that provides 150 mA for power-hungry cards. MicroSD board and its pin connection are shown in Figure 5.9 and Table 5.6 respectively.

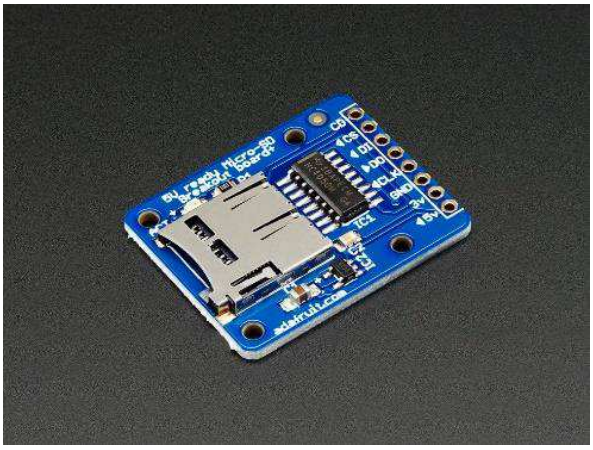

Figure 5.9 – MicroSD breakout board [47]

Table 5.6 – Pin connection for Micro SD breakout board

Boards	Pins					
Genuino Mega	5 V	GND	52	50	51	53
Micro SD breakout board	5 V	GND	CLK	DO	DI	CS

(vi) Real-Time Clock breakout board DS3231

The DS3231 is a low-cost, extremely accurate I²C real-time clock (RTC) with an integrated temperature-compensated crystal oscillator and crystal. The device incorporates a battery

input, and maintains accurate timekeeping when the main power to the device is interrupted. The integration of the crystal resonator enhances the long-term accuracy of the device.

The RTC maintains seconds, minutes, hours, day, date, month, and year information. The date at the end of the month is automatically adjusted for months with fewer than 31 days, including corrections for leap year. The clock operates in either the 24-hour or 12-hour format with an active-low AM/PM indicator [47]. RTC board is shown in Figure 5.10.

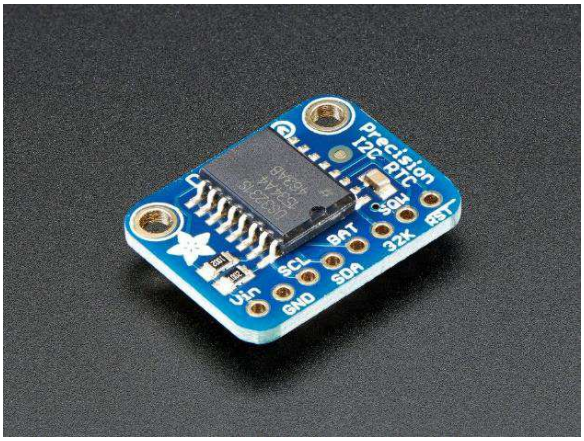

Figure 5.10 – RTC breakout board [47]

Table 5.7 – Pin connection for RTC breakout board

Boards	Pins			
Genuino Mega	5 V	GND	21 (I²C bus)	20 (I²C bus)
RTC breakout board	5 V	GND	SCL	SDA

(vii) Analog-to-Digital converter (ADC) ADS1115

The ADS1115 (Figure 5.11) is used when an analog-to-digital conversion or when just a higher-precision ADC is required. This ADC provides 16-bit precision at maximum

of 860 samples/second over I^2C connection. The chip can be configured as 4 single-ended input channels. This ADC can run from 2V to 5V power, can measure a large range of signals and its super easy to use [47]. It is a great general purpose 16-bit converter. Interfacing is done via I^2C. Without the converter, Genuino Mega provides only 10-bit analog to digital conversion. Pin connection is shown in Table 5.8.

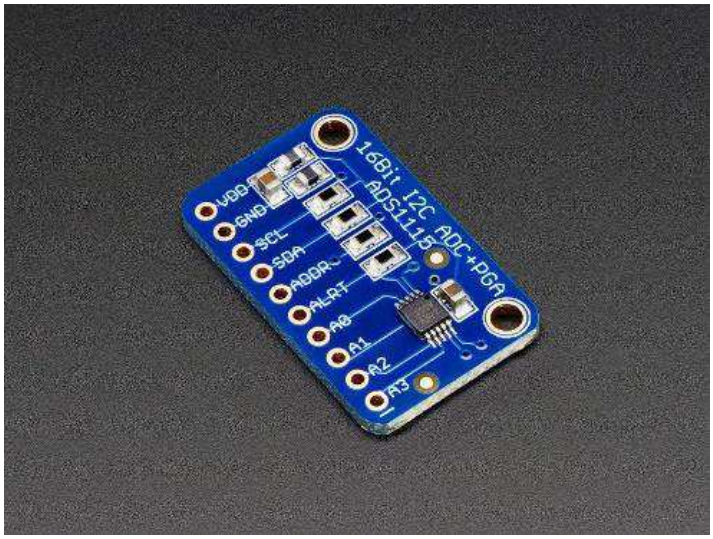

Figure 5.11 – Analog to digital converter ADS1115 [47]

Table 5.8 – Pin connection for analog to digital converter ADS1115

Boards	Pins				
Genuino Mega	5 V	GND	21 (I²C bus)	20 (I²C bus)	2
ADS1115	5 V	GND	SCL	SDA	ALRT

Complete circuit diagram and Operation manual for the DAQ system are shown in Appendices C and D respectively.

5.4 Field trials at Pine Cove mine

During the field trials the DAQ system was installed and tested. To collect sufficient amount of data, 37 blast holes were drilled on two different test locations (blast 545 and 546). The majority of the holes were drilled in the anticipated ore zones (Figures 5.12, 5.13). For each hole the following parameters were recorded:

- Hole depth;
- Feed pressure;
- Damping pressure;
- Percussion pressure;
- Rotation pressure;
- Flushing air pressure.

Data recording frequency was set at 10 Hz.

Initially 7×3 holes pattern was planned for both test locations. However, for the first location one row of the holes (#244776-244782) was not drilled due its proximity to the bench (preventing undercut). Instead, two more holes (#244813, 244798) were added to the test location, forming a final pattern of 8×2. Each hole was drilled approximately 7.5 meters deep. Cuttings samples were collected for 5 holes (indicated in red) with depth interval of 0.5 meters. Sometimes it was impossible to collect cuttings sample due to flooded holes (#244791-244793).

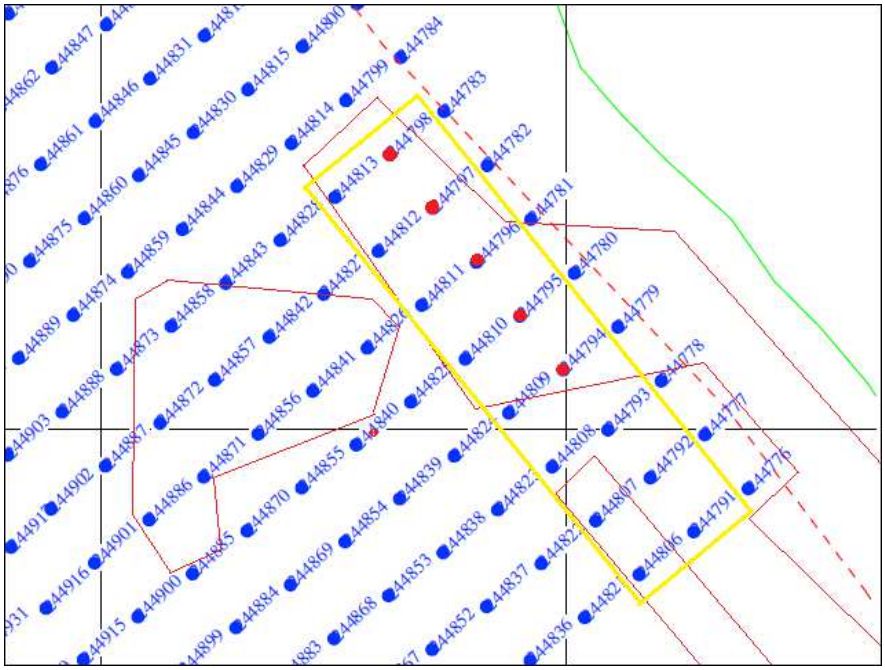

Figure 5.12 – Blast 545 with indicated ore zones (red) and test location (yellow)

In total, 16 holes were drilled, and 68 cuttings samples were collected on this test location. For the second location, twenty-one (7×3 pattern) test hole was drilled. Cuttings samples were collected for all seven holes in the middle row (Figure 5.13, indicated in red). Similarly to the previous location, samples were collected every 0.5 meters. For some holes collection started at the depth of 1 or 1.5 m, because of very loose rock at the top part of the hole. During drilling these holes, the bit simply "fell" through the rock and no cuttings were generated. Eighty cuttings sample were collected on this location. Considering the fact that all the operational parameters during drilling were kept nearly constant analysis on cuttings size was out of interest. Only grade analysis was performed on cuttings samples to define the gold content and identify rock as waste or ore. The grade varied from 0.14 to

11.9 g/t. For this type of mine, the samples with grades higher than 0.8 g/t were considered as ore.

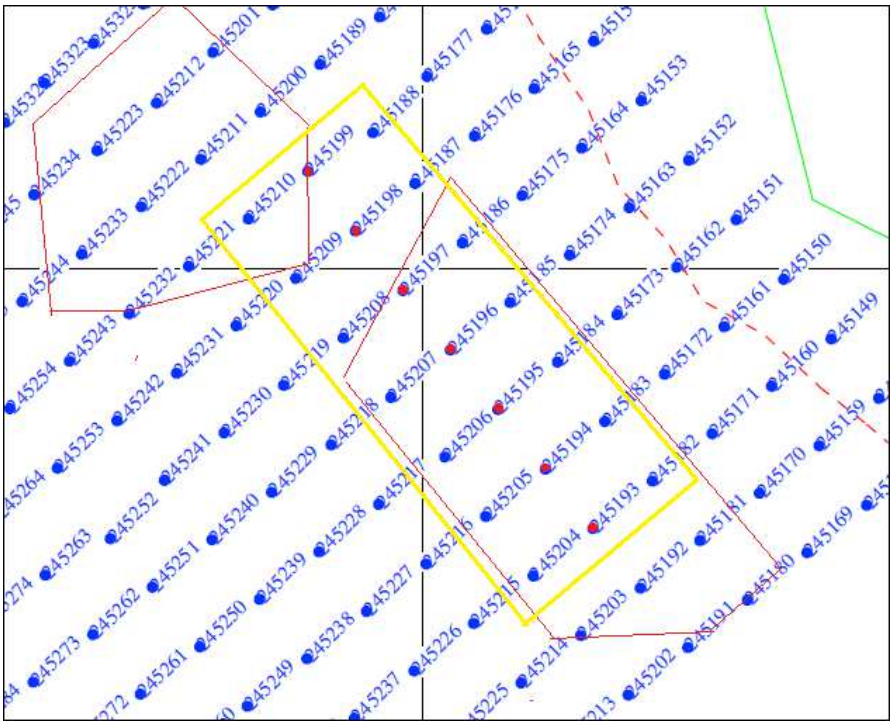

Figure 5.13 – Blast 546 with indicated ore zones (red) and test location (yellow)

5.5 Data analysis and discussion

As mentioned above, the main goal of the field trials is to find out if it is possible to detect ore/waste boundaries by monitoring drilling parameters recorded by the DAQ system. All the files recorded were processed in Microsoft Excel and later were transferred to Strater software to generate the logs for each hole. An example of the log, which shows all recorded parameters, is shown in Figure 5.14. However, preliminary analysis has shown, that only ROP, damping and feed pressure showed significant change along the course of the hole, which can potentially serve as the indicators of the formation change. All other

parameters were eliminated from the logs to facilitate the analysis. Also, ore grade log was added for the several holes (only those where cuttings were collected). Due to imperfection in the original version of the code uploaded to the DAQ microcontroller, the bit position and ROP for the second and third rods were recalculated manually. Unfortunately, only average ROP for every second could be calculated manually. This lead to reduction of the sample rate from 10 Hz to 1 Hz, what affected the quality of data and can be observed on the logs.

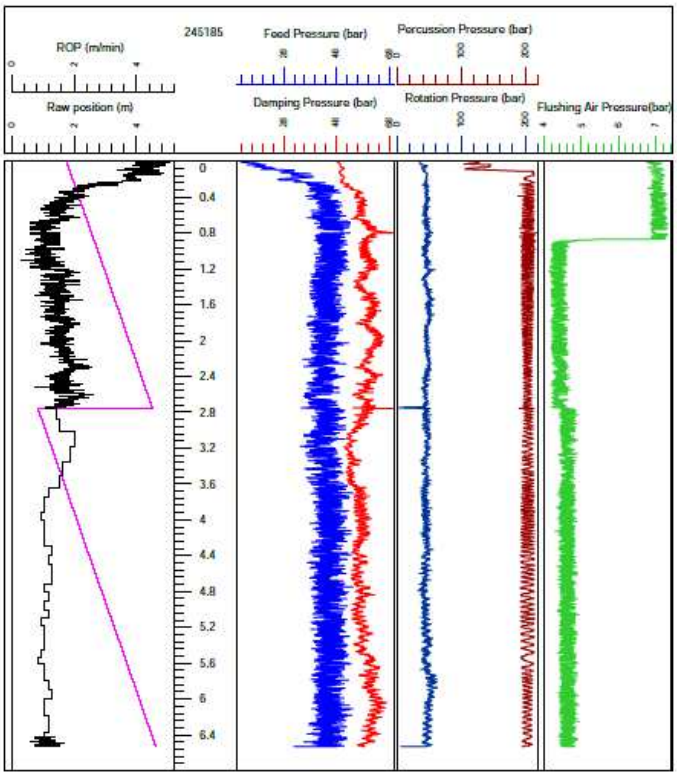

Figure 5.14 – Example of complete log

Also from preliminary analysis it was noticed that the damping pressure log has the same pattern for all the blast holes. Damping pressure tends to increase towards the end of each rod (Figure 5.15).

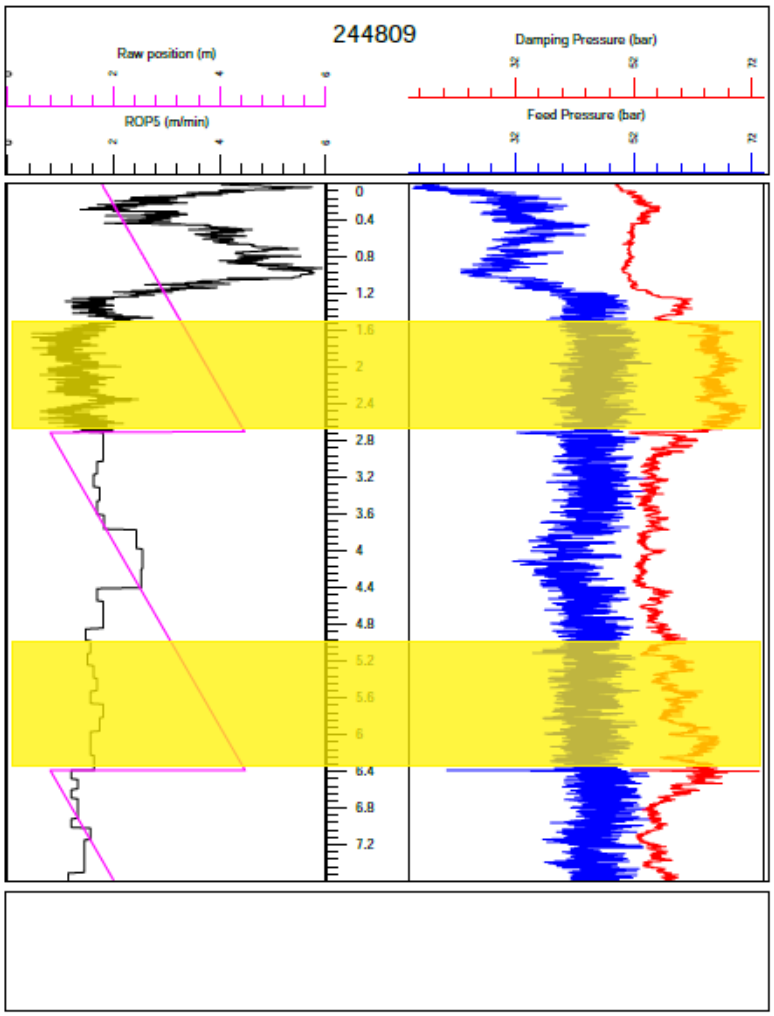

Figure 5.15 – Increase in damping pressure

Such pattern, to some extent, was observed for all of the test holes. Considering the fact that there is a big distance between the holes (different test location), it is possible to assume that these changes in damping pressure are not related to the formation change, even though they are observed at the same depth. This assumption is also supported by the assay results, as ore grade (waste/ore) values fluctuates a lot throughout the location. This phenomenon can be explained by the fact that some axial vibrations are transformed to the

lateral movement of the “unconfined” (above the ground) part of the drilling rod. When the bit penetrates through the rock and bigger part of the drilling rod is “confined” in the hole, a contact between the rod and a wall may occur, which restricts lateral movement on the rod (and the mast itself), reducing damping ability of the rod and making the system stiffer. It is well known, that a rate of penetration (ROP) is related to the strength of the drilled formation. The higher the ROP is, the softer is the formation (if other parameters kept constant). It also known from previous research, that ore should have lower strength than the waste rock. For this reason, the ROP will be used as one of the prime indicators for detecting the boundary between softer and harder (potentially ore and waste) formation.

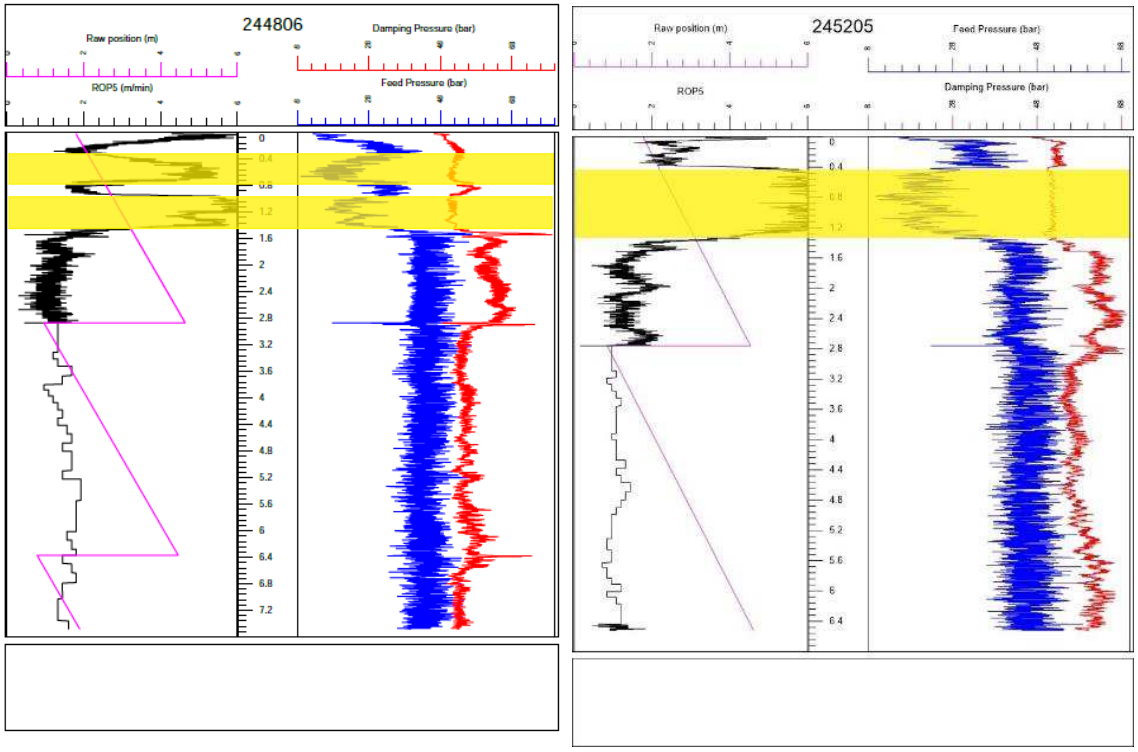

Figure 5.16 – High ROP zones in subdrill (logs for 2 different holes)

The analysis has shown that, damping pressure also be can used to characterize the rock: lower damping pressure corresponds to softer formation and vice versa. It was also observed that feed pressure tends to decrease with increase of ROP.

Initially feed pressure was considered as constant and independent parameter, but current data shows that it shows the same trend as damping pressure. The initial assumption was partially correct, as it seems that feed pressure decreases with a spike in ROP, but then is automatically adjusted by the system and goes back up to the original value (around 40 bar). This pattern is especially noticeable while drilling through loose rock at top section of the hole, called subdrill. (Figure 5.16). Log on the left (black) represent ROP and logs on the right represents damping and feed pressure (blue and red color respectively).

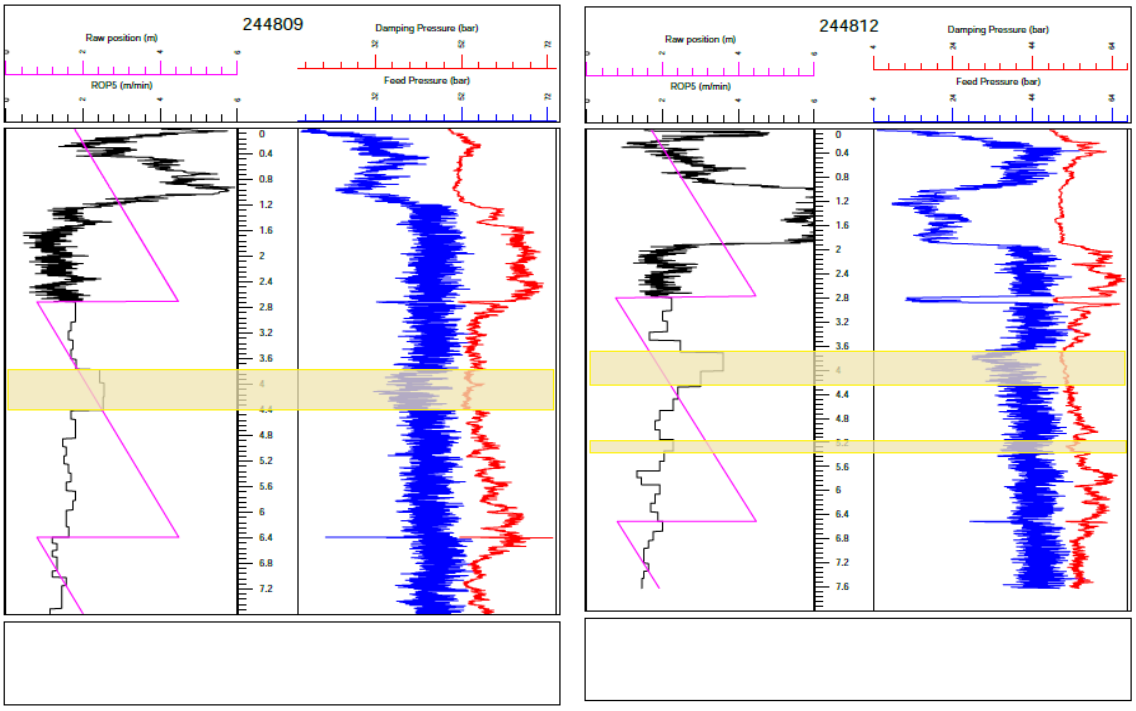

Figure 5.17 – Drilling logs with indicated high ROP zones (location 1: blast 545)

Figures 5.17 and 5.18 show the same trend of feed and damping pressure for sections deeper in the hole. Many examples of such trend were observed throughout holes drilled in both test locations.

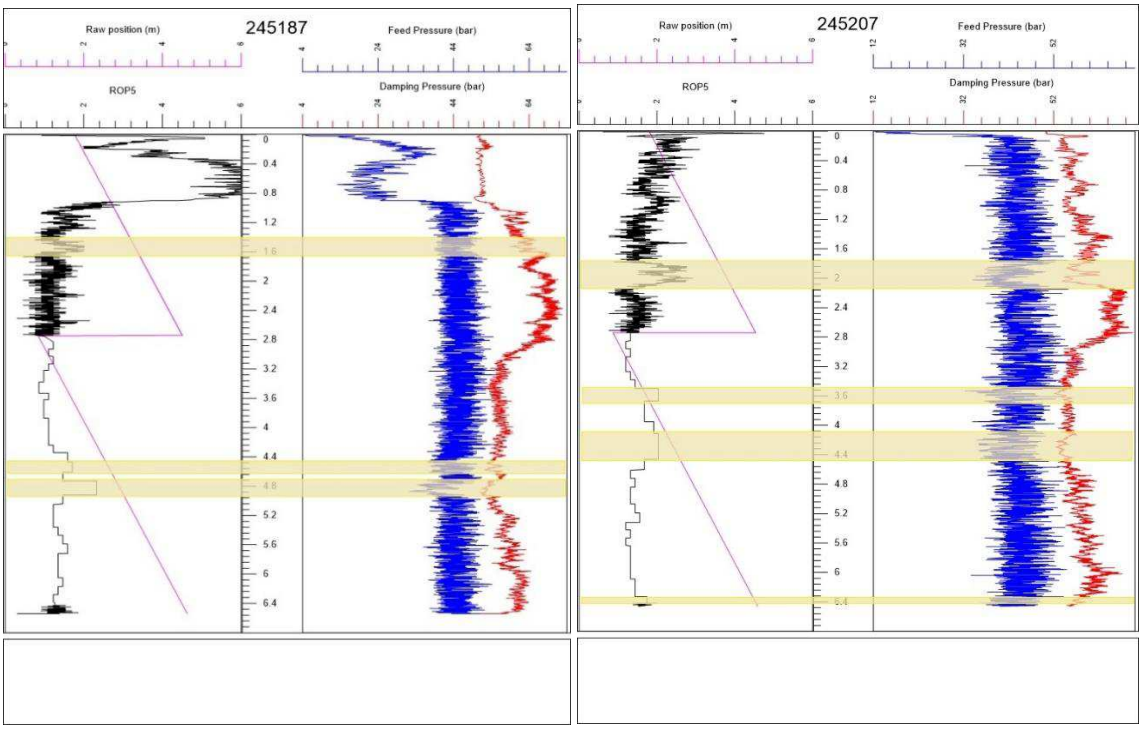

Figure 5.18 – Drilling logs with indicated high ROP zones (location 2: blast 546)

From the logs shown above it could be observed that decrease in feed and damping pressure along with increase of ROP can serve as indicators of softer or possibly loose or fractured formations (indicated in yellow). This hypothesis can be supported by the fact that high ROP and low damping pressure is observed while drilling in subdrill – top section of the hole, which was fractured by the blasting operations. However in deeper sections of the hole, the decrease in damping pressure is very slight and cannot be used as a strong indicator alone without ROP log.

The question yet to be answered, if those indicated zones were drilled in ore or just in softer waste rock. For this purpose, cuttings samples were collected on each test location. Initially it was thought, that the geology (ore presence) within adjacent holes is similar and geological cross section of the test location can be built just using cuttings collected from several holes (7 holes in one line, middle row). However, the assay results show that ore grade/presence changes from hole to hole and drilling logs for adjacent holes cannot be compared. In other words, all the soft zones indicated on the logs above cannot be correlated to the formation type, as the geological cross section could differ from the ones for the middle row holes.

Figure 5.19 shows the logs for the holes with indicated ore zones, defined based on cuttings analysis. Multiple spikes can be observed on these logs, which represent drilling breaks due to samples collection (every 0.5 m). All these interruptions to some extent distort final logs, because drilling system requires certain time to adjust parameters to normal values after a break. Especially damping and feed pressure logs are affected by these drilling breaks, what makes them very hard to analyze. Mainly ROP logs were used for analysis in this case.

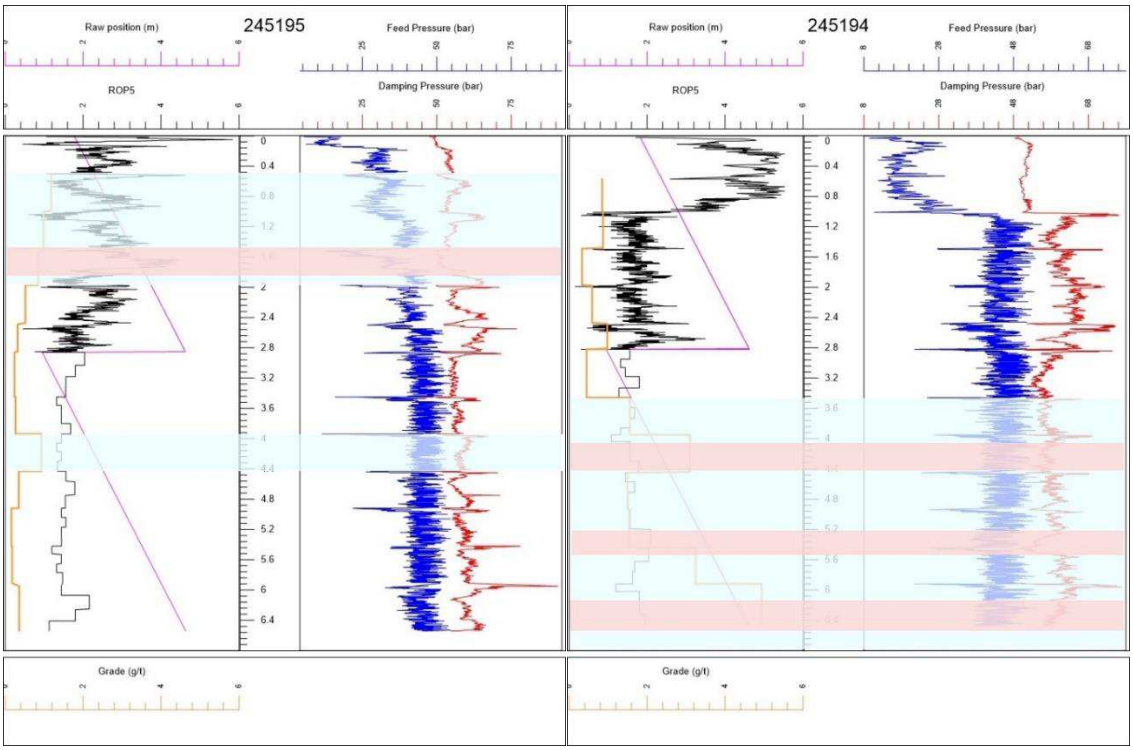

Figure 5.19 - Logs with indicated ore zones (blue) and high ROP zones (pink) within ore

On these figures, ore zones (high grade) are marked in blue and high ROP zones within the ore are marked in pink. Ore grade log is shown in orange on the left.

The analysis shows that many intervals within the ore were drilled with high ROP. However, there are even more intervals within ore drilled with low ROP. Often the ROP was even lower in ore than it was in waste rock. It leads to a conclusion that the difference in properties between waste and host rock is not significant enough to detect the boundary based on ROP logs. It makes the system not capable to detect ore/waste boundary. No relationship was observed between ROP and ore grade.

CHAPTER 6

SUMMARY AND CONCLUSION

6.1 Summary of present work

The constantly increasing cost and complexity of processes in oil and gas production has lead the industry to focus on drilling optimization. Drilling is one of the most challenging and expensive operations in hydrocarbon production and even slight increase in its efficiency can potentially save millions of dollars. Understanding of the penetration mechanism and how it is influenced by different parameters, is a key part in improving of the drilling efficiency. Cuttings generated during drilling process represent the result of interaction between the bit, rock and drilling mud. For this reason, it can be used as a valuable source of information for performance evaluation and following optimization.

Multiple methods and required equipment for cuttings collection are presented along with methodology for cuttings preparation. Different methods can be chosen for analysis, depending on the desired accuracy, cuttings size, available equipment, time for analysis, etc. Cuttings samples are mainly analyzed in term of their size, which is presented as coarseness index or mean particle size. These are compared with such drilling parameters as, rate of penetration, weight on bit, torque on bit, bit hydraulics, mechanical specific energy and bottom hole pressure. The established relationships between above-mentioned parameters allows to evaluate drilling efficiency based on cuttings analysis.

6.2 Concluding remarks

- Modern technology can provide real-time particle size distribution with high precision. It can greatly facilitate and accelerate cuttings analysis. Nevertheless, some methods have limitations for particle size, concentration and media particles are contained in.
- Multiple factors can affect real particle size distribution of the samples and distort final results, among them:
    - collection of incomplete samples;
    - mixing of the particles from different tests;
    - some particles can be trapped in the system, especially in the load cell;
    - fine particles (<67 μm) are lost during the limitation of cuttings collection system;
    - fine particles tend to stick together and form lumps;

    - presence of cavings in the samples (for field data).

- Coarseness Index and mean particles size can be used as a numerical representation of the cuttings size. These two parameters are mainly interchangeable as they show the same relationship with major drilling parameters.
- Proposed Bar PSD is a useful way to analyze incomplete cuttings samples. It allows to compare different size fraction within different samples.
- Coarseness index has a strong correlation with major drilling parameters:
    - It increases with increase of WOB, ROP and TOB;
    - It decreases with increase in BHP and flowrate;
    - Higher MSE is associated with lower CI values.
- Results in grey shale show that cuttings size increase only with increase of WOB up to a certain point. After reaching a threshold value of WOB, cuttings size tend to decrease. It may be related to cuttings regrinding and to highly brittle and laminate structure of the grey shale.
- Percentage of fine particles in samples tend to increase with increase in BHP. It may be explained by regrinding of cuttings before they are removed by drilling fluid. Chip hold down effect may greatly contribute to this process.
- Established relationships allow to do the reverse analysis on performance evaluation. However, such analysis can be performed only on cuttings generated during drilling with the same bit, drilling mud and use of same rock type and strength.

- Drill cuttings is great source of information about subsurface formation. They greatly help with identification of formation type and construction of geological cross-sections. Cuttings also used for ore grade analysis in ore-waste boundaries identification.
- The DAQ system installed and tested during field trials in Pine Cove mine is not capable of detecting ore-waste boundaries. Nevertheless, it can detect softer or fragmented rock which can potentially help in determination of powder factor in blasting operations.

6.3 Future work

Due to limitation on the drilling system, small range of weight on bit was tested. As a future work, testing of higher WOB is recommended. It can potentially help to find founders point. The region above this point is a key area of interest for cuttings analysis. The effect of higher bottom hole pressure and rotary speed on cuttings size to be investigated in future work. The above-mentioned activities can be performed using Large Drilling Simulator that is currently being tested in the Drilling Technology Laboratory. It has much higher WOB and BHP capacity and can vary rotary speed.

Extensive laboratory research is recommended for natural rock. Cuttings generating mechanism can be different for highly anisotropic rock like grey shale. Drilling in multiple layer orientations for such rock must be performed, as it highly affects penetration mechanism. Natural rock specimens should be prepared and tested.

Comparison of the experimental data with simulation study is also being considered for future work. Results of the cuttings analysis performed in the lab, can be compared to the results of simulation performed in PFC2D or other software.

For the investigation of the ore-waste boundary, the increase of sampling frequency of the DAQ system is recommended. Data collected with higher sampling rate will allow to derive the secondary parameters, percussive index, which can potentially be used for rock characterization.

References

[1] BP Statistical Review of World Energy June 2017, [online]. Available: https://www.bp.com/content/dam/bp/en/corporate/pdf/energy-economics/statistical-review-2017/bp-statistical-review-of-world-energy-2017-oil.pdf.

[2] Halliburton. Reduce Non-Productive Time (NPT), [online]. Available: http://www.halliburton.com/en-US/ps/solutions/deepwater/challenges-solutions/reduce-non-productive-time.page?node-id=hgjyd452&Topic=DeepwaterWestAfrica.

[3] M. Karimi, "Drill cuttings analysis for real-time problem diagnosis and drilling performance evaluation", SPE Pacific Oil & Gas Conference and Exhibition, Jakarta, Oct. 2015.

[4] D.T. Georgi, D.G. Harville, H.A. Robertson, "Advances in cuttings collection and analysis", SPWLA 34th Annual Logging Symposium, Jun. 1993.

[5] B. Akbari, S. Miska, M. Yu, E. Ozbayoglu, "Relation between the mechanical specific energy, cuttings morphology, and PDC cutter geometry", 33rd International Conference on Ocean, Offshore and Arctic Engineering, San Francisco, California, USA, June 8-13, 2014.

[6] R. Altindag, "Evaluation of drill cuttings in prediction of penetration rate by using coarseness index and mean particle size in percussive drilling", Geotechnical and Geological Engineering 22: 417–425, 2004.

[7] A. Saasen *et al.,* "Automatic measurement of drilling fluid and drill cuttings properties", IADC/SPE Drilling Conference, Orlando, Florida, USA, Mar. 2008.

[8] T.H. Omland *et al.,* "Improved drilling-process control through continuous particle and cuttings monitoring", SPE Digital Energy Conference and Exhibition, Houston, Texas, USA, Apr. 2007.

[9] Williams, R.D. and Ewing, S.P. Jr., “Improved methods for sampling gas and drill cuttings”, SPE 62nd Annual Technical Conference and Exhibition, Dallas, Texas, September 27-30, 1987.

[10] R. Han *et al.,* “Real-time borehole condition monitoring using novel 3D cuttings sensing technology”, IADC/SPE Drilling Conference, Hague, Netherlands, Mar. 2017.

[11] Naegel, M., E. Pradie, T. Delahaye, C. Mabile, and G. Roussiaux, “Cuttings flow meters monitor hole cleaning in extended reach wells”, SPE European Petroleum Conference, The Hague, Netherlands, 20-22 October, 1998.

[12] Schlumberger, “CLEAR hole cleaning and wellbore risk reduction service”, [online]. Available: http://www.slb.com/~/media/Files/geoservices/product_sheets/clear_ps.pdf.

[13] Marana, A.N., J.P. Papa, M. Ferreira, K. Miura, and F. Torres, “An intelligent system to detect drilling problems through drilled-cuttings-return analysis”, IADC/SPE Drilling Conference and Exhibition, New Orleans, Louisiana, USA, 2-4 February, 2010.

[14] Jillavenkatesa, A., Dapkunas, S.J., Lin-Sien Lum, “Particle size characterization”, NIST Special Publication 960-1, 2001.

[15] Retsch, “The basic principles of sieve analysis”, [online]. Available: http://www.ninolab.se/fileadmin/Ninolab/pdf/retsch/documents/af_sieving_basics_2004_en.pdf.

[16] M. Hrncirova, J. Pospisil, M. Spilacek, “Size analysis of solid particles using laser diffraction and sieve analysis”, Engineering Mechanics, Vol. 20, No. 3/4, p. 309–318, 2010.

[17] J. Sliwinski, M. Le Strat and M. Dublonko, “A New Quantitative Method for Analysis of Drill Cuttings and Core for Geologic, Diagenetic and Reservoir Evaluation”, CSPG CSEG CWLS Convention, Calgary, Alberta, Canada, 2009.

[18] J. J. Kumara, K. Hayano and K. Ogiwara, “Image Analysis Techniques on Evaluation of Particle Size Distribution of Gravel”, International Journal of GEOMATE, Vol. 3, No. 1 (Sl. No. 5), pp. 290-297, Sept., 2012.

[19] Horiba Scientific, “The CAMSIZER Image Analyzer”, [online]. Available: http://www.horiba.com/scientific/products/particle-characterization/technology/dynamic-image-analysis/

[20] D. Greaves et al., “Measuring the particle size of a known distribution using the focused beam reflectance measurement technique”, Elsevier, Chemical Engineering Science 63, 5410-5419, 2008.

[21] H. Geers, W. Witt, “Ultrasonic extinction for in-line measurement of particle size and concentration of suspensions and emulsions”, Particulate System Analysis, Harrogate, UK, 2003

[22] Brezani, I. and F. Zelenak, “Improving the effectivity of work with rosin-rammler diagram by using MATLAB (R) GUI tool” Acta Montanistica Slovaca. 15(2): 152-157, 2010.

[23] Wills, B.A., Napier-Munn, T.J., “Particle Size Analysis. 7th edition”, Mineral Processing Technology. Elsevier Science & Technology Books. Chapter 4. pp. 90 – 108, 2006.

[24] Rosin, P., Rammler, E., “The laws governing the fineness of powdered coal”, Journal of the Institute of Fuel, 29–36, 1933.

[25] Allen, T., “Particle Size Measurement: Powder sampling and particle size measurement”, Chapman & Hall, 5th edition, Chapter 2.13, 1997.

[26] Roxborough, F.F and Rispin, A., “The mechanical cutting characteristics of the lower chalk”, University of Newcastle, 1972.

[27] Blott Simon J., Pye Kenneth, Sedimentology [Peer Reviewed Journal] Vol.55(1), pp.31-63, February 2008.

[28] G.W. Stachowiak, “Particle angularity and its relationship to abrasive and erosive wear”, Elsevier, Wear 241. 214–219, 2000.

[29] F.J. Santarelli, A.F. Marsala, M. Brignoli, E. Rossi, N. Bona, "Formation evaluation from logging on cuttings", SPE Reservoir Evaluation & Engineering, June 1998.

[30] M. Haftani *et al.*,"A new method for correlating rock strength to indentation tests", Elsevier: Journal of Petroleum Science and Engineering 112, pp.24–31, 2013.

[31] Meyers A.G., Hunt S.P., Frick R., Behr S., "Point load testing of drill cuttings for the determination of rock strength", ARMA: The 40th U.S. Symposium on Rock Mechanics, Anchorage, Alaska, USA, June 25-29, 2005.

[32] C. Carugo *et al*., "Advanced cuttings analysis improves reservoir characterization and reduces operating times in shale gas drilling projects", International Petroleum Technology Conference, Beijing, China, 26-27 March, 2013.

[33] R. Lenormand, O. Fonta, "Advances in measuring porosity and permeability from drill cuttings', SPE/EAGE Reservoir Characterization and Simulation Conference, Abu Dhabi, U.A.E., 28-31 October, 2007.

[34] Ersoy, A. and M. Waller, "Drilling detritus and the operating parameters of thermally stable PDC core bits", International Journal of Rock Mechanics and Mining Sciences. 34(7): 1109-1123, 1997.

[35] R. Reyes, "Bit-rock interaction in roary drilling: Numerical and experimental study", M.Eng. thesis, Faculty of Engineering and Applied Sciences, MUN, St. John's, NL, 2017.

[36] H. Khorshidian, "Phenomena affecting penetration mechanisms of polycrystalline diamond compact bits," M.Eng. thesis, Faculty of Engineering and Applied Sciences, MUN, St. John's, NL, 2012.

[37] Z. Zhang, "Development and Characterization of Synthetic Rock-Like Materials for Drilling and Geomechanics Experiments," M.Eng. thesis, Faculty of Engineering and Applied Sciences, MUN, St. John's, NL, 2016.

R. Majidi, S. Z. Miska, S. Tammineni, “PDC single cutter: the effect of depth
[38] of cut and rpm under simulated borehole conditions”, Wiertnictwo Nafta Gaz, Tom 28, Zeszyt 1-2, 2011.

[39] Rana, P.S., Field Trial Report. Unpublished document, 2014

[40] Reyes, R., Kyzym, I., Rana P.S., Molgaard J. and Butt, S.D, “Cuttings Analysis for Rotary Drilling Penetration Mechanisms and Performance Evaluation”, 49th US Rock Mechanics / Geomechanics Symposium, San Francisco, CA, USA, 28 June- 1 July 2015.

[41] Anaconda Mining. “NI 43-101 Technical report, mineral resource and mineral reserve update on the Pine Cove mine and mineral resource estimate on the Stog’er Tight deposit, Point Rouse Prolect”, October 2015.

[42] Paone, J., Madson, D., Bruce, W. E., “Drillability studies: laboratory percussive drilling”, Bureau of Mines, Twin Cities, MN (USA). Twin Cities Mining Research Center, 1969.

[43] Schunnesson, H., “Rock characterisation using percussive drilling”, International journal of rock mechanics and mining sciences, 35(6), 711-725, 1998.

[44] Atlas Copco website [online]. Available: https://www.atlascopco.com/en-ca/mrba/products/drill-rigs/surface-drill-rigs/flexirpc-t40

[45] E. Flynn, “Pine Cove Mine Field Visit Summary Report”, April 2016. Unpublished document.

[46] Arduino electronics, [online]. Available: https://www.arduino.cc/

[47] Adafruit shield and boards, [online]. Available: https://www.adafruit.com/

[48] I. Kyzym, A. Lopez, “Data acquisition system v2.0 Field trial summary report”, July 2017. Unpublished document.

APPENDIX A

ARDUINO SKETCH FOR GENUINO MEGA (MASTER BOARD)

```
#include <Arduino.h>
#include <stdio.h>
#include <string.h>
#include <stdlib.h>
#include <ctype.h>
#include <Wire.h>
#include <RTClib.h>
#include <SdFat.h>
#include <SdFatUtil.h>
#include <MB_textLCDinterface.h>
#include <MB_TextUtility.h>
#include <MB_SDTools.h>
#include <mbDebug.h> //some debug libraries
#include <ADS1115.h>
#define LCD_NUMBER_OF_COLS 20
#define LCD_NUMBER_OF_ROWS 4
#if LCD_INTERFACE_DISPLAY_TYPE ==
LCD_INTERFACE_DISPLAY_TYPES_LICQUIDCRYSTALI2C
        #include <LiquidCrystal_I2C.h>
        LiquidCrystal_I2C lcd(0x20, LCD_NUMBER_OF_COLS,
LCD_NUMBER_OF_ROWS);
#elif  LCD_INTERFACE_DISPLAY_TYPE ==
LCD_INTERFACE_DISPLAY_TYPES_ADAFRUITI2CBACKPACK
        #include <LiquidTWI.h>
        LiquidTWI lcd(0);
#elif LCD_INTERFACE_DISPLAY_TYPE ==
LCD_INTERFACE_DISPLAY_TYPES_MBSERIALTERMINAL
#else
        #error unknown LCD type:
#endif
#include <MB_KeypadSerial.h>
RTC_DS3231 rtc;
```

```
ADS1115 adc0(ADS1115_DEFAULT_ADDRESS);
//=Coefficients============================
float coefPositionSensor=(2*1.120*3.0480/5000.0);
float coefFlushingAir=(13.78952/1024.0);
float coefFeed=(344.738/1024.0);
float coefRotation=(344.738/5000.0);
float coefPercussion=(344.738/5000.0);
float coefDamperPressure=(344.738/5000.0);
#define KEYPAD_ROWS_NUMBER 4
#define KEYPAD_COLS_NUMBER 4
uint8_t pinsKeypadCols[KEYPAD_COLS_NUMBER]={28,26,24,22};
uint8_t pinsKeypadRows[KEYPAD_ROWS_NUMBER]={30,32,34,36};
#define PIN_SDCARD_CS 53
#define PIN_ADC_READY_ALERT          2
char keys[KEYPAD_ROWS_NUMBER][KEYPAD_COLS_NUMBER] = {
        {KEY_1,KEY_2,KEY_3, KEY_A}
        ,{KEY_4,KEY_5,KEY_6, KEY_B}
        ,{KEY_7,KEY_8,KEY_9, KEY_C}
        ,{KEY_START,KEY_0,KEY_STOP,KEY_D}
};
SdFat sd;
SdFile loggerFile;
MB_KeypadSerial keypad;
MB_textLCDinterface interface(LCD_NUMBER_OF_COLS,
LCD_NUMBER_OF_ROWS);
boolean loggingStarted=false;
boolean isDrilling=false;
uint32_t holeID=0;
char drillingDeptString[10];
uint32_t loggingStartMillis;
#define RTC_TIME_LENGHT 20
char currentRTCTimeString[RTC_TIME_LENGHT];
uint32_t samplesPerSeconds=10; //default value of sample rate
//uint32_t samplesPerSeconds=1;
uint32_t nextloggingTimeMillis;
uint8_t currentVersion=0;
```

```
char fileName[20]; //filename for logging
//temporary buffers for a choice of filename
#define FILENAME_LENGHT (8+1+3+1)
char originalName[FILENAME_LENGHT];
char versionalName[FILENAME_LENGHT];
//====VARIABLES FOR MEASUREMENTS================
float rawPosition, rawFlushingAir, rawFeed, rawRotation, rawPercussion, rawDamper;
//====VARIABLES FOR LOGGING=====================
uint32_t previousMeasurementTime;
uint32_t currentMeasurementTime;
float lastLowestPosition;
float zeroLevelDelta;
float realPosition;
float realROP;
float realFlushingAir;
float realFeed;
float realRotation;
float realPercussion;
float realDamperPressure;
DateTime startTime;
//===Forward panels and commands declaration=====
void panelMain(int);
void panelEnterName(int);
void cmdStop(int);
void cmdRun(int);
void panelChangeSettings(int);
void writeHeader();
void doLogging();
void cmdRun();
void readRTCTime(){
        static uint32_t nextRTCUpdateMillis=0;
        if (millis()> nextRTCUpdateMillis){
                DateTime now = rtc.now();

        snprintf(currentRTCTimeString,RTC_TIME_LENGHT,"%d.%02d.%02d~%02d:
```

```
%02d:%02d", now.year(), now.month(), now.day(), now.hour(), now.minute(),
now.second());
                nextRTCUpdateMillis=millis()+300;
        }
}
boolean pollAlertReadyPin() {
        for (uint32_t i = 0; i<100000; i++){
                if (!digitalRead(PIN_ADC_READY_ALERT)) return true;
        }
        Serial.println("Failed to wait for AlertReadyPin, it's stuck high!");
        return false;
}
void panelRunning(int par=0){
        interface.initPanel(panelRunning);
        interface.addLabelStaticProgmem(F("Data~recording..."),0,0);
        interface.addLabelStaticProgmem(F("Depth:"),0,1);
        interface.addDynamicString(drillingDeptString,6,1,7);
        interface.addLabelStaticProgmem(F("File:"),0,2);
        interface.addLabelStaticRAM(fileName,6,2);
        interface.addLabelStaticProgmem(F("Press~STOP~when~done"),0,3);
        interface.assignAction(KEY_STOP,&cmdStop);
        interface.redrawPanel(true);
}
//returns 0 if file NNNNNN.txt doesn't exists, otherwise returns the first available
filename
//template is NNNNNN.Vxt, where V - number of version
uint8_t getVersionNumber(){
        SdFile file;
        char tmpFilename[FILENAME_LENGHT];
        boolean fileExists;
        snprintf(originalName,FILENAME_LENGHT, "%06lu_0.txt", holeID);
        fileExists=file.open(sd.vwd(), originalName, O_READ);
        file.close();
        if (!fileExists) {
                return (0);
        }
```

```
        //===file exists - trying to find versions
        for (int i = 1; i <10  ; i++){
                snprintf(versionalName,FILENAME_LENGHT, "%06lu_%1u.txt",
holeID, i);
                fileExists=file.open(sd.vwd(), versionalName, O_READ);
                if (!fileExists) {
                        file.close();
                        return (i);
                }
                file.close();
        }
        return (9);
}
void cmdRunOriginal(int parInt=0){
        snprintf(fileName,FILENAME_LENGHT, originalName);
        cmdRun();
}
void cmdRunVersional(int parInt=0){
        snprintf(fileName,FILENAME_LENGHT, versionalName);
Serial.println(fileName);
        cmdRun();
}
void panelAskForVersion(int par=0){
        interface.initPanel();
        interface.addLabelStaticProgmemCentered(F("!File~exists!"),0);
        interface.addLabelStaticProgmem(F("F1:Over"),0,1);
        interface.addDynamicString(originalName, 8,1,12);
        interface.addLabelStaticProgmem(F("F2:New "),0,2);
        interface.addDynamicString(versionalName, 8,2,12);
        interface.addLabelStaticProgmem(F("STOP:~Cancel"),0,3);
        interface.assignAction(KEY_F1,&cmdRunOriginal);
        interface.assignAction(KEY_F2,&cmdRunVersional);
        interface.assignAction(KEY_STOP,&cmdStop);
        interface.redrawPanel(true);
}
void cmdEnterID_AndStart(int par=0){
```

```
        interface.initPanel();
        interface.printColRow(F("START:Run"),0,2);
        interface.printColRow(F("STOP:Cancel"),0,3);
        holeID=0;
        if (interface.inputKeypad_UInt(holeID, "Enter~hole~ID",8, false)){
                //check filename here!!!!
                currentVersion=getVersionNumber();
                //here we already have filenames
                if (currentVersion==0)
                {
                        cmdRunOriginal();
                }else{
                        panelAskForVersion(0);
                }
        }else{
                panelMain(0);
        }
}
void getValues(){
        //position
        adc0.setMultiplexer(ADS1115_MUX_P0_NG);
        adc0.triggerConversion();
        if(pollAlertReadyPin()){
                rawPosition=adc0.getMilliVolts(false);
        }else{
                rawPosition=0;
        }
        previousMeasurementTime=currentMeasurementTime;
        currentMeasurementTime=millis();
        //rotation
        adc0.setMultiplexer(ADS1115_MUX_P1_NG);
        adc0.triggerConversion();
        if(pollAlertReadyPin()){
                rawRotation=adc0.getMilliVolts(false);
        }else{
                rawRotation=0;
```

```
        }
        //percussion
        adc0.setMultiplexer(ADS1115_MUX_P2_NG);
        adc0.triggerConversion();
        if(pollAlertReadyPin()){
                rawPercussion=adc0.getMilliVolts(false);
        }else{
                rawPercussion=0;
        }
        //damping
        adc0.setMultiplexer(ADS1115_MUX_P3_NG);
        adc0.triggerConversion();
        if(pollAlertReadyPin()){
                rawDamper=adc0.getMilliVolts(false);
        }else{
                rawDamper=0;
        }
        rawFlushingAir=analogRead(4);
        rawFeed=analogRead(5);
//==========Calculating real values of the parameters============
                realPosition=coefPositionSensor* rawPosition-zeroLevelDelta;
                realFlushingAir = coefFlushingAir * rawFlushingAir;
                realFeed = coefFeed * rawFeed;
                realRotation = coefRotation * rawRotation;
                realPercussion = coefPercussion * rawPercussion;
                realDamperPressure=coefDamperPressure*rawDamper;
                dtostrf(lastLowestPosition,5,1, drillingDeptString);
        if (realPosition>lastLowestPosition){
        if (isDrilling)   {
                                realROP=(realPosition-
lastLowestPosition)/(currentMeasurementTime-previousMeasurementTime)*60*1000;
        }else{
        realROP=0;//drilling just started, we don't know when the previous position was
reached, so we skip this measurement
        isDrilling=true;
                        }
```

```
        lastLowestPosition=realPosition;
                }else{
        realROP=0;
        isDrilling=false;
                }
}
void writeFooter(){
        SdFile file;
        if(!file.open(fileName, O_APPEND|O_WRITE)){
                interface.showMessage(F("SD~ERROR!"), 2000, 100);
                Serial.println(F("\nFailed to open for writing\n"));
                return;
        }
        file.seekEnd();
        DateTime now = rtc.now();
        char timeStrBuf[40];
        snprintf(timeStrBuf,sizeof(timeStrBuf),"Date;%d.%02d.%02d", now.year(),
now.month(), now.day());
        file.println(timeStrBuf);
        snprint (timeStrBuf,sizeof(timeStrBuf),"Start Time; %02d:%02d:%02d",
startTime.hour(), startTime.minute(), startTime.second());
        file.println(timeStrBuf);
        snprintf(timeStrBuf,sizeof(timeStrBuf),"End Time; %02d:%02d:%02d",
now.hour(), now.minute(), now.second());
        file.println(timeStrBuf);
        file.print(F("Hole ID;"));
        file.println(holeID);
        file.print(F("Depth, m;"));
        file.println(lastLowestPosition);
        file.close();
}
void cmdRun(){
        loggingStarted=true;
        loggingStartMillis=millis();
        nextloggingTimeMillis=millis();
        startTime= rtc.now();
```

```
        //==create file, write header.
        writeHeader();
        //===write a first line
        lastLowestPosition=0;
        zeroLevelDelta=0;
        realPosition=0;
        getValues(); //get a current position to determine a zero level
        zeroLevelDelta=realPosition; //use it like a "zero level"
        lastLowestPosition=0;
        getValues(); //refresh values
        doLogging(); //write the first line
        panelRunning(0);
void cmdStop(int par=0){
        loggingStarted=false;
        writeFooter();
        interface.clearScreen();
        interface.printCentered(F("Great~job~Angus..."),0);
  interface.printCentered(F("Saving~file..."),2);
  interface.printCentered(F("Please~wait..."),3);
        //SDTools_DumpFile(fileName);
        panelMain(0);
}
void panelMain(int par=0){
        interface.initPanel(panelMain); //here we remember a pointer to the current panel
        interface.addLabelStaticProgmemCentered(F("-=READY=-"),0);
        interface.addLabelStaticProgmem(F("Press~START~to~Run"),0,1);
        interface.addDynamicString(currentRTCTimeString,0,2,sizeof(currentRTCTimeS
tring));
        interface.addLabelStaticProgmem(F("F1:Change~settings"),0,3);
        interface.assignAction(KEY_START, &cmdEnterID_AndStart);
        interface.assignAction(KEY_F1, &panelChangeSettings);
        interface.redrawPanel(true);
}
void cmdSetSamplesPerSeconds(){
        interface.initPanel();
        interface.addLabelStaticProgmem(F("Set~samples/sec"),0,0);
```

```
        interface.addLabelStaticProgmem(F("START:~Save"),0,2);
        interface.addLabelStaticProgmem(F("F3:~Backspace"),0,3);
        interface.redrawPanel(true);
        interface.inputKeypad_UInt(samplesPerSeconds,"",4, false);
        panelChangeSettings(0);
}
void cmdSetRTCTime(){
        DateTime now = rtc.now();
        uint8_t tmpHours=now.hour();
        uint8_t tmpMin=now.minute();
        uint8_t tmpSec= now.second();
        interface.clearScreen();
        interface.setCursorColRow(0,2);
        interface.print(F("F3:Backspace"));
        interface.setCursorColRow(0,3);
        interface.print(F("START:OK;STOP:Cancel"));
        if (interface.inputKeypad_Time(tmpHours, tmpMin, tmpSec, "Enter~time",false))
        {
                DateTime newTime=DateTime(now.year(), now.month(),
now.day(),tmpHours, tmpMin, tmpSec);
                rtc.adjust(newTime);
                }else{
        }
        interface.redrawPanel(true);
void cmdSetDate(){
        DateTime now = rtc.now();
        uint16_t tmpYYYY=now.year();
        uint8_t tmpMM=now.month();
        uint8_t tmpDD= now.day();
        interface.clearScreen();
        interface.setCursorColRow(0,2);
        interface.print(F("F3:Backspace"));
        interface.setCursorColRow(0,3);
        interface.print(F("START:OK;STOP:Cancel"));
        if (interface.inputKeypad_Date(tmpYYYY, tmpMM, tmpDD,
"Enter~date",false))
```

```
        {
                DateTime newTime=DateTime(tmpYYYY, tmpMM, tmpDD,now.hour(),
now.minute(), now.second());
                rtc.adjust(newTime);
        }else{
        }
        interface.redrawPanel(true);
}
void panelChangeSettings(int par=0){
        interface.initPanel(panelChangeSettings); //here we remember a pointer to the
current panel
        interface.addLabelStaticProgmem(F("F1:~Set~samples/sec."),0,0);
        interface.addLabelStaticProgmem(F("F2:~Set~time"),0,1);
        interface.addLabelStaticProgmem(F("F3:~Set~date"),0,2);
        interface.addLabelStaticProgmem(F("STOP:~Main~screen"),0,3);
        interface.assignAction(KEY_F1, &cmdSetSamplesPerSeconds);
        interface.assignAction(KEY_F2, &cmdSetRTCTime);
        interface.assignAction(KEY_F3, &cmdSetDate);
        interface.assignAction(KEY_STOP, &panelMain);
        interface.redrawPanel(true);
}
void panelEnterName(int par=0){
        interface.initPanel(panelEnterName); //here we remember a pointer to the current
panel
        interface.addLabelStaticProgmem(F("Enter~hole~ID"),0,0);
        //interface.addValueLongUInt(holeID,F(""),,0);
        interface.addLabelStaticProgmem(F("START:~Run"),0,2);
        interface.addLabelStaticProgmem(F("STOP:~Cancel"),0,3);
        interface.redrawPanel(true);
}
void setup(){
        Serial.begin(115200);
        Serial.println(__TIME__);
        Serial3.begin(9600);
        delay(1000);
        Serial3.println("P test");
```

```
        delay(1000);
        #if 0
                keypad.begin(&Serial);
                Serial.println("Debug: serial0 instead of terminal's serial 3 is used");
        #else
                keypad.begin(&Serial3);
        #endif
        // initialize the lcd
        #if LCD_INTERFACE_DISPLAY_TYPE ==
LCD_INTERFACE_DISPLAY_TYPES_LICQUIDCRYSTALI2C
                lcd.init();
                lcd.backlight();
        #elif  LCD_INTERFACE_DISPLAY_TYPE ==
LCD_INTERFACE_DISPLAY_TYPES_ADAFRUITI2CBACKPACK
                lcd.begin(LCD_NUMBER_OF_COLS, LCD_NUMBER_OF_ROWS);
                lcd.setBacklight(HIGH);
        #elif LCD_INTERFACE_DISPLAY_TYPE ==
LCD_INTERFACE_DISPLAY_TYPES_MBSERIALTERMINAL
        #else
                #error unknown LCD type:
        #endif
        interface.clearScreen();
        interface.printCentered(F("Initialization..."),1);
        interface.setup(panelMain);
        if(!sd.begin(PIN_SDCARD_CS, SPI_FULL_SPEED)){
                interface.showMessage(F("SD~CARD~FAILURE"),5000,500);
                interface.clearScreen();
                interface.printCentered(F("SD~CARD~FAILURE"),1);
                interface.printCentered("Please~replace",2);
   interface.printCentered("the~card~and~restart",3);
                while(1); //freeze
        }
        if (! rtc.begin()) {
                Serial.println("Couldn't find RTC");
                interface.showMessage(F("CLOCK~FAILURE"),5000,500);
                interface.clearScreen();
```

```
            interface.printCentered(F("CLOCK~FAILURE"),1);
            while (1);
        }

        adc0.initialize(); // initialize ADS1115 16 bit A/D chip
        // We're going to do single shot sampling
        adc0.setMode(ADS1115_MODE_SINGLESHOT);
        adc0.setRate(ADS1115_RATE_128);
        // Set the gain (PGA) +/- 6.144v
        // Note that any analog input must be higher than 0.3V and less than VDD +0.3
        adc0.setGain(ADS1115_PGA_6P144);
        pinMode(PIN_ADC_READY_ALERT, INPUT_PULLUP);
        adc0.setConversionReadyPinMode();
        //for test purposes only
        //rtc.adjust(DateTime(F(__DATE__), F(__TIME__)));
        interface.redrawPanel(true);
void writeHeader(){
        SdFile file;
        if(file.open(fileName, O_WRITE)){
            Serial.println("Old file removed");
            file.remove();
        }
        if(!file.open(fileName, O_CREAT|O_APPEND|O_WRITE)){
            interface.showMessage(F("SD~ERROR!"), 2000, 100);
            return;
        }
        file.seekEnd();
        Serial.println();
        file.print("Time, ms;Total depth (m);Position (m);ROP (m/min);Feed Pressure
(bar);Percussion Pressure (bar);Damping Pressure (bar);Rotation Pressure (bar);Flushing
Air Pressure(bar); Raw position (m)");
        file.println("");
        file.close();
}
void printFileFloat(float parFloat
        , SdFile *parFile
```

```
        ){
                parFile->print(";");
                parFile->print(parFloat);
}
void doLogging(){
uint32_t startMillis=millis();
                SdFile file;
                if(!file.open(fileName, O_APPEND|O_WRITE)){
                        interface.showMessage(F("SD~ERROR!"), 2000, 100);
    interface.clearScreen();
    interface.printCentered("Please~replace",2);
    interface.printCentered("the~card~and~restart",3);
                        return;
                }
                file.seekEnd();
Serial.print("\t fop:");
Serial.print(millis()-startMillis          );
startMillis      =millis();
        file.print(currentMeasurementTime-loggingStartMillis);
        printFileFloat(lastLowestPosition, &file);
        printFileFloat(realPosition, &file);
        file.print(";");
        file.print(realROP,3); //additional precision
Serial.print("\t l1:");
Serial.print(millis()-startMillis          );
startMillis      =millis();
        printFileFloat(realFeed, &file);
        printFileFloat(realPercussion, &file);
        printFileFloat(realDamperPressure, &file);
 printFileFloat(realRotation, &file);
 printFileFloat(realFlushingAir, &file);
 printFileFloat((coefPositionSensor* rawPosition), &file);
Serial.print("\t l2:");
Serial.print(millis()-startMillis          );
startMillis      =millis();
        Serial.println("");
```

```
        file.println("");
        file.close();
Serial.print("\t fcl:");
Serial.print(millis()-startMillis        );
startMillis     =millis();
}
void loop(){
        if (loggingStarted){
                if (millis()>nextloggingTimeMillis)   {
uint32_t startMillis    =millis();
                        getValues();
Serial.print("\t get:");
Serial.print(millis()-startMillis);
startMillis     =millis();
                        doLogging();
Serial.print("\t log:");
Serial.print(millis()-startMillis        );
startMillis     =millis();
                        readRTCTime();
Serial.print("\t rtc:");
Serial.print(millis()-startMillis        );
startMillis     =millis();
                        interface.loop();
Serial.print("\t inter:");
Serial.print(millis()-startMillis        );
startMillis     =millis();
                        nextloggingTimeMillis+=(uint32_t)1000/samplesPerSeconds;
                }
        }else{
                readRTCTime();
                interface.loop();
        }
}
```

APPENDIX B

ARDUINO SKETCH FOR GENUINO MEGA (MASTER BOARD)

```
#include <mbDebug.h>
#include <MBCommandParser_v3.h>
#define LCD_INTERFACE_DISPLAY_TYPES_LICQUIDCRYSTALI2C 21
#define LCD_INTERFACE_DISPLAY_TYPES_ADAFRUITI2CBACKPACK 22
//#define LCD_INTERFACE_DISPLAY_TYPE
LCD_INTERFACE_DISPLAY_TYPES_LICQUIDCRYSTALI2C
#define LCD_INTERFACE_DISPLAY_TYPE
LCD_INTERFACE_DISPLAY_TYPES_ADAFRUITI2CBACKPACK
#define LCD_NUMBER_OF_COLS 20
#define LCD_NUMBER_OF_ROWS 4
#if LCD_INTERFACE_DISPLAY_TYPE ==
LCD_INTERFACE_DISPLAY_TYPES_LICQUIDCRYSTALI2C
        #include <LiquidCrystal_I2C.h>
        LiquidCrystal_I2C lcd(0x20, LCD_NUMBER_OF_COLS,
LCD_NUMBER_OF_ROWS);
#elif  LCD_INTERFACE_DISPLAY_TYPE ==
LCD_INTERFACE_DISPLAY_TYPES_ADAFRUITI2CBACKPACK
        #include <LiquidTWI.h>
        LiquidTWI lcd(0);
#else
        #error unknown LCD type:
#endif
SerialCommandParser_v3 commandParser(&Serial, &Serial);
char printingString[SERCMDPARSER__SERIAL_BUFFER_SIZE];
#include <Keypad.h>
#define KEYPAD_ROWS_NUMBER 4
#define KEYPAD_COLS_NUMBER 4
//===PINS
uint8_t pinsKeypadCols[KEYPAD_COLS_NUMBER]={6,7,8,9};
uint8_t pinsKeypadRows[KEYPAD_ROWS_NUMBER]={5,4,3,2};
char keys[KEYPAD_ROWS_NUMBER][KEYPAD_COLS_NUMBER] = {
        {'1','2','3','A'}
```

```
        ,{'4','5','6','B'}
        ,{'7','8','9','C'}
        ,{'*','0','#','D'}
};
Keypad keypad = Keypad( makeKeymap(keys), pinsKeypadRows, pinsKeypadCols,
KEYPAD_ROWS_NUMBER, KEYPAD_COLS_NUMBER);
void cmdClearScreen(){
        #if LCD_INTERFACE_DISPLAY_TYPE ==
LCD_INTERFACE_DISPLAY_TYPES_LICQUIDCRYSTALI2C
                lcd.clear();
        #elif  LCD_INTERFACE_DISPLAY_TYPE ==
LCD_INTERFACE_DISPLAY_TYPES_ADAFRUITI2CBACKPACK
                lcd.clear();
        #else
                #error unknown display type
        #endif
}
void cmdGoXY(){
        uint8_t curX, curY;
        curX=commandParser.getParameterInt(0);
        curY=commandParser.getParameterInt(1);
        #if LCD_INTERFACE_DISPLAY_TYPE ==
LCD_INTERFACE_DISPLAY_TYPES_LICQUIDCRYSTALI2C
                lcd.setCursor(curX, curY);
        #elif  LCD_INTERFACE_DISPLAY_TYPE ==
LCD_INTERFACE_DISPLAY_TYPES_ADAFRUITI2CBACKPACK
                lcd.setCursor(curX, curY);
        #else
                #error unknown display type
        #endif
}
void cmdSetBlink(){
        uint8_t blinkState=commandParser.getParameterInt(0);
        if (blinkState){
                #if LCD_INTERFACE_DISPLAY_TYPE ==
LCD_INTERFACE_DISPLAY_TYPES_LICQUIDCRYSTALI2C
```

```
                lcd.blink_on();
            #elif  LCD_INTERFACE_DISPLAY_TYPE ==
LCD_INTERFACE_DISPLAY_TYPES_ADAFRUITI2CBACKPACK
                lcd.blink();
            #else
                #error unknown display type
            #endif
        }else{
            #if LCD_INTERFACE_DISPLAY_TYPE ==
LCD_INTERFACE_DISPLAY_TYPES_LICQUIDCRYSTALI2C
                lcd.blink_off();
            #elif  LCD_INTERFACE_DISPLAY_TYPE ==
LCD_INTERFACE_DISPLAY_TYPES_ADAFRUITI2CBACKPACK
                lcd.noBlink();
            #else
                #error unknown display type
            #endif
        }
}
void cmdSetCursorVisible(){
        uint8_t cursorVisible=commandParser.getParameterInt(0);
        if (cursorVisible){
            #if LCD_INTERFACE_DISPLAY_TYPE ==
LCD_INTERFACE_DISPLAY_TYPES_ADAFRUITI2CBACKPACK
                lcd.cursor();
            #elif  LCD_INTERFACE_DISPLAY_TYPE ==
LCD_INTERFACE_DISPLAY_TYPES_LICQUIDCRYSTALI2C
                lcd.cursor_on();
            #else
                #error unknown display type
            #endif
        }else{
            #if LCD_INTERFACE_DISPLAY_TYPE ==
LCD_INTERFACE_DISPLAY_TYPES_LICQUIDCRYSTALI2C
                lcd.cursor_off();
```

```
                #elif  LCD_INTERFACE_DISPLAY_TYPE ==
LCD_INTERFACE_DISPLAY_TYPES_ADAFRUITI2CBACKPACK
                        lcd.noCursor();
                #else
                        #error unknown display type
                #endif
        }
}
void cmdSetBacklight(){
        uint8_t backlight=commandParser.getParameterInt(0);
        if (backlight){
                #if LCD_INTERFACE_DISPLAY_TYPE ==
LCD_INTERFACE_DISPLAY_TYPES_LICQUIDCRYSTALI2C
                        lcd.backlight();
                #elif  LCD_INTERFACE_DISPLAY_TYPE ==
LCD_INTERFACE_DISPLAY_TYPES_ADAFRUITI2CBACKPACK
                        lcd.setBacklight(HIGH);
                #else
                        #error unknown display type
                #endif
        }else{
                #if LCD_INTERFACE_DISPLAY_TYPE ==
LCD_INTERFACE_DISPLAY_TYPES_LICQUIDCRYSTALI2C
                        lcd.noBacklight();
                #elif  LCD_INTERFACE_DISPLAY_TYPE ==
LCD_INTERFACE_DISPLAY_TYPES_ADAFRUITI2CBACKPACK
                        lcd.setBacklight(LOW);
                #else
                        #error unknown display type
                #endif
        }
}
void cmdPrint(){
        char tmpBuff[100];
        strcpy(tmpBuff, commandParser.getParameterString(0));
        for (int i = 0; i < strlen(tmpBuff) ; i++){
```

```
                if(tmpBuff[i]=='~'){
                        lcd.print(" ");
                }else{
                        lcd.print(tmpBuff[i]);
                }
        }
}
void setup(){
        Serial.begin(9600); //works only when you use SoftSerial
        #if LCD_INTERFACE_DISPLAY_TYPE ==
LCD_INTERFACE_DISPLAY_TYPES_LICQUIDCRYSTALI2C
                lcd.init();
                lcd.backlight();
        #elif  LCD_INTERFACE_DISPLAY_TYPE ==
LCD_INTERFACE_DISPLAY_TYPES_ADAFRUITI2CBACKPACK
                lcd.begin(LCD_NUMBER_OF_COLS, LCD_NUMBER_OF_ROWS);
                lcd.setBacklight(HIGH);
        #else
                #error unknown LCD type:
        #endif
        lcd.print("Connecting,         please wait...");
        commandParser.storeCopyOfIncomingBuffer(printingString);
        commandParser.addCommand('S', F("cLear Screen"), cmdClearScreen, 0);

        commandParser.addCommand('X', F("cursor to Xy"), cmdGoXY, 2);
        commandParser.addCommand('B', F("set cursor Blink 1/0"), cmdSetBlink, 1);
        commandParser.addCommand('V', F("set cursor Visible 1/0"),
cmdSetCursorVisible, 1);
        commandParser.addCommand('L', F("set backLight 1/0"), cmdSetBacklight, 1);
        commandParser.addCommand('P', F("Print"), cmdPrint, 1);
        /*
        commandParser.printOptionsSettings();
        commandParser.printCommandList();
        */
}
```

```
void loop(){
        commandParser.processSerialReading();
        commandParser.parseSerialCommand();
        char curKey=keypad.getKey();
        if (curKey!= NO_KEY){
                Serial.write(curKey);
        }
}
```

APPENDIX C

CIRCUIT DIGRAM FOR DAQ v2.0 SYSTEM

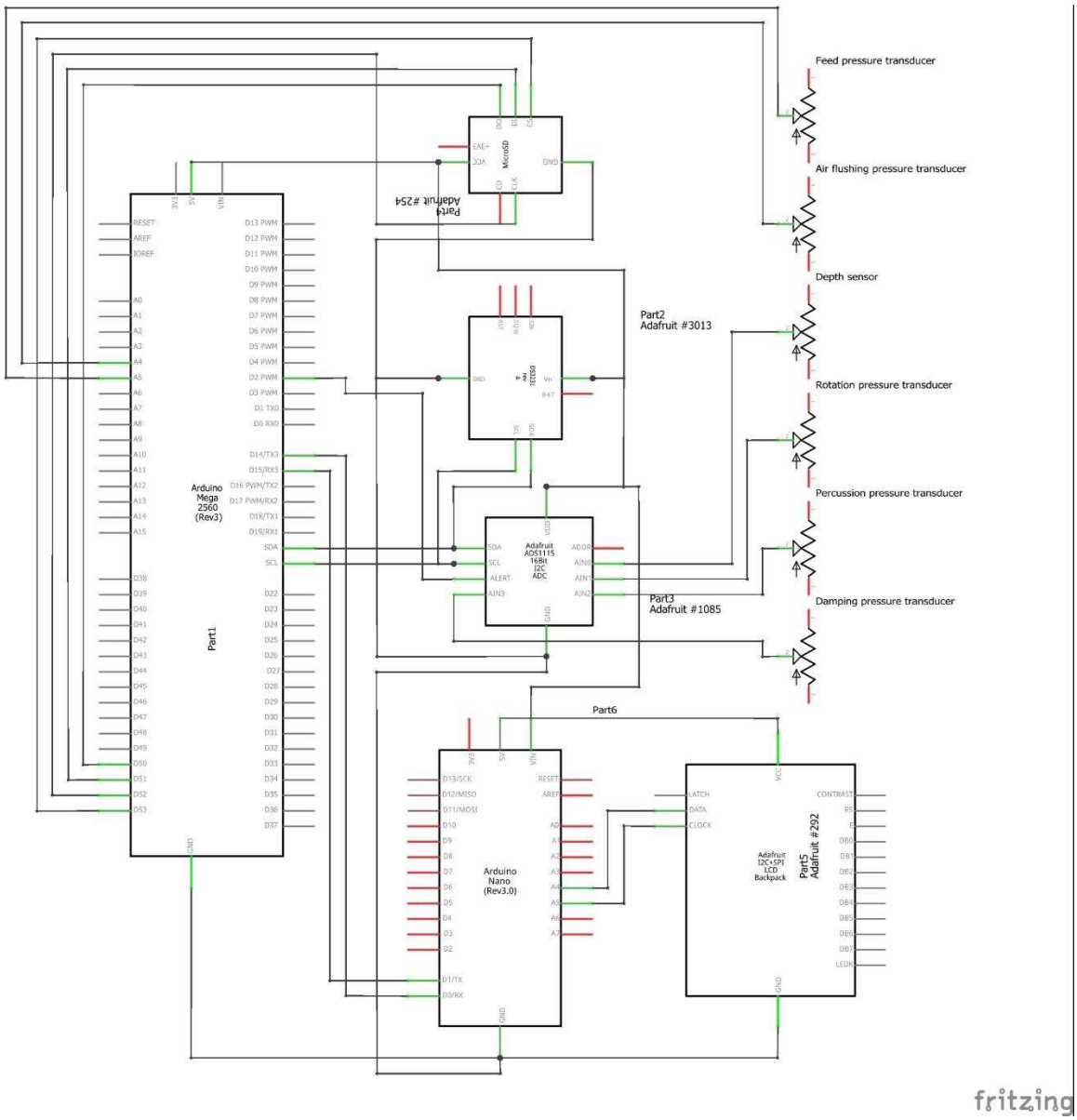

APPENDIX D

DATA ACQUISITION SYSTEM v2.0:

OPERATION MANUAL

Designed by: Igor Kyzym

Emily Flynn

Last Updated: March 1, 2017

TABLE OF CONTENTS

SECTION 1: GENERAL

The following operation manual provides instruction on how to use, retrieve data, and operate the Data Acquisition system v2.0 (DAQ v2.0). This manual provides a description of the system and its operation for use with the Atlas Copco T40 FlexiROC blast-hole drill rig operated by Anaconda Mining Inc. located at the Pine Cove open pit gold mine in Baie Verte, Newfoundland.

1.1. Configuration

The DAQ v2.0 system is a modified version of an old DAQ v1.0 system, which was installed on the rig prior to March 2017. New DAQ system configured to properly log data while drilling. Similar to old system, this system can be configured to log data from other blast hole drilling rigs; however, sensors and system are calibrated to work with the Atlas Copco T40 FlexiROC.

NOTE: Consult with the contacts given below before attempting to switch any major components or configurations of this system.

1.2 System modification

Multiple modifications were implemented in the DAQ v2.0 system. Microcontroller and breakout boards where updated to newer versions. Old RTC breakout board was replaced with high precision RTC DS3231 board, which has an integrated crystal inside the chip and a temperature sensor next to it. This sensor compensates for the frequency changes (caused by temperature fluctuations) by adding or removing clock ticks so that the timekeeping stays on schedule. Also, an Analog-to-Digital Converter (ADC) board was added to the system. This ADC board provides 16-bit precision (instead of 10-bit as it was before) and helps to acquire more precise data from the sensors. Another improvement that was implemented in the new system is a remote control. It is installed in the cabin and

allows operator to create and name individual data files for each hole, to control start and stop moment of data recording and to adjust system time and data recording frequency.

Old depth sensor was replaced with a new more reliable one. The sensor has a higher torque value on power spring; this supposed to prevent the cable from slacking during high accelerations and eventually jamming the spool.

1.3 Contact Information

If any problems or questions arise that are not covered in this manual, please contact the following members of the Drilling Technology Lab (DTL) group located at Memorial University of Newfoundland (MUN):

Dr. Stephen Butt

Email: sdbutt@mun.ca

Igor Kyzym

Email: igor.kyzym@gmail.com

SECTION 2: OPERATION

The following section is a set of instructions for operation while drilling as well as data logging and transferring after logging has occurred.

2.1. On/Off Function

There is an on and off switch located on the exterior of the box. This switch controls the 24V supply of power to the system. When this switch is in the “On” position, all sensors and the DAQ system will be powered.

At the beginning of each day, this switch should be moved to the “on” position (Figure 1). If system is correctly hooked up to a voltage supply, the red light on the Genuino Mega board located into the system enclosure should be lit up. Also, after all drilling has occurred for the day, switch should be moved to the “off” position.

NOTE: When T40 FlexiROC rig is on, 24V will be supplied to the DAQ system if switch is in “on” position. When rig turns off, no voltage will be supplied to the system. Therefore, DAQ system does not need to be turned on and off every day. **For the T40 FlexiROC system, it can be left on.**

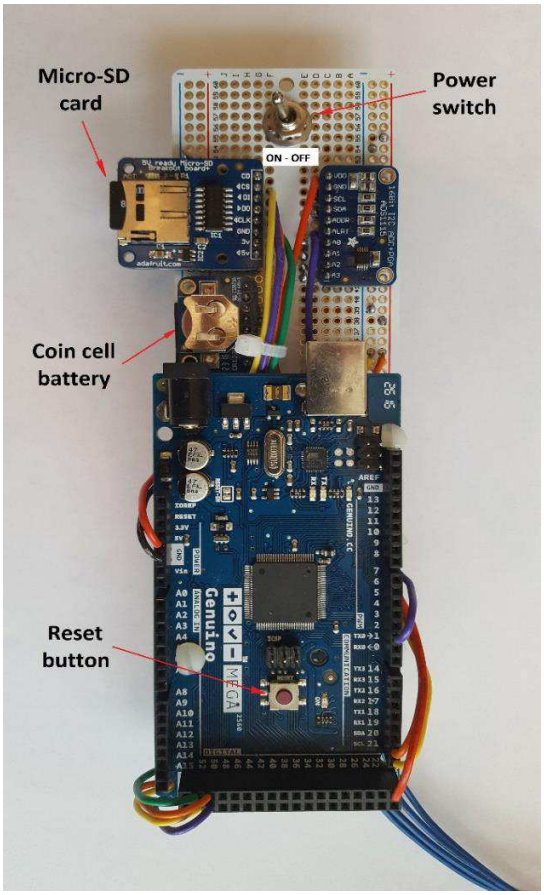

Figure 1 – Microcontroller Genuino Mega and breakout boards

2.2. Micro SD Card

Inside the DAQ box there are four small circuit boards. One of the boards is a “Micro-SD Breakout Board”, which contains the slot for insertion of the micro SD card (Figure 1).

At the beginning of each day, the micro SD card should be inserted if it has not already been inserted into the slot on the Breakout Board. Once, inserted the data from the sensors will write to this card.

NOTE: The system is programmed to initially check to see if the micro SD card is present for logging. If the micro SD is not present during this check, the system will not log the code an error will appear on the display (Figure 2). Even if the card is inserted after the DAQ system is powered, it will not write to the file on the card. To fix this, the card must first be inserted and then the system must be RESET (see section 2.3).

Figure 2 – Micro-SD card error message

2.3. RESET Function

Resetting the system will restart the programmed set-up code. The set-up code checks for the correct work of RTC, ADC boards and micro SD card. Start-up will take only a few seconds and if micro SD card was inserted, then system will be ready to start logging the

data. During the start-up message “Connecting” will appear on the display for a couple of seconds and will be replaced by “Main screen” when the system is ready to log (Figure 3).

To RESET the system, one of two procedures should be followed:

1. Turn the system off, and then on again.
    - To do this, locate the on/off switch on the exterior of the DAQ system enclosure. First, turn the switch to the “off” position. Then turn the switch to the “on” position.

2. Press the RESET button on the Genuino Mega
    - Open the enclosure of the system, locate the Genuino Mega Board, and press the RESET button (Figure 1). This will reset the code.

Figure 3 – Remote control with the Main menu on the display

2.4 Data recording

After the system was powered and the set-up code checked for the correct work of all the boards, the Main menu will appear on the display. This will indicate that system is working correctly and is ready for logging.

To RECORD A DATA FILE please follow the steps below:

1. Lower a drilling bit on the ground. The DAQ system will read a signal from the depth sensor and record this value as a "zero depth";
2. Press "START". A request to name a file will appear on the display (Figure 4);
3. Name a file using the keypad. Each file should be named with a corresponding hole ID and should contain no more than 6 digits.

Figure 4 – Naming the file

Key "F3" is assigned a backspace function and should be used for correction of inputted characters.

4. Press “START”. Data recording will start. Corresponding message, along with the file name and current depth value (Figure 6) will appear on the display.

   NOTE: After the START button was pressed, the system will automatically check if a file with such name already exists. If it does exist, a warning message will appear on the screen (Figure 5) and the operator should make a choice between two options:

   1. Press “F1” – This option will overwrite the existing file. In other words, the old file will be discarded and a new one will be created with the exactly same name and version number (e.g. 777777_0.txt). This option should be chosen in case the original hole was not completed (drilling was interrupted because of technical or any other issues and desired depth was not reached).
   2. Press “F2” – This option will create a new file with the same name, but with a new version number in the end (e.g. 777777_**1**.txt). In this case both files will be saved (777777_0.txt and 777777_1.txt). This option should be picked in case of redrilling (drilling a new hole adjacent to the original one).

Figure 5 – Warning message about already existing file

Figure 6 – Data recording screen

5. Proceed with the drilling a hole;
6. Press “STOP” when drilling is complete (hole is complete). The system will stop recording and will save the file. This will take just a couple of seconds (Figure 7).

Figure 7 – Message about saving the file

After the file was closed, Main menu (Figure 3) will pop up on the display again. This will indicate that the system is ready to record next data file.

2.5 Additional Functions

Some additional functions like data recording frequency and time/date adjustment are incorporated into the system.

2.5.1 Time and date adjustment

Real time clock (RTC) board used in the system is a high precision device and maximum error should nor exceed ±2 min/year. Even though it maintains accurate timekeeping when main power to the device is interrupted, time adjustment will be needed if the coin cell battery rans down.

To ADJUST TIME/DATE please follow the steps below:

1. Ensure the Main menu is on the display. If not, press “STOP” and Main menu will appear on the display;
2. Press “F1”. Change settings menu will appear on the display (Figure 8)

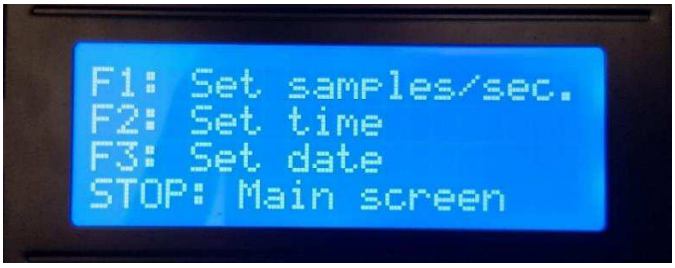

Figure 8 – Settings screen

3. Press “F2” or “F3” to go to time or date adjustment menu respectively (Figure 9);
4. Use the keypad to adjust time/date. Use an “F3” for correction in case a wrong key was accidentally pressed (backspace function);
5. Press “START” to confirm new time/date or “STOP” to discard changes.

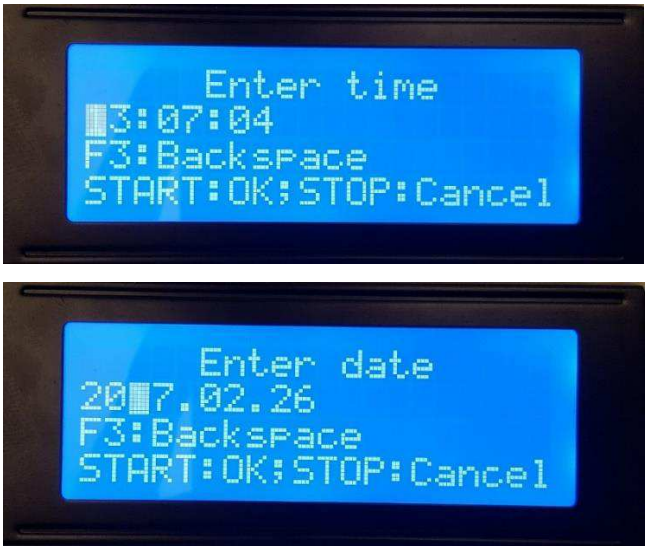

Figure 9 – Time/date adjustment

2.5.2 Sample rate adjustment

Data recording frequency is set to 10 samples/second by default.

To change the SAMPLE RATE value, please follows the steps below:

1. Ensure the Main menu is on the display. If not, press "STOP" and Main menu will appear on the display;
2. Press "F1". Change settings menu will appear on the display (Figure 8)
3. Press "F1" to go to sample rate adjustment menu (Figure 10);
4. Use the keypad to adjust the sample rate value. Use an "F3" for correction, in case a wrong key was accidentally pressed (backspace function);
5. Press "START" to confirm new sample rate value or "STOP" to discard changes.

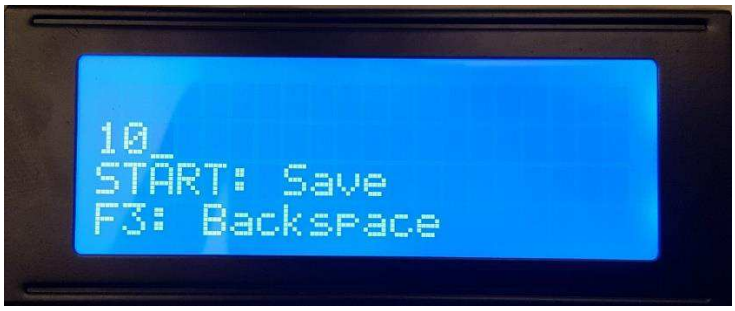

Figure 10 – Sample rate adjustment

NOTE: Please do NOT adjust the sample rate value unless requested by DTL members.

2.6. Saving/Sending Data Files

The data files will have to be saved onto a safe hard drive or onto the host PC.

To save logged data from the DAQ system please follow the steps below:

1. Ensure the DAQ system is switched off, before removing any components.
2. Next, locate the SD card breakout board, and remove the micro SD card (Figure 1).
3. Bring the micro SD card to the host PC used for saving.
4. Insert micro SD card into host PC. Use micro SD card reader/writer if there is not SD card slot on the PC being used.
5. Copy all data files into one folder. Name that folder with a time when the data was recorded.
6. Format a micro SD card before installation back on the DAQ system.

Sending Logged Data:

Once the files have been saved on the host PC, the files can be sent to MUN for further analysis. Text files will be sent through email. Please follow the template below:

Send To: adjlopezober@mun.ca Alejandro Lopez
igor.kyzym@gmail.com Igor Kyzym
cc: sdbutt@mun.ca Stephen Butt

Subject: Data Logged for Week of March 6 - 13

Attachment: Archive file with all saved data files for week stated above.

SECTION 3: MAINTENANCE

The T40 DAQ system contains some small components that may need replacement as time progresses. However, these items can easily be replaced as needed. The protocol on how to handle the replacement and maintenance of these items is described below.

3.1. Replacing Components

Before replacing any components or making any changes on the T40 DAQ system, please consult the DTL at MUN for further assistance **(see section 1.3.)**. Do not order or add any components to the system before contacting the authorized personnel at Memorial University.

Once confirmed with the DTL group, the replacement for the component can be chosen to fix the problem that has occurred.

Coin Cell Battery

The coin cell battery inside the DAQ system enclosure will need replacement if the system has been in use for a number of years. Although, the battery can last up to 10 years, it may die before this time. If the battery has run end, time will stop counting on the clock. This can be an indication to replace this battery.

Coin cell batteries can be purchased locally for approximately 1$. Lithium 3V 12mm Coin Cell Battery should be purchased.

Fuse

The current system uses a 250 mA fuse. However, if a short or an electrical error occurs this fuse will blow. The error will then have to be corrected and the fuse will have to be replaced.

APPENDIX E

ARMA 15-764

Cuttings Analysis for Rotary Drilling Penetration Mechanisms and Performance Evaluation

Reyes, R., Kyzym, I., Rana P.S., Molgaard J. and Butt, S.D
Memorial University of Newfoundland, St. John's, NL, Canada

This paper was prepared for presentation at the 49th US Rock Mechanics / Geomechanics Symposium held in San Francisco, CA, USA, 28 June-1 July 2015.

ABSTRACT: Drillability or drilling efficiency of rock depends on three main parameter groups: rock characteristics, drill rig parameters and operational parameters. This paper describes the methodology of rock cuttings collection, preparation and their analysis for evaluation of the drilling efficiency and the performance of a passive Vibration Assisted Rotary Drilling (pVARD) tool in particular. The pVARD tool utilizes rock bit interactions to create axial vibrations in order to improve rock penetration. Analyses showed the correlation of such parameters as rate of penetration and weight on bit to cuttings size distribution. Several parameters such as mean particle size and coarseness index were used for numerical representation of cuttings size. Also a new particle size distribution bar diagram was proposed for cuttings samples comparison.

1. INTRODUCTION

One of the purposes of an effective drilling fluid system is to convey the cuttings from around the bit to the surface [1].

Several studies have been carried out on drilling cuttings as these are commonly used for the geological description of wells. Also studies on the petrophysical properties of formations, such as porosity and permeability have been conducted [2,3]. These studies have outlined the importance of cuttings analysis.

However, few studies have focused on studying cuttings as a mean of understanding the cutting action of the drilling tools. By analyzing the way that the cutter affects the different drilled formations and establishing relations between drilling parameters, drilling performance and cuttings, it is more feasible to make assumptions on the rock-bit interaction models for different drilling techniques.

Drilling performance is often defined as the drillability of a rock, that is, how fast a certain formation can be drilled. It is characterized by the rate of penetration (ROP). The parameters that define the drillability of a rock are usually separated in three groups: Rock characteristics (physical, mechanical, and micro-structural properties of the drilled formation), machine parameters (rotation, force, cuttings removal, etcetera.) and operating processes (drilling techniques, state of the equipment, etcetera.) [4].

In previous studies, some relations have been established between these three parameter groups and the cuttings analysis. Pfleider and Blake [5] concluded that the size and shape of cuttings are strongly related to ROP, i.e., the higher the ROP, the coarser the particles. This statement has been supported by other studies, both in percussion drilling and rotary drilling. [4,6].

The use of different drilling bits and drilling through different geological formations has also been evaluated in these studies. In general, there is unanimity in diamond drilling studies that the size of cuttings is related to the speed of advance. Most of these studies have also shown that this advance is proportional to the increase in rotary speed and the weight on bit during the drilling up to certain point. Above this point the relation tends to be inversely proportional due to the grinding of the particles [5].

In terms of quantifying and comparing the particle size of drill cuttings, several techniques have been developed, but the most used method has been to plot the cumulative percentage of undersized particles (or oversized) against particle size [6]. This graphical method has been done using different combinations of scales (linear, log, log-log) each with specific benefits depending on the application [7]. For powder materials and others obtained as a result of grinding, crushing and

milling, the double logarithmic scale diagram, hereinafter called Rosin-Rammler (RR) distribution, has been shown to be well suited. Its graphical representation can be approximated to a straight line for better evaluation and comparison of samples [8].

The purpose of the present work is to describe a process for the analysis and comparison of cuttings sizes, its relationship with the drillability parameters and to apply this procedure to the evaluation of the performance of the passive Vibration Assisted Rotary Drilling (pVARD) tool, developed by the Advanced Drilling Technology Laboratory of Memorial University of Newfoundland.

2. BACKGROUND

Several Vibration Assisted Rotary Drilling (VARD) tools were designed and evaluated by the Advanced Drilling Laboratory. Multiple laboratory tests of reduced scale tools and various stages of numerical simulations were conducted.

Laboratory-scale prototype testing of a passive Vibration Assisted Rotary Drilling (pVARD) tool showed a considerable increase in the rate of bit penetration (ROP) by providing axial compliance at the bit-rock contact. To confirm the results obtained in the laboratory, a full-scale model of pVARD tool was designed and fabricated for further testing in field conditions.

3. FIELD WORK

Several potential field sites were identified and evaluated on the Avalon Peninsula of Newfoundland, Canada. The site selected for the present study was a quarry site owned and operated by Greenslades Construction in Conception Bay South.

Some preliminary studies indicated that the rocks drilled would be grey (green) and red shale with a basement of granite. During the field work, an Ingersoll Rand T3W drill rig was used. The rig was equipped with four drill bits that were used alternately during the drilling; however, this report will only focus on the results obtained during the drilling with PDC and RC bits. TSP bit data was not analyzed because of insufficient number of collected samples (less than 2 ft were drilled). Also percussive bit is out of interest, as the paper is focused only on rotary drilling.
The drilling of three wells was performed up to a depth of 121.92 m, 123.44 m and 63.73 m respectively. Several Bottom Hole Assembly (BHA) configurations were tested under different values of weight on bit (WOB). Other parameters like flowrate of the drilling fluid system and rotary speed of the drill string fluctuated because of the nature of drilling rig. During the drilling, cuttings were collected from the return fluid line (water) of the well into plastic containers. The latter were left for 5-10 minutes to give cuttings enough time to settle. After water was drained, cuttings were placed in separate sealed bags for each interval of drilling. Sometimes it was problematic to collect the samples that mainly consisted of very fine grains, as they required a very long time to settle. Consequently, the weight of those samples was relatively small (30-40 grams) compared to others (a few hundred grams). The following parameters were recorded for each interval: drilling depth, net drilling time, feed pressure, rotary speed, pump flowrate. The data was obtained either through the rig's control panel or through direct measurement.

To compensate for the fluctuations of rotary speed, a normalized ROP value was calculated as follows:

$$ROP_n = ROP\frac{100}{n} \qquad (1)$$

where ROP - is rate of penetration corresponding to rotary speed n.

This means that the normalized ROP's values correspond to a rotary speed of 100 rpm.

4. LABORATORY WORK

4.1 Procedure of cuttings size analysis

Since there is no a standard procedure for particle size analysis of cuttings from well drilling, the ASTM D422 Standard Test Method for Particle-Size Analysis of Soils [9] was adapted for this type of sample.

The cuttings were dried in an oven at the temperature of 60~70 °C. While drying, clumps formed in several samples. These were carefully crushed with a rubber mortar. A hundred grams, as a representative weight of the sample, was taken from each sample for sieving. If the sample weight was less than a hundred grams, the entire sample was sieved.

The set of sieves, included the following mesh sizes

- 2300 μm;
- 1180 μm;
- 850 μm;
- 425 μm;
- 300 μm;
- 100 μm.

An automatic shaker was used to provide the proper separation of different size fractions. Finally, all size

fractions were weighed and put into separate plastic bags.

The cumulative weight percentage of passing particles was calculated for each size of mesh. A total of 79 sieved samples were obtained and a Rosin-Rammler (RR) diagram was plotted for each sample. From the RR diagram, using a Matlab code [8], the particle mean size (d') was taken as a size parameter; this is the particle size for which 36.79% of the particles are bigger. An example of RR diagram is shown on Fig. 3.

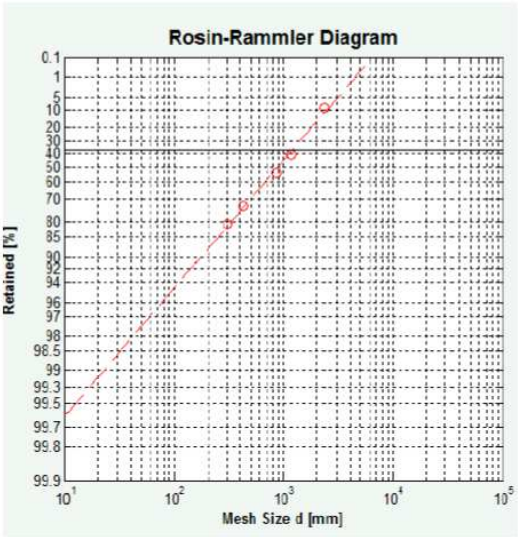

Fig. 3 - Rosin-Rammler (RR) distribution diagram

Another size parameter calculated is the coarseness index (CI); the coarseness index is a non-dimensional number obtained by adding the cumulative weight percentage of particles retained in each size of a set of sieves [10]. The CI will vary depending on the mesh sizes selected but will be suitable for comparison if the same sieves are used throughout the process. This parameter is very useful, because the overall sample can be characterized by one number, however it cannot provide complete information about the particle size distribution. The coarseness index calculation procedure is shown in Table 1.

A regular particle size distribution diagram (PSD) (Fig. 4) could be used for graphical representation of cuttings size distribution. Horizontal and vertical axes represent sieve mesh size and the cumulative percentage of particles finer than corresponding mesh size respectively. The horizontal axis is plotted on a logarithmic scale for a better distribution of the curve. The further right this curve is, the larger the particles are.

Table 1 Sieve analysis of Sample #36. Well 2 Grey Shale with quartz veins

Size (mm)	Weight (%)	Cumulative weight (%)
+2.36	7.52	7.52
-2.36+1.18	27.44	34.96
-1.18+0.850	12.83	47.79
-0.850+0.425	20.98	68.77
-0.425+300	7.34	76.11
-300	23.89	100.0
$\sum$	100	
Coarseness index (CI)		335.15

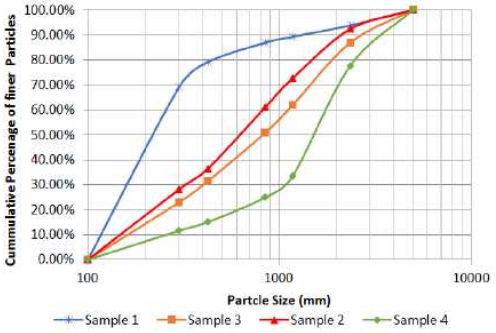

Fig. 4 – PSD diagram

From the diagram shown above it is possible to see that Sample 1 has the finest grains and Sample 4 has the coarsest. However, a PSD diagram can be confusing and the comparison of cuttings samples may be difficult, especially when representative curves intersect (Fig. 5).

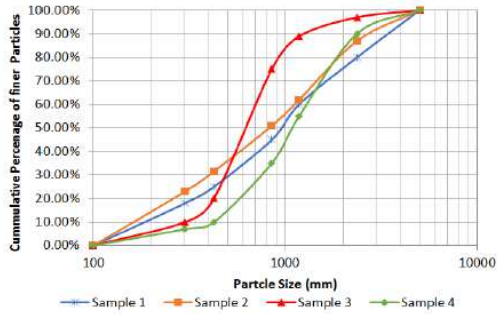

Fig. 5 – PSD diagram with crossing curves

For this reason, a bar particle size distribution (BPSD) diagram was proposed (Fig. 6). Each color represents a different size range in the sample. These diagrams present information in a simple and more convenient way. The bar diagram makes particle size distribution

easier to perceive than a regular curve diagram. Also BPSD diagrams facilitate the comparison between different size fractions of different samples. This representation is more complete and precise than numerical parameters such as the coarseness index (CI) or mean particle size (d). Also, it was found that a bar PSD is much more useful than a regular PSD diagram, which might be quite confusing and may lead to inaccurate interpretations of the results.

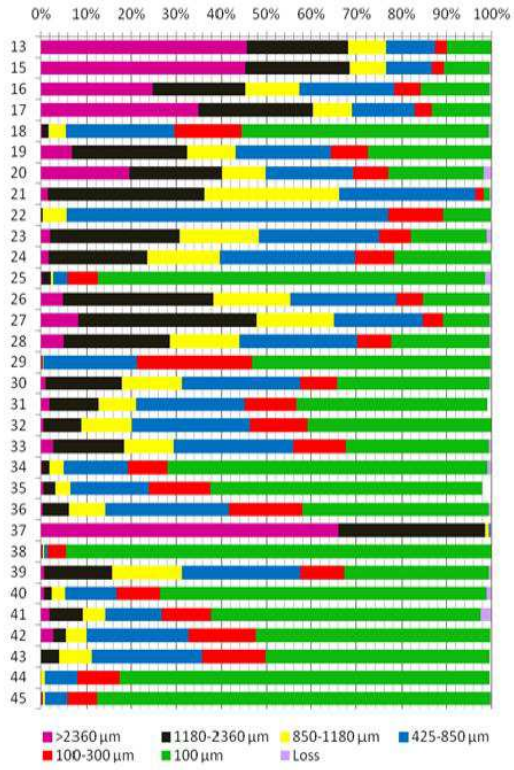

Fig. 6 – PSD bar diagram for cutting samples collected from Well 1

4.2 Geological Studies

Visual and microscopic analyses of cuttings allows for an opportunity to identify the type of drilled formation. For this purpose two microscopes (a Wild at 128x and Reichert ME4 at 2000x magnification) were used.

Analyses showed that the drilled formations were prevalently grey and red shale. The upper 60 m (200 ft) consist of pure grey shale. Deeper formations are mainly consecutively changing, thin, layers of grey and red shale, or red shale interbedded in a grey layer and vice versa. The last 15 m (50 ft) of Well 1 and 2 are mainly grey shale with a high content of quartz. Microscopic pictures of cuttings that represent three drilled formations are shown in Fig. 7.

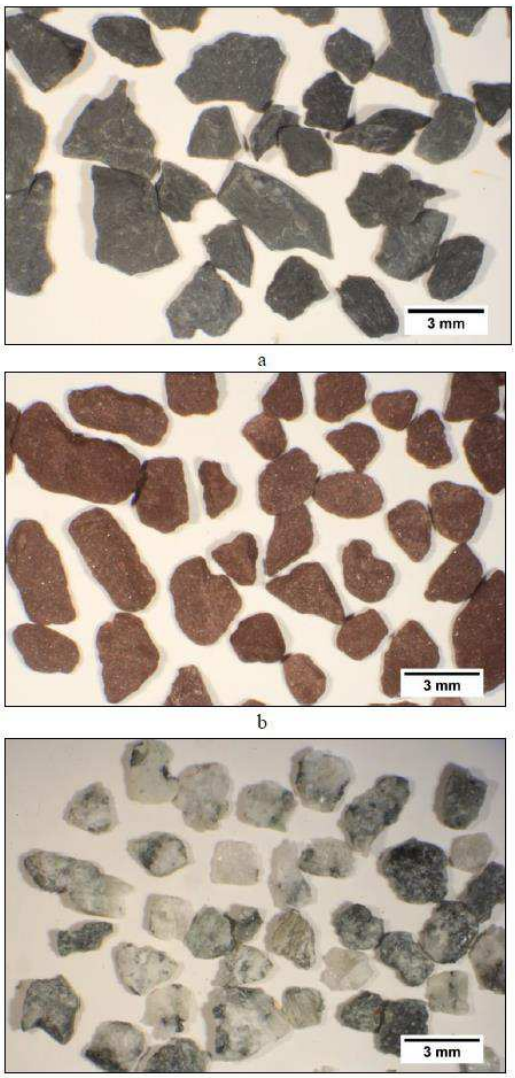

Fig. 7 – Cuttings geological analysis (a – grey shale, b – red shale, c – formation with a high content of quartz)

The last sections of Wells 1 and 2 appeared to be highly heterogeneous due to the differing amount of quartz in each sample; for this reason, no further cuttings analysis, or any drillability evaluation while drilling through this formation, was done. Therefore, the investigation was focused mostly on the depth interval of 0-105 m (0-350 ft) for all three wells. The obtained results allowed us to construct a geological cross-section of the site (Fig. 8).

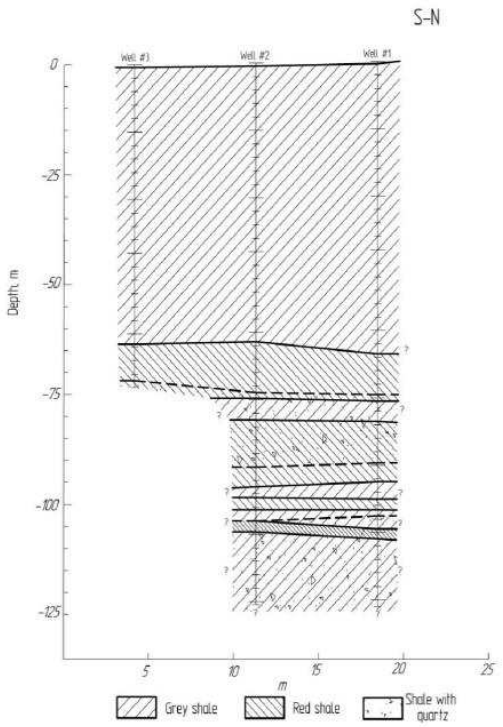

Fig. 8 – Geological cross-section of the site

The section from 72-90 m (240-300 ft) deep also has some quartz veins; however, the percentage of quartz is quite small and it had a negligible effect on the drilling performance.

Additionally, some samples were collected from exposures of shale on the surface of the field site for rock characterization. A brief observation of these samples shows that grey shale (Fig. 9) is a highly brittle sedimentary rock with a brightly expressed laminate structure, while red shale (Fig. 10) is expected to be much more compact and intact rock. However, unconfined compressive strength values, estimated from point load index test (load was applied in direction normal to bedding), are approximately equal for both rocks.

Unconfined compressive strength results for these rocks are shown in Table 2.

Table 2 Unconfined compressive strength of the rocks

Rock type	Value (MPa)
Grey shale	61
Red shale	56

Fig. 9 – Grey shale sample

Fig. 10 – Red shale sample

4.3 Cuttings size interpretation

From each well, several intervals were chosen for further analysis. For each sample from those intervals ROP, WOB, CI and mean particle size (d) values were plotted. WOB values are shown in kN, ROP in meters per hour.

4.3.1 Particle size distribution analysis in grey shale

As section 1, samples 12-21 (39.3-63.6 m) of Well 1 have been analyzed. Drilling was performed with a roller cone bit and without the pVARD tool.

In Fig. 11 a bar PSD diagram for this section is shown, along with CI, d, WOB and ROP values for each sample. In this section, samples 16-17 were not considered because visual analysis of cuttings showed a high content of quartz in these samples.

These diagrams show that cuttings size has a tendency to increase first and then decrease after certain point. Conversely, WOB and ROP values are continuously increasing. From the CI and d plots it can also be observed that both parameters are equivalent for size representation.

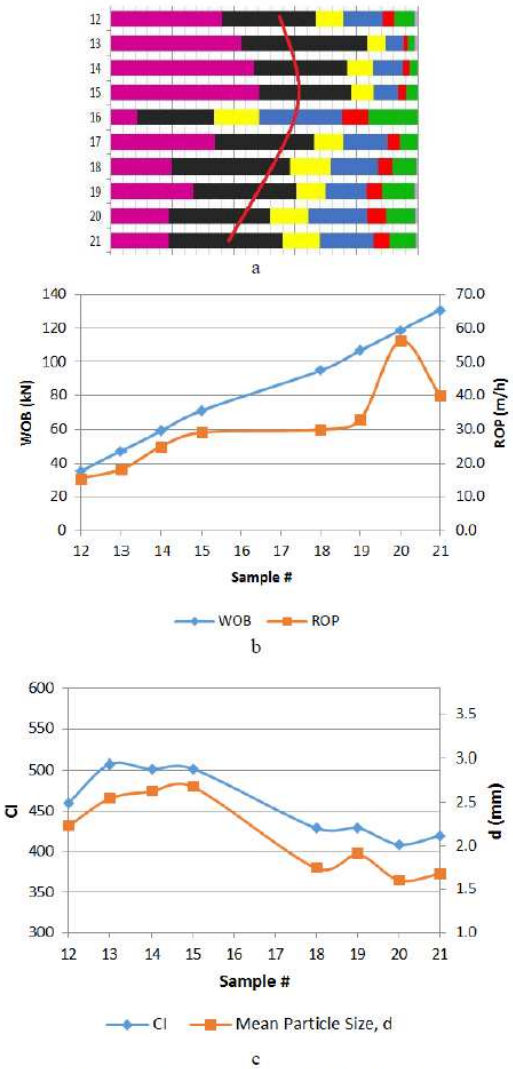

Fig. 11 – PSD analysis of Section 1 (a-bar PSD, b-Performance Parameters, c-Size Parameters)

Section 2 (samples 18-21, Well 3, 82.3-91.4 m), which was drilled with a PDC bit and no VARD tool, shows the same results as Section 1. The corresponding results are shown in Fig. 12.

Analyzing both sections, it is possible to say that after reaching a certain threshold of WOB cuttings get smaller because of crushing by the bit before they can be removed from the borehole by the drilling fluid. In both cases (Section 1 and 2) this threshold value is around 70-75 kN. After this value, the positive relation between ROP (WOB) and cuttings size changes into a negative one.

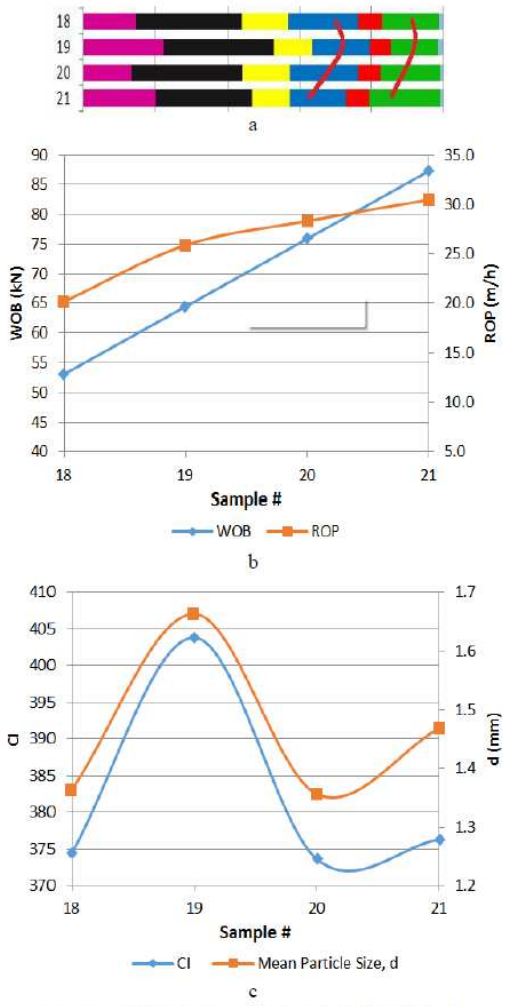

Fig. 12 – PSD analysis of Section 2. (a-bar PSD, b-Performance Parameters, c-Size Parameters)

This phenomenon could be explained by the laminate structure and brittleness of the grey shale. It is worth noticing that ROP is still increasing, while smaller cuttings are being generated. We might expect that, with more efficient cleaning of the borehole (a higher flowrate) ROP could be even higher, as additional energy would not be spent in regrinding cuttings. This leads us to conclude that, for weak and brittle formations efficient cleaning is a very important factor.

The other two sections (plots are not shown in the paper) analyzed from the grey shale showed a negative relationship between ROP and cuttings size. In both cases drilling was performed with a WOB over 65 kN, what supports the hypothesis about threshold value.

4.3.2 Particle size distribution analysis in red shale

Section 3 comprises samples 39-43 (71.6-73.6 m) from Well 3. These samples contain quartz, but as the percentage is quite small and constant for all samples we assume that it has no significant effect on the performance and cuttings size. Drilling was performed with the PDC bit and with the pVARD tool.

The bar PSD diagram for this section and the corresponding CI, d, WOB and ROP graphs are shown in Fig. 13.

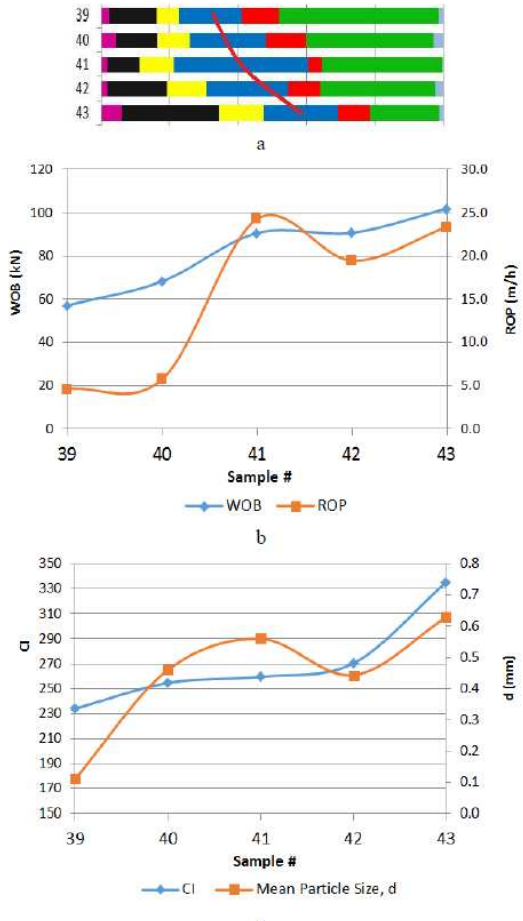

Fig. 13 - PSD analysis of Section 3. (a-bar PSD, b-Performance Parameters, c-Size Parameters)

For drilling in red shale, the cuttings size and ROP (as well as WOB) have a positive relationship for all the WOB range; in other words, bigger cuttings are generated while drilling with higher ROP. Additional analyses performed on other sections of the red shale are consistent with this affirmation.

The same particle size analysis against performance parameters was made for the bottom section of Wells 1 and 2. Although it was mentioned that this formation was highly heterogeneous, the results obtained also support the statement that ROP and cuttings size have a positive relationship. However, is important to keep in mind that, in this case, the change in cuttings size could be due to changing formation (from quartz veins to shale and vice versa).

Also due to natural brittleness of the shale and drillsrting vibrations cavings could occur and consequently affect original particle size distribution of the drill cuttings samples. However, the extent to which cavings could affect particle size distribution is yet to be investigated.

There is no apparent relationship found for ROP and cuttings size in highly interbedded formations.

On the other hand, no conclusive results could be obtained for the use of the pVARD tool. Even though the use of this tool showed an increased performance in the red shale [12], the cuttings analyses did not show a consistent increase in size for all the sections analyzed.

Heterogeneity in the formations and fluctuations in the flushing flowrate and drill string rotary speed might be a reason for the irregularity of the results. It is clear that further work is required to solve this inconsistency.

So far, some preliminary studies performed by ADL members Yingjian Xiao and Jinghan Zhong on concrete samples with different strength values, have shown good results for the cuttings size in drilling with the pVARD tool. Laboratory work on natural rock drilling is expected to be performed later to confirm these results.

5. CONCLUSIONS

The analysis of the results obtained from the field and laboratory work that has been performed lead us to the following conclusions:

- Bar particle distribution diagram (BPSD) is a very useful instrument for graphical representation of cuttings samples. It is easier to perceive information from BPSD than from regular PSD.
- The mean particle size (d) and the Coarseness Index (CI) are suitable for rough numerical characterizing of cuttings size and comparison between samples. Mean size and CI are mainly interchangeable and show a similar relationship with ROP and WOB. Nevertheless, a bar PSD diagram provides more detailed information about cuttings samples.

- ROP and cuttings size (CI, d) have a mainly positive relationship. For very brittle and laminate structure formations like grey shale, this relation might become negative if the WOB is increased over a certain value.
- Efficient cleaning of the borehole is important for drilling through weak, brittle formations.
- The PSD analysis shows consistent results for homogeneous formations. For heterogeneous formations results are not consistent.
- Inconsistency in field data could be caused by formation heterogeneity, cuttings collection issues (incomplete samples were collected), fluctuations in flowrate and rotary speed.

REFERENCES

1. Caenn, R., H. C. H. Darley, and G.R. Gray. 2011. Introduction to drilling fluids. In *Composition and properties of drilling and completion fluids*, 6th ed. Gulf Professional Pub, 1-2.
2. Lenormand, R. and O. Fonta. 2007. Advances in measuring porosity and permeability from drill cuttings. In *Proceedings of the 2007 SPE/EAGE Reservoir Characterization and Simulation Conference, Abu Dhabi, 28 – 30 October 2007,* eds. Curran Associates Inc, 135-143.
3. Carugo, C., A. Malossi, P. Balossino, R. Galimberti, L. Gioacchini, F. Pingitore, and F. Rivolta, 2013. Advanced cuttings analysis improves reservoir characterization and reduces operating times in shale gas drilling project. In *Proceedings of the International Petroleum Technology Conference 2013: Challenging Technology and Economic Limits to Meet the Global Energy Demand, IPTC 2013,Beijing, 26 - 28 March 2013,* eds. Society of Petroleum Engineers *7* 5654-5668.
4. Altindag, R. 2003. Estimation of penetration rate in percussive drilling by means of coarseness index and mean particle size. *Rock Mechanics and Rock Engineering.* 36(4): 323-332.
5. Pfleider, E. and R. L. Blake, 1953. Research on the cutting action of the diamond drill bit. *Mining Eng.* 5: 187-195.
6. Ersoy, A. and M. Waller, 1997. Drilling detritus and the operating parameters of thermally stable PDC core bits. *International Journal of Rock Mechanics and Mining Sciences.* 34(7): 1109-1123.
7. Wills, B.A. and T.J. Napier-Munn, 2006. Particle Size Analysis. In *Wills' Mineral Processing Technology*, ed. Elsevier Science & Technology Books, 90 – 108.
8. Brezani, I. and F. Zelenak. 2010. Improving the effectivity of work with rosin-rammler diagram by using MATLAB (R) GUI tool. *Acta Montanistica Slovaca.* 15(2): 152-157.
9. ASTM D422-63 2007-e2, Standard Test Method for Particle-Size Analysis of Soils, ASTM International, West Conshohocken, PA, 2007, www.astm.org
10. Roxborough, F. and A. Rispin. 1973. Mechanical cutting characteristics of lower chalk. *Tunnels & Tunnelling International.* 5(3)
11. Deely, C. 1947. Diamond core drilling methods and problems. *Petroleum Engineer.* 18(9).
12. Rana, P.S. 2014. Field Trial Report. Unpublished document.